U.PORTO

FEUP FACULDADE DE ENGENHARIA
UNIVERSIDADE DO PORTO

Thermal Behaviour of Filament Wound CFRP Struts for a Deployable Space Antenna

José Henrique dos Santos Faria

Supervisors:

António Torres Marques, Emeritus Professor

Pedro Teixeira, Ph.D.

Submitted in fulfilment of the requirements for
the degree of Master of Science in Mechanical Engineering
to the Faculty of Engineering of the University of Porto

Porto, July 2021

To my grandparents.

‘It is an important and popular fact that things are not always what they seem. For instance, on the planet Earth, man had always assumed that he was more intelligent than dolphins because he had achieved so much - the wheel, New York, wars and so on - whilst all the dolphins had ever done was muck about in the water having a good time. But conversely, the dolphins had always believed that they were far more intelligent than man - for precisely the same reasons.’

Douglas Adams, ‘The Hitchhiker’s Guide to the Galaxy’

Abstract

The space environment is synonym of harsh conditions, particularly for polymer matrix composites. As spacecrafts move in and out of Earth's shadow while in orbit, they are exposed to a cyclic rise and drop between extreme temperatures that represents a thermal fatigue event capable of degrading composite components. The distinct behaviour between constituents under thermal cycling originates stresses that potentiate the advance of damage mechanisms within the laminate. The mechanical and physical properties of composite systems can be heavily jeopardised by the progression of damage, risking the integrity of the structure that they compose.

This study delves into the thermal behaviour of filament wound CFRP struts that form the frame for a deployable space antenna. As this is a highly sensitive structure, the dimensional stability of the composite struts must be guaranteed throughout the entire life cycle of the artificial satellite, along with its structural integrity. The response of this component to conditions similar to the ones encountered while in orbit is assessed by exposing it to thermal cycling, and evaluating its consequences. Along this work, the influence of the production parameters in the definition of the thermal behaviour, as well as the expected consequences of thermal cycling, are reviewed and further discussed with the aid of experimental data. It is concluded that thermal fatigue environments undoubtedly lead to damage in composite systems, but the initial forms of degradation are not necessarily worrying, as they might not affect the physical and mechanical properties of the component.

Keywords: Composite Systems, Filament Winding, Thermal Fatigue

Resumo

O ambiente espacial é sinónimo de condições adversas, particularmente para compósitos de matriz polimérica. Os satélites artificias que se encontram em órbita são expostos a variações cíclicas de temperatura, definidas pela sua posição face ao Sol, o que se traduz num ambiente de fadiga térmica capaz de degradar os sistemas compósitos. O comportamento distinto entre os constituintes destes materiais durante variações térmicas leva ao aparecimento de tensões que potenciam o avanço de mecanismos de dano no seio do laminado. As propriedades físicas e mecânicas dos materiais compósitos podem ser postas em causa pela progressão destes danos, colocando em risco a integridade da estrutura que compõem.

O estudo em mãos foca-se no comportamento térmico de tubos em fibra de carbono e resina de épóxi produzidos por enrolamento filamentar. Estes componentes fazem parte de uma antena espacial que requer uma enorme estabilidade dimensional ao longo de todo o intervalo de temperaturas experienciado em órbita. A resposta deste componente às condições encontradas no Espaço é avaliada através da sua exposição a ciclos térmicos, cujas consequências são escrutinadas. Ao longo desta dissertação, a influência dos parâmetros de produção na definição do comportamento térmico, bem como as consequências da exposição a fadiga térmica, são exploradas e discutidas com o auxílio de dados experimentais. É possível concluir que os ambientes de fadiga térmica levam indubitavelmente à propagação de dano em sistemas compósitos, mas os modos de degradação manifestados numa fase inicial podem não ser alvo de preocupação quanto ao comportamento destes materiais, na medida em que não afetam significativamente as suas propriedades físicas e mecânicas.

Palavras-chave: Sistemas Compósitos, Enrolamento Filamentar, Fadiga Térmica

Acknowledgements

Firstly, I would like to express my gratitude to Professor António Torres Marques for his endless support, interest and patience over the past months. The vast experience and knowledge transmitted pushed me to excel and certainly elevated the quality of the work developed.

It is also imperative to thank everyone at Frezite High Performance for the warm welcome and express my heartfelt appreciation to my supervisor Pedro Teixeira, along with Nuno Vieira and José Cerqueira. It is certainly uncommon to have the opportunity to become part of such an exciting project and even more unlikely to be heard as a contributing part of such a demanding operation. The fascinating scope of this project, coupled with the genuine sympathy of everyone I worked with, resulted in an incredibly enriching experience.

Moreover, I must acknowledge the help of Prof. António Magalhães and Prof. Luis Durão, from ISEP, as well as Prof. Joaquim Magalhães, from FEUP, in the search for non-destructive inspection methodologies. This recognition is extended to Emília Soares and Armanda Marques for their kindness and availability during this process.

Completing a journey of this kind is far from being just the result of a single semester or even the knowledge acquired through my entire education. It is also, and perhaps most importantly, the culmination of multiple years of growth under the love and company of friends and family that define who I am and still aspire to become. For that reason, I am immeasurably grateful to them.

I could not stress enough the importance of those closest to me in any goal I will ever achieve. I must mention Elisabete and Mafalda for the unquestionably reciprocal unbounded care nurtured towards me. The role of my grandparents, Idalina and Joaquim, is particularly impossible to describe, as every part of me was impacted by their love. To my father, José, I credit my terrible jokes and enormous passion for engineering. Lastly, to my mother, Felismina, I owe absolutely everything.

Contents

Abstract **v**

Resumo **vii**

Acknowledgements **ix**

1 Introduction **1**

1.1 Copernicus Programme at Frezite High Performance 1

1.2 Motivation 2

1.3 Main Goal 3

1.4 Thesis Outline 3

2 Filament Winding **5**

2.1 Brief Historical Review 6

2.2 Process Description 7

2.2.1 Process Parameters 8

2.2.2 Raw Materials 10

2.2.3 Mandrel Preparation 10

2.2.4 Impregnation Methods 11

2.2.5 Fibre Tension 13

2.2.6 Curing Stage 14

2.2.7 Advantages and Limitations 15

2.3 Winding Pattern 16

2.3.1 Geodesic Paths and Nonslip Strategies 19

2.3.2 Axisymmetric Shapes 20

3 Thermal Behaviour of Composite Materials **23**

3.1 Space Environment 24

3.1.1 Ultraviolet and Particulate Radiation 24

3.1.2 Atomic Oxygen . . . 25
3.1.3 Vacuum . . . 25
3.1.4 Thermal Cycling . . . 26
3.2 Defining Thermal Behaviour . . . 27
3.2.1 Glass Transition Temperature . . . 27
3.2.2 Coefficient of Thermal Expansion . . . 29
3.2.3 Thermally Induced Stress . . . 31
3.3 Parameters Affecting Thermal Behaviour . . . 35
3.3.1 Constituent Selection and Fibre Volume Fraction . . . 35
3.3.2 Layup and Fibre Orientation . . . 38
3.3.3 Curing Stage . . . 39
3.4 Effect of Thermal Cycling . . . 44
3.4.1 Fatigue Damage Mechanisms . . . 44
3.4.2 Mechanical Properties . . . 49
3.4.3 Glass Transition Temperature . . . 52
3.4.4 Coefficient of Thermal Expansion . . . 54

4 Experimental Characterisation **57**
4.1 Manufactured Struts . . . 58
4.2 Thermal Cycling . . . 60
4.3 Non-Destructive Inspection . . . 62
4.3.1 Microscopic Observation . . . 63
4.3.2 X-Ray Radiography . . . 63
4.3.3 Thermography . . . 64
4.4 Mechanical Properties . . . 65
4.4.1 Compression Test . . . 65
4.4.2 Four-Point Bending . . . 67
4.5 Thermal Properties . . . 69
4.5.1 Coefficient of Thermal Expansion . . . 70
4.5.2 Glass Transition Temperature . . . 72

5 Results and Discussion **75**
5.1 Non-Destructive Inspection . . . 76
5.1.1 Microscopic Observation . . . 76
5.1.2 X-Ray Radiography . . . 82
5.1.3 Thermography . . . 86
5.2 Mechanical Properties . . . 87
5.2.1 Compression Properties . . . 87

5.2.2 Flexural Properties 89
5.3 Thermal Properties 91
5.3.1 Coefficient of Thermal Expansion 91
5.3.2 Glass Transition Temperature 93
5.4 Discussion 95

6 Conclusions and Future Work **99**
6.1 Conclusions 99
6.2 Future Work 100

References **103**

List of Figures

2.1 Simplified representation of a helical horizontal filament winding machine, based on illustrations in [1, 7, 8]. 8
2.2 Representation of the doctor blade action in the impregnation stage. . . . 13
2.3 Representation of helical filament winding, adapted from [14]. 17
2.4 Representation of the winding sequence, adapted from [7]. 18

3.1 Evolution of the coefficient of thermal expansion with the fibre volume fraction of composite systems composed by different fibres, based on the rule of mixtures. 37
3.2 Generalised time-temperature transformation (TTT) isothermal cure diagram for a thermoset resin, adapted from [30, 59, 60]. 41
3.3 Simplified representation of the curing stage of a thermoset resin, based on the illustrations in [41, 47, 62]. 42
3.4 Damage progression in composite systems, inspired by illustrations in [72, 73]. 45
3.5 Illustration of damage in a cross-ply laminate. 47

4.1 X-ray radiography setup. 64
4.2 Compression test setup. 66
4.3 Four-point bending test setup. 68
4.4 Test setup for thermomechanical analysis. 71

5.1 Micrographs of one BOL specimen highlighting defects resulting from the manufacturing stage. 78
5.2 Micrographs of one BOL sample showing the presence of cracks before thermal cycling. 79
5.3 Micrographs of one EOL specimen showing multiple intralaminar cracks. 80
5.4 Micrographs of an EOL sample revealing how voids attract the growth path of cracks. 81

5.5 Micrographs of one EOL sample showing cracks with varying dimensions. 82
5.6 Radiographs of BOL specimens. 84
5.7 Radiographs of EOL specimens. 85
5.8 Thermograms of EOL sample. 86
5.9 Stress-strain curves of multiple BOL and EOL specimens under compression. 88
5.10 Compression properties of BOL and EOL specimens. 89
5.11 Stress-strain curves of multiple BOL and EOL specimens under four-point bending. 90
5.12 Flexural properties of BOL and EOL specimens. 90
5.13 Evolution of the length-corrected strain with temperature during three runs of one EOL and one BOL sample from the same tube. 92
5.14 Average longitudinal coefficient of thermal expansion of BOL and EOL specimens between -78ºC and 91ºC. 93
5.15 Curves obtained from differential scanning calorimetery (DSC) to determine T_g. 94
5.16 Values obtained for the glass transition temperature of every BOL sample (BOL [All]), BOL samples only from tube W (BOL [W]) and EOL samples also from tube W (EOL [W]). 95

List of Tables

2.1 Comparison of different impregnation methods, adapted from [2]. 11

3.1 Properties of generic fibres and epoxy resin. 37

4.1 Properties of the adopted carbon fibres from Torayca®. 58
4.2 Properties of the hot curing epoxy matrix system from Huntsman®. 59
4.3 Conditions defined for the thermal cycling (TC) and thermal vacuum cycling (TVC) stages. 61
4.4 Number of specimens cut from tube sections exposed to TC and TVC stages, designated as EOL (end-of-life) samples. 62
4.5 Summary of the number of tubes and sections per tube analysed by x-ray radiography. 64
4.6 Specimens for compression tests. 67
4.7 Specimens for four-point bending. 69
4.8 Specimens considered for thermomechanical analysis and the correspondent number of measuring runs. 72
4.9 Number of samples for DSC procedure. 73

5.1 Summary of the compression properties of BOL and EOL specimens, with indication of the mean percentage difference taking BOL value as the baseline. 88
5.2 Summary of the flexural properties of BOL and EOL specimens, with indication of the mean percentage difference taking BOL value as the baseline. 91
5.3 Summary of the mean longitudinal CTE ($\overline{\alpha_L}$) between -78ºC and 91ºC for BOL and EOL specimens, with indication of the mean percentage difference taking BOL value as the baseline. 93
5.4 Summary of the glass transition temperature of BOL and EOL specimens. 95

Chapter 1

Introduction

The use of composite systems is now quite widespread across every industry, which is justified by their undeniable advantages. Composite materials are known to present excellent specific strength and modulus, permit substantial design flexibility, and can be tailored to fit very demanding applications. However, the intricate nature of composite systems, which allows obtaining a broad range of properties, makes it harder to comprehend the complex mechanisms that define its characteristics.

This thesis focuses on the thermal behaviour of filament wound CFRP tubes that act as struts in the frame of a deployable space antenna. The aerospace industry deals with high responsibility missions, which translates to numerous requirements that these components must meet to guarantee their successful implementation. By studying the factors that define the thermal response of composite systems, the development of these tubes can be further optimised to achieve the predefined goals, assuring their durability while exposed to the space environment.

Section 1.1 introduces the programme where this project lays and the company responsible for its development. The motivation for this work is further developed in section 1.2, and its main goal is summarised in section 1.3. Lastly, section 1.4 provides a brief outline of the entire thesis.

1.1 Copernicus Programme at Frezite High Performance

The work described along this thesis arose from industrial need and was performed along with the expertise of the collaborators at FHP - Frezite High Performance, the company responsible for the development of this project. Since its foundation, FHP focuses in providing engineering services and mechanical hardware to the space and industrial sectors, branching its capabilities in three main areas - multilayer insulation, mechanical ground support equipment and lightweight mechanical components - the

latter being the one where this project lays. This study focuses on the development of filament wound CFRP tubes, which are a flagship product of FHP. Achieving a more detailed characterisation of this component facilitates the optimisation of its properties and guarantees the success of its application.

These composite struts are a fundamental constituent of a deployable space antenna conceived for the Copernicus Imaging Microwave Radiometer (CIMR) mission. This satellite mission falls under the Copernicus Programme, which is an Earth observation initiative helmed by the European Union in an effort of solidifying Europe's independence regarding space technologies. The CIMR mission in particular is expected to monitor the ocean and sea ice along the Arctic environment, providing a tremendous amount of data that should help characterise the state of these regions - a particularly pressing concern under the consequences of climate change. The tubes produced by FHP are part of the large deployable reflector attached on the observation satellite, and thus their behaviour must fall within a series of rigorous requirements. This further stresses the importance of finding optimal production parameters and design solutions in search of operational viability.

1.2 Motivation

The CFRP tubes compose the deployable frame of a large antenna reflector, which is a high sensitivity platform that requires an exceptional perseverance of its structural integrity and dimensional stability. The space environment places obstacles on those goals, as it imposes a multitude of harsh conditions that are particularly menacing to polymer matrix composites. The work at hands tackles these issues in two ways - assessing how the production choices define the thermal behaviour of these tubes, and evaluating their durability under the conditions encountered while in orbit.

When satellites revolve around the Earth, they enter an environment of thermal fatigue with cyclic rises and drops in temperature according to their position relatively to the Sun. This exposure to thermal cycling justifies why the thermal behaviour of the filament wound struts is of paramount importance. One of the main concerns regarding temperature changes is how it jeopardises the dimensional stability of the deployable frame. The CFRP tubes are bonded to titanium end-fittings, which present a positive expansion upon heating. Oppositely, laminates reinforced with carbon fibres tend to present a negative coefficient of thermal expansion along fibre direction. A comprehensive understanding of the designed laminate allows the production of tubes whose contraction compensates the expansion of the end-fittings, guaranteeing the dimensional stability of the structure. Another important consequence of exposure to extreme temperatures is the temperature-dependent response

of the polymeric matrix. For example, if the glass transition temperature of the composite tubes is surpassed, their mechanical properties can drop to the point of endangering the integrity of the entire assembly. Furthermore, thermal cycling is known to promote the advance of damage mechanisms in composite systems, and this degradation endangers every characteristic of the laminate. The complexity of these intricate phenomena translates to a need of extensively characterising the thermal behaviour of the composite struts, and how thermal cycling can affect its characteristics.

1.3 Main Goal

The production of composite parts, and the filament winding process in particular, comprehends a large number of parameters that define the resulting behaviour of the components. By identifying the decisions that most affect the thermal behaviour of the filament wound struts, the necessary alterations can be performed to meet the requirements of the application. Moreover, it is necessary to assess the impact of the working environment on the properties of the material. As thermal cycling is one of the conditions of the space environment that affects composite materials the most, studying its consequences is fundamental to guarantee that the CFRP tubes maintain the necessary properties for their application to be successful. In summary, this study aims at evaluating how the thermal response is defined by the production parameters, and investigates how thermal cycling can alter the initial characteristics of composite parts.

1.4 Thesis Outline

The first step in characterising the composite struts under study is to acquire a deeper understanding of its production process. Chapter 2 tackles that matter by describing the main steps of the filament winding process, and reporting the particularities that should be considered when this method is adopted. Chapter 3 performs a review on the main focus of this thesis - the thermal behaviour of composite systems. This chapter starts by justifying the motivation for this study with a brief depiction of the space environment, followed by the definition of the factors that define and affect thermal behaviour, and ending with a study on the effect of thermal cycling. Chapter 4 describes the experimental procedures adopted in order to investigate the thermal behaviour and reaction to thermal fatigue of the filament wound struts. The analysis of the results and their discussion is carried out in chapter 5, with multiple conclusions drawn from the consequences of the adopted manufacturing process and the changes in the composite tubes provoked by exposure to thermal cycling. Finally, chapter 6 summarises the conclusions extracted from the entire

work, and reflects on future studies that would help achieve a deeper understanding of the characteristics of the filament wound struts.

Chapter 2

Filament Winding

The filament winding process is a composite fabrication method where resin impregnated continuous fibres are wound around a rotating mandrel at a defined angle. Typically, a carriage moves along the revolution axis of the mandrel while fibres are drawn and gradually cover its shape. By its level of automation and relative simplicity, this is often recognised as a very cost-efficient composite fabrication method amongst the numerous others now available, and it is particularly sought after to produce tubular parts or highly specialised components, such as pressure vessels [1, 2]. Axisymmetric parts, such as the struts considered in this project, represent the highest share of components produced by filament winding, but its evolving degree of automation also allows the production of more complex shapes through personalised winding patterns, as this can be described as a very flexible process [2].

As this chapter looks to provide an in-depth review of the filament winding process, section 2.1 delves into the history of this manufacturing method, from its early beginnings in the development of the aerospace industry to current applications. Section 2.2 describes this process through an extensive depiction of its most significant stages, considering modern literature and classical findings, balanced with commentary on the strengths and weaknesses of filament winding. This section should provide the necessary basis of knowledge to understand the intricacies of the process that are known to affect the behaviour of the produced struts with the manipulation of the process parameters.

The winding pattern is a particular concern of this composite manufacturing method, and thus deserves an independent section - 2.3 - where a brief introduction to the geometrical considerations and physical consequences of the generated winding trajectories is performed. The winding stage goes beyond machine kinematics, as the different types of patterns applied in this process have a notorious impact on the characteristics of the obtained component.

2.1 Brief Historical Review

As the use of composite materials, to its most basic premise, traces back in millennia, it is no surprise that the application of circumferential wrappings to increase the bursting strength of structures such as cannon barrels, a philosophy close to filament winding, dates back in centuries [3]. Naturally, the advent of filament winding comes only with the surge of advanced composite materials observed in the XX century, and early applications of this process appear in the 1950s, as a novel technique to obtain rocket engine cases [4].

The demands associated with the aerospace industry, and particularly with the design of rocket boosters, require lightweight materials capable of withstanding severe structural stresses and sustain high temperatures. Commercial applications often take advantage on lower weight too, as was the case with railway tank cars whose manufacturers also capitalised on the development of filament winding [3] - an optimal way of obtaining axisymmetric composite components. As the motivation to develop this technology was evident, numerous government agencies sponsored research projects that allowed it to grow, while focusing on the production of lightweight pressure vessels, with an inaugural crowning achievement of producing filament wound motors or cases for the Atlas and Polaris missiles [3].

The fundamental, and thus timeless, components of a winding machine are easily identified as the mandrel and the reinforcement feeding head, which can operate at a different level of complexity [3]. Evidently, the most basic techniques were the ones implemented at the early stages of this technology, with the lathe winder being the predominant choice at the very beginning [3, 4]. In this configuration, the mandrel rotates as the feeding head moves along the mandrel's length, meaning that these were very limited two axis machines. The mandrel is usually placed horizontally, but its axis of revolution could also be vertical, which is actually preferred with large mandrels in order to reduce deflection [3]. The tumble winder was another common early invention where the mandrel rotates perpendicular to the main longitudinal axis of revolution which is offset by a certain angle that defines the winding pattern [3]. The polar winder and the racetrack winder are additional examples of initial takes on the filament winding process [4], and paved the way for the more advanced systems that are seen today, ranging from two-axes to six-axes CNC filament winding machines [1].

A special remark should be made regarding the role of the textile industry in the birth of filament winding. The knitting and weaving industries were already highly developed around the 1950s, and the equipment used in those sectors - such as tensioning devices, rotating spindles and traversing mechanisms for control of the winding angle - influenced directly the filament winding machines created at the time [3].

Through time, the introduction of cross carriage movement lead to the production of more complex shapes, and computer aided manufacturing, with its incessant development, resulted in higher quality components as fibre placement and speed are now more precisely controlled [4]. As this is a simple process, at least in regard to its machine kinematics, filament winding became highly automated - even in the 1960s, winding patterns could be controlled by punch tape data processing techniques [3]. Its simplicity, along with the high degree of automation, guarantee the success of this process up to this day. In comparison with other composite fabrication methods, filament winding allows for excellent accuracy in the placement of the rovings, very high fibre volume fractions and consistent production quality [4] - natural consequences of such a machine-oriented process, where room for human error is quite reduced. The current offer of CAD/CAM software aimed at this process grants the possibility to perform detailed simulations and guarantees a high degree of control over the multiple manufacturing parameters, resulting in the creation of new production approaches and establishing a seamless working environment along with the CNC filament winding machines [4].

The interest of the aerospace industry in this process is still present, ranging from the production of Composite Overwrapped Pressure Vessels (COPV) - lighter and capable of withstanding higher internal pressures than metallic predecessors [5] - to simple tubes as the ones studied along this thesis. As composite materials remain dominant in especially demanding applications, a process as cost-efficient as filament winding will prevail as a natural choice for the production of many components. Other industries have also welcomed this manufacturing process, with transmission drive shafts, pole vaulting poles, chemical storage tanks, fishing rods, compressed natural gas cylinders and golf club shafts being often produced as filament wound parts in search of lower weight and optimised mechanical properties [5, 6].

2.2 Process Description

As previously mentioned, the filament winding machine shares its core principals with the lathe machine. While the mandrel revolves around itself, a carriage that holds the payout eye translates across its length and lays the fibres at a predefined angle. Through the decades, new machine systems have distanced themselves from the early two-axes machines, and CNC-controlled six-axes configurations are now common [1]. Taking the six-axes machine as an example, the mandrel rotation, the carriage translations on x, y and z, and rotation of two of those axes compose the six degrees of freedom of those advanced configurations [1, 7].

The typical configuration for the production of simple cylindrical components such

as the tubes considered on this thesis is the helical horizontal filament winding machine, which presents as main components the following: creel, feed eye, tensioning system, resin impregnator, motion control system, heating and curing devices, mandrel and carriage [7]. Figure 2.1 shows a simplified top view illustration of a horizontal filament winding machine.

The traversing carriage that holds the feed eye moves along the axis of revolution of the mandrel, from one end to the other, placing bands of fibre pulled from the creel on the rotating mandrel that becomes covered in angled ply patterns [7]. The fibres are impregnated right before passing the feed eye, and when the mandrel is fully covered on the desired mosaic of fibre bands, the curing stage takes place and the final component is obtained. The carriage movement and mandrel rotation are connected, either mechanically or solely by control systems, in order to precisely define the winding trajectories [7]. The input parameters defined by the operators to obtain the desired component can vary between mandrel speed, band width, winding angle, among others, depending on the utilised software [1].

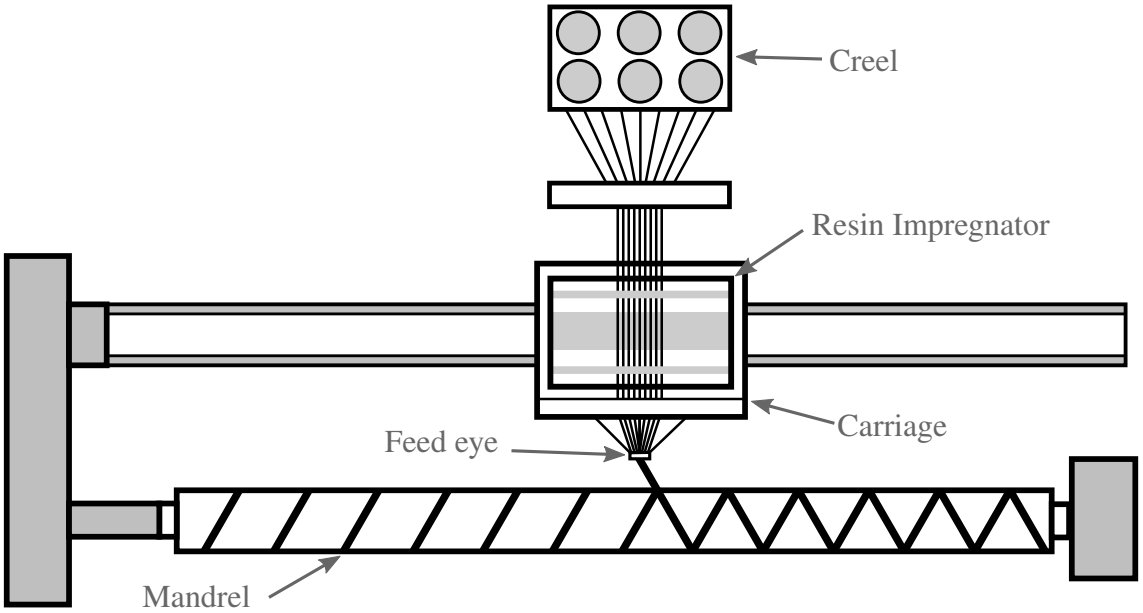


Figure 2.1: Simplified representation of a helical horizontal filament winding machine, based on illustrations in [1, 7, 8].

2.2.1 Process Parameters

In any process, some parameters are more of a direct consequence of the user-end actions, and others are a result of the inherent intricacies of the process and how it unfolds as a concatenation of every variable. Taking into account the work developed by Faria [9],

the following parameters are the ones resulting directly from the design choices and the variables introduced in the filament winding machines:

- constituents of the composite system;
- mandrel geometry;
- initial fibre tension;
- fibre band cross-section;
- fibre band pattern;
- lay-up sequence;
- winding angle;
- winding speed;
- initial degree of fibre impregnation;
- processing temperature; and
- curing time after winding.

Confirming the mentioned duality, some processing conditions of filament winding are not directly induced by the user but represent the natural reaction to the introduced controllable parameters, following the intrinsic physical phenomena associated with composite laminates. These dependent properties may vary through time and space during the entirety of the filament winding process, and particularly with thermoset matrices the main ones are:

- fibre motion;
- matrix flow;
- matrix viscosity and degree of cure;
- temperature;
- thermal expansion;
- chemical changes (shrinkage);
- fibre bed compaction; and
- fibre, resin and void content.

The parameters listed up to this point serve as a backbone for the description of the filament winding process, and expanding on all of them would be superfluous to the main goal of this project. With this in mind, in the following sections an overview of the areas where these parameters are included is made with the intention of creating a comprehensive but pragmatic description of the filament winding process.

Identifying the variables that govern filament winding is a crucial step in the assessment of how this process defines the characteristics of the resulting composite parts. Nonetheless, as section 3.3 delves into the conditions that affect thermal properties transversely to every

production method, this chapter mainly aims at emphasising the distinctive factors that surround filament winding.

2.2.2 Raw Materials

As established before, filament winding utilises continuous fibre and thermoset resins - even though thermoplastics are already applied in some variants of the process, thermoset polymers are clearly predominant.

When this process emerged in the 1940s, glass fibres were already widely popular, mainly in the USA, and an obvious choice for mechanically demanding applications, with its high specific strength compensating for the tendency to break during handling and notorious hygroscopy [3]. Following the advances in composite materials and the advent of more highly capable filaments, carbon, aramid and even natural fibres are now also commonly applied, as epoxy, unsaturated polyester and vinylester are popular choices as a matrix [1, 6].

Carbon and aramid fibres present mechanical and thermal properties more suitable for demanding applications than glass fibres, but their cost might be prohibitive. Epoxy resins present the best operative properties while also being the most expensive. The glass transition temperature of the chosen thermoset matrix also needs to be taken into account as it affects the necessary curing temperatures of the final part and its resistance to elevated temperatures - a topic developed in sections 3.2.1 and 3.3.3 [10].

The excellent interface shear strength obtained between carbon fibres and epoxy resins turn this pairing into a very popular choice for filament wound components in the aerospace industry. Lower cost solutions may reside in the use of glass fibres with a polyester resin [1]. If highly uniform through thickness fibre distribution and resin presence is required, preimpregnated tows are a proven solution [1].

2.2.3 Mandrel Preparation

The final component should be easily separated from the mandrel with specialised extraction tools or even by hand, and in order to facilitate that process the mandrel is coated with a release agent before the actual winding process [1, 7]. If a higher quality surface finish is required on the inside of the tubular structure, a gel coat is also applied over the release agent [1].

The mandrel is a simple component that plays a vital role in the filament winding process. For a mandrel to be suitable, it must withstand the winding tension, avoid any deflection caused by the weight of the laminate or its own, maintain its properties under the curing stage, respect the geometric tolerances, present such durability that it can be

reused, and be removable from the final part [3, 7].

The mandrel is typically extracted and reused, but there are some applications where the last two demands for the mandrel may not be respected. For example, when filament wound pressure vessels are produced, leaving the mandrel inside as an integral constituent can mitigate gas or liquid leakages as it creates a barrier between the composite system and the contained fluid [1], acting as a liner.

The wooden mandrels utilised in the 1940s gave way to the current metallic mandrels [7]. Steel mandrels are the most popular choice and can be chrome-plated for higher quality inner surface finish and easier extraction. Aluminium mandrels also exist but are not as sought after. Some designs create the need for collapsible or even destructible mandrels made of sand or plaster of Paris. The low cost of the mandrels is one of the great advantages of the filament winding process, as it represents its main tooling component [1].

2.2.4 Impregnation Methods

Impregnation represents the phase where fibres are engulfed by the material that will then act as a matrix, usually a resin system. For filament winding, there are three identifiable impregnation methods on the market - wet winding, prepreg winding and dry winding [2, 10]. Note that prepreg winding can also be described as dry winding in current literature, however, in this review, a difference will be established between these two. Table 2.1 shows a generalised comparison between this three variants based on the considerations of Sofi et al. [2], whose work focuses on the use of dry fibre winding.

Table 2.1: Comparison of different impregnation methods, adapted from [2].

Winding Process	**Advantages**	**Disadvantages**
Wet Winding	Low raw material cost	Poor control over resin content
	Simple material storage	Relatively high variability
		Resin dripping and accumulation
		Poor surface finish
		Poor quality/speed relation
Prepreg Winding	High control over resin content	High material cost
	High mechanical properties	Difficult material storage and handling
		High manufacturing cost
Dry Winding	High control over resin content	Two steps - preforming and impregnation
	Low raw material cost	Difficult preform handling
	Simple material storage	
	High mechanical properties	

Prepreg winding utilises preimpregnated fibres without any need of additional impregnation during the winding operation. This impregnation method results in higher mechanical performance than the components obtained by wet winding, but the material costs are higher, meaning that it is only appropriate for high performance parts [10].

Dry winding, also known as post-impregnation in current literature, represents the winding of fibres on the mandrel without any resin, producing a preform that is then impregnated [2]. The high costs of processes that utilise prepregs, such as prepreg winding, are justifying a shift in research interest for methods where dry preforms are impregnated through liquid composite moulding (LCM). With dry winding, high fibre contents, repeatable product quality and precisely controlled resin content have been attainable at relatively low costs - but this process is far from the technology readiness stage of prepreg and wet winding, representing now a technology that is bound to gain a significant position on the market through further investigation [2].

Wet winding is not only the most applied impregnation method in filament winding processes, but also the one utilised for the production of the CFRP tubes studied along this thesis, meaning that it deserves the most attention on the context of this project. The dry fibre yarns encountered in spools at the creels are pulled through guiding pins or combs and into a resin bath, that may be at the carriage platform, right before converging at the feed eye, forming the fibre band that is applied on the mandrel [1, 7, 10]. As this process directly utilises raw materials, the significant process variables inherent to the process are more than the ones encountered with prepreg winding - resin viscosity and fibre tension are crucial aspects of this impregnation method [10].

The control of resin viscosity has a great impact on the finished product. If the viscosity is too low or too high, it is difficult to achieve an even distribution of the matrix system along the axisymmetric shape of the component, either by aggravated inertia of the matrix flow or excess of mobility leading it do drip off of the part and resulting in a deficit of resin content [10].

The fibre volume fraction is heavily influenced by the impregnation of the fibres, and achieving a component with a constant fibre content along its volume is particularly difficult. As fibres have a tendency to adhere to an excessive amount of resin while being bathed on it, the container where fibres are impregnated usually has rolls that help achieve uniform impregnation of the fibres and extract excess of resin [1, 8, 10]. In some cases a single roll of larger dimensions is half-emerged in the bath, while in others multiple rolls are placed completely inside of the bath - many variations are possible, with some rolls being heated. Passing carbon fibre through multiple rolls might severely damage it, and utilising a single large roll is thus the most common solution for CFRP components. Air bubbles formed inside of the fibre bands due to incorrect impregnation leads to the

creation of voids on the final component, and that is why wetting is a crucial detail of this process [8].

Figure 2.2 shows a simplified representation of the setup utilised in the production of the filament wound tubes studied in this thesis - a single roll setup with a doctor blade. The distance from the doctor blade to the roll controls the amount of resin that the fibre is bathed in, which has shown to have a direct influence in the resulting fibre volume fraction of the final component.

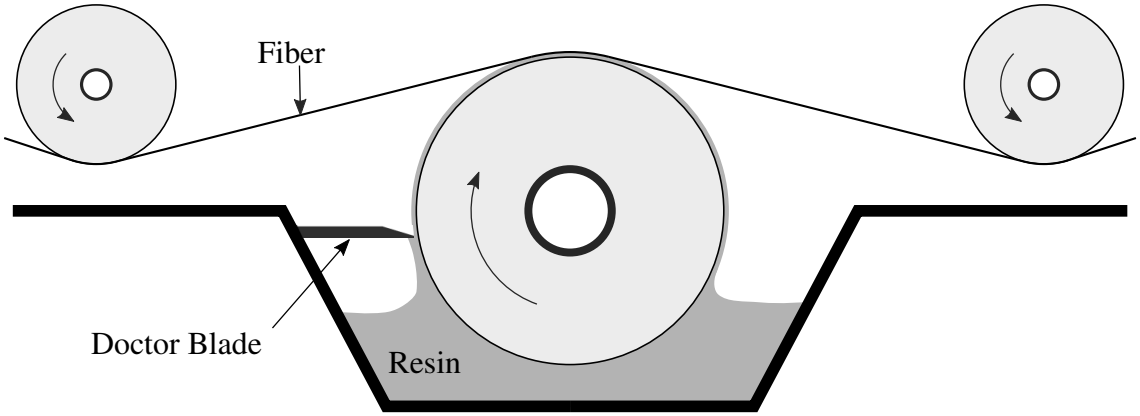


Figure 2.2: Representation of the doctor blade action in the impregnation stage.

Bad impregnation can also be a result of intrinsically low wettability of the raw materials, which is affected by the permeability of the fibre bands and resin viscosity. A high void content can be avoided by slightly heating the resin, lower winding speeds or increasing the distance in which fibre bands are passing through the resin bath [8].

The outer surface finish is usually of low quality in filament wound parts, which can be mitigated by the use of shrink tape or teflon-coated air breathers that remove some of the excessive resin amounts. Additional finishing operations can be conducted to guarantee optimal geometric tolerances and lower surface rugosity [1], as is the case with the studied tubes.

2.2.5 Fibre Tension

Controlling fibre tension is also crucial to achieve correct impregnation during the wet winding process. A tensioning device must allow the control of fibre tension throughout the process, as the bands cover the mandrel in the desired pattern and the thickness of the laminate grows larger [1]. Fibre tension is usually controlled between the creel, where the continuous fibres in the form of tows or rovings are pulled from, and the impregnation bath [7, 10]. Companies such as Pultrex [11] offer servo controlled, electronic closed looped or self compensating tensioners. The creel itself, the following pulleys, band brakes and guides can act as a controllable tensioning device.

To avoid fibre damage, the fibres should have as little contact as possible with the guiding systems, as well as avoid abrupt changes in direction because friction and bending can damage the fibres and affect the properties of the final component. Twisting is another concern while designing the guidance system due to the creation of voids and unevenness of the plies [7]. Changes in direction at the impregnation stage and at the feed eye are usually the strongest, and the highest local changes in fibre tension and band width will be directly connected to these points where the fibre path is deflected the most [8].

The tension at which the rovings are kept has a significant effect on the mechanical properties of the final component, representing a very important design variable of the process [10]. Akkus and Genc [12] studied the influence of pretension on the mechanical properties of carbon fibre by creating a tensioning device similar to the ones used in filament winding. It was shown that parameters such as roller diameter, contact angle between the fibre and rollers, and tensioning force are connected to a reduction in tensile strength up to 43%. Due to increased friction, higher contact angles resulted in damage of the carbon fibres, with the same happening with higher tensioning forces. The use of smaller diameter pulleys on the tensioning device also resulted in greater damage due to the bending of the fibres. This implies that low contact angles and larger diameter pulleys represent a good solution to avoid fibre damage.

Mertiny and Ellyin [13] investigated the influence of fibre tension on composite components produced by filament winding and stated that laminate compaction is heavily influenced by fibre tension, meaning that the fibre volume fraction can be manipulated through this parameter. Failure of specimens was also impacted by distinct fibre tension - higher winding tensions increased strength in fibre dominated loading scenarios, but the opposite occurred with matrix dominated properties, where higher compaction was slightly detrimental to the component's behaviour. Erdiller [10] also studied the effect of fibre tension on the mechanical properties of filament wound tubes and found that higher tension resulted in increased longitudinal and hoop tensile strength. In general terms, if fibre tension is too low, laminate compaction might be scarce and result in an excessive resin content. On the other hand, if tension is too high, the fibres might be damaged and some plies might suffer from a resin deficit [1].

2.2.6 Curing Stage

The winding stage that distinguishes filament winding does not represent the whole process chain, since the curing stage is another critical phase, as with any other composite part fabrication method - polymerisation hardens the resin and guarantees that the expected mechanical and physical properties are achieved. Filament winding machines may be equipped with radiation devices - infrared, ultraviolet, electron beam - that heat the wound

fibre bands, but utilising independent hot air ovens or heated turning rigs are more common solutions [1, 7]. Depending on the designed component and the chosen constituents, the part can also be cured at room temperature or go through intermediate curing stages between winding phases due to high thickness [1].

The use of autoclaves for a controlled pressure environment is usually not required, since fibre tension creates such compression of the laminate on the convex mandrel that no additional compaction is needed, even for a high performance component. For the production of large parts, appropriate autoclaves could be hard to find and its usage increases the production costs - being able to dismiss that equipment represents a significant advantage of this particular process [1, 7]. However, this lack of external pressure does create parts with weaker through-thickness properties and increased void content when compared with autoclaved parts. This means that in applications where matrix-dominated properties are important, autoclaves may be used to cure filament wound parts, keeping in mind the possibility of fibre crimping along the process [7].

It is of paramount importance that the wound components are slowly rotated during the curing cycle up to the point where resin no longer flows [7]. If this condition is not respected, resin will accumulate on the lower side of the wound part, possibly dripping off of the component, and result in a severely unbalanced and defective piece.

Section 3.3.3 expands on the importance of the curing stage in the production of polymer matrix composites, particularly regarding the definition of the glass transition temperature of the material.

2.2.7 Advantages and Limitations

Filament winding presents itself as an optimal manufacturing method for several components, and thus prevails with a strong commercial presence. The ability to precisely define the winding angle and completely transform the mechanical properties of a component according to its projected needs is of paramount importance. The directional strength ratio of filament wound components can be easily modified, which results in very efficient designs where each loading condition is accounted for - such design liberty is not possible with isotropic materials [3].

The mechanical properties obtained with this process, such as high specific strength and modulus, make it suitable for demanding applications, while presenting a satisfactory degree of repeatability [10]. The attainable values for fibre volume fraction, well above 60%, are also an important advantage of this method.

This process presents relatively low costs on raw material and particularly on tooling while producing high performance parts, allowing it to be a predominant choice for the production of specialised components such as fuel tanks and pressure vessels [1], and

a cost-effective method to obtain tubular components in general. Its high degree of automation turn this into a suitable method for high-volume components and assure a constant production quality [1].

Considering specifically the production of pipes, which translates directly to the struts considered along this thesis, filament winding and its highly modifiable winding trajectory can lead to improved bending strength, increased buckling strength through the addition of hoop layers, or optimised axial strength with lower angle helical patterns [7].

Filament winding is not limited to cylindrical or even axisymmetric shapes, but the kinematics involved in the winding process limit its application, as it can generally only be applied to closed and convex geometries [1]. Open geometries would not be correctly covered by the fibre bands because these would form bridge-like trajectories over the mandrel.

Despite being praised for its high range of design possibilities, there are limitations to the applied winding angle due to fibre slipping concerns. Although not mandatory, geodesic paths and those close to it are preferred because it guarantees higher stability during fibre placement - this is discussed in higher detail in section 2.3.1 [1]. Obtaining an uniform through-thickness fibre positioning and resin volume can also be a hard task [1].

The simplicity of this process has been pointed out before, but this statement might be deceiving, to a certain extent. As the kinematics involved on the fibre placement stage appear to be simple, the inherently complex physical processes surrounding composite materials dismantle that hypothesis and the whole process cannot be taken as lightly as a lathe cutting operation would, for example. As mentioned, the winding stage itself does not guarantee the quality of the desired part, as numerous phases influence its properties [7]. Producing a filament wound part lighter and cheaper than a metallic counterpart is so easily obtainable that many mistakes can be made in the process while remaining competitive on the market [7], but those processing errors should evidently be avoided, namely those concerning fibre pattern, fibre impregnation, curing temperatures, as well as many others. These ill practices usually result in walls thicker than necessary, wasting raw material [7].

2.3 Winding Pattern

The winding pattern is a particular concern of the filament winding process and the defined trajectories display a significant role in the mechanical and thermal properties of the obtained components. Three types of filament winding patterns can be easily identified - helical, polar and hoop winding.

Helical winding is not only the most applied and versatile winding strategy, but also the one utilised in the production of the tubes studied in this thesis. The rotating mandrel and

the traversing carriage that holds the wind eye are connected through a defined motion ratio that dictates the angle at which the fibres are laid on the mandrel [1, 7]. When the carriage moves to one end of the mandrel, it creates a ply oriented in a certain angle ($+\theta$ ply), and as it comes back, it generates a ply with opposite fibre orientation ($-\theta$ ply), resulting in a balanced laminate [7] - figure 2.3 shows a simplified schematic representation of the helical winding process. Helical winding, with off-axis plies, typically presents a winding angle between 5º and 80º [2].

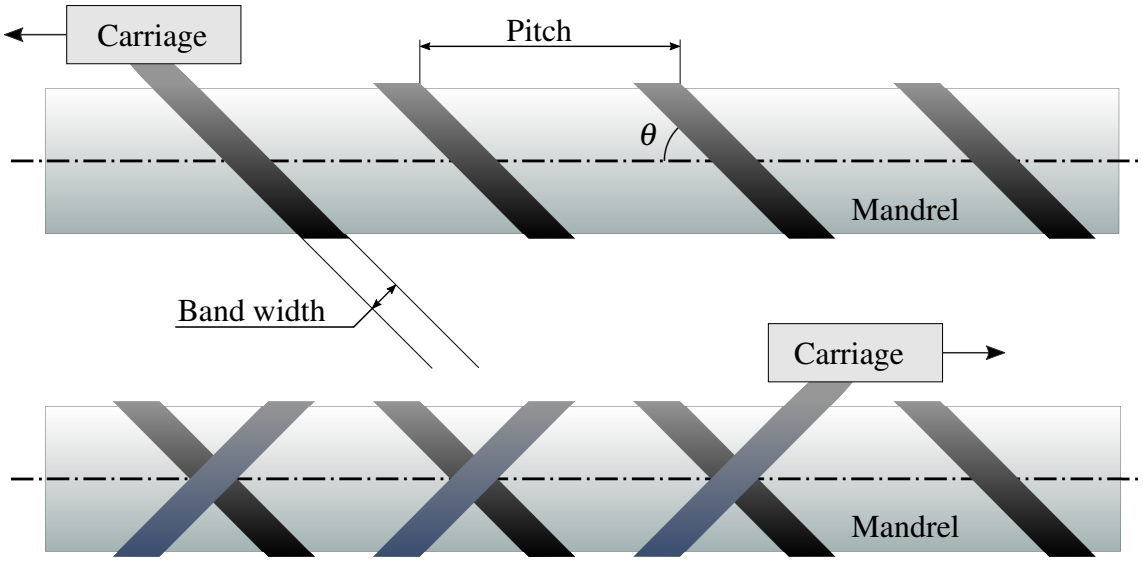


Figure 2.3: Representation of helical filament winding, adapted from [14].

Polar winding is almost parallel to the axis of revolution of the mandrel, as the carriage moves around it forming winding angles from 0º to 5º. Hoop winding describes a close to circumferential wrap of the mandrel - winding angle very close to 90º - which is a popular approach for applications that require high bursting strength [2, 6, 7]. Some applications may require a combination of these three winding trajectories to obtain the desired mechanical properties, as each of these have a different effect on the final component. This freedom in fibre orientation allows a tailored directional strength according to the predicted loading scenarios.

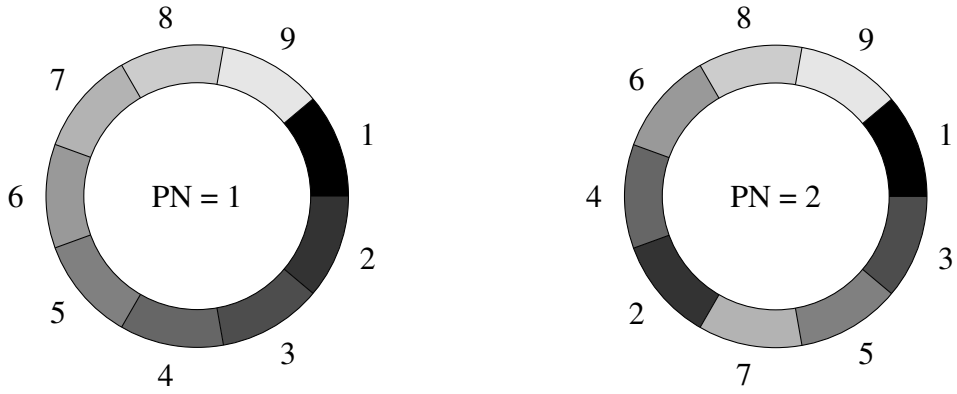
The winding angle, θ, is defined as the angle formed between the mandrel's axis of revolution and the direction of the fibre as it is laid on the mandrel [7]. This means that polar winding is identified by $\theta = 0º$, and hoop winding is associated with $\theta = 90º$. The influence of mandrel geometry on the winding angle is shown in equation 2.1, where $\varnothing$ is the mandrel's diameter and P is the pitch.

$$\tan(\theta) = \frac{\pi \cdot \varnothing}{P} \tag{2.1}$$

The impregnated fibres that go through the wind eye, before covering the mandrel, form a band whose geometry is dependent on the number of fibre tows, the thickness and the cross-sectional area [7]. Naturally, the shape of the fibre band changes as it is laid on the mandrel due to the applied tension and its interaction with other bands. The way in which these bands are laid on the mandrel - with a given orientation, pitch and repetitive sequence - results in the winding pattern, or band pattern, of the filament wound component [7].

Consider that a carriage circuit represents the movement of the carriage from its starting point to one end of the mandrel and back. The distance between the bands that are laid down in each carriage circuit has a great impact in how interwoven the laminate is [7].

The *Pattern Number* (PN) indicates the number of circuits completed before a band is placed adjacent to the first one [5, 7] - figure 2.4 shows the order in which each band is wound for a PN of 1 and 2. With a PN of 1, every band is placed next to the previous one, but with a PN equal to 2, odd numbered circuits and even numbered circuits are adjacent, resulting in two separate waves of material that gradually cover the mandrel. Increasing the pattern number leads to greater distances between consecutive bands during the winding process, which results in more interwoven patterns that typically present a higher void fraction, lower fibre volume fraction, and generalised loss in mechanical properties due to cross-over crimp - on the other hand, these highly intertwined patterns are preferred in high energy absorption applications [7].



(a) Pattern Number 1 (b) Pattern Number 2

Figure 2.4: Representation of the winding sequence, adapted from [7].

The turnaround zones, at the extremities of the mandrel, see a change in the fibre band's trajectory as the carriage prepares to advance in the opposite direction, meaning that the winding angle will go from θ to $180^{\circ} - \theta$. During this dwell stage, as the carriage reaches one end of the mandrel, the winding angle gradually increases to 90° - the dwell position from where the carriage starts going in the reverse direction and the winding angle will

return to the desired value [5, 7].

In order to actually reach the dwell position, the mandrel rotation must be long enough while the winding angle steepens - this leads to a higher effective thickness of the band, due to its geometrical projection on the mandrel's cross section, resulting in material thickening, besides having a significant portion of the component where the fibres were not laid in the desired orientation. Simply reducing dwell to a point where this transitioning position is not reached creates unpredictable winding lengths requiring experimentation to achieve a non-defective component. Authors such as Peters [7] and others present optimal winding strategies where fibre orientation is changed at a minimum portion of the mandrel, material thickening is minimised and winding length is precisely determined. In some components, such as the CFRP tubes studied in this thesis, the areas affected by the turnaround may be cut so that there are no consequences from this limitation.

2.3.1 Geodesic Paths and Nonslip Strategies

While defining the winding pattern, machine kinematics and the desired properties are not the only areas of concern. Successful fibre placement is crucial in a correct operation, and geometrical principles heavily affect the physical phenomena involved.

Geodesic paths are a popular approach on filament winding trajectories as they assure the most stable fibre placement, reducing slipping to virtually zero [5, 7]. Geodesic curves describe the shortest path between two points of a given surface - in this case, a geodesic path is the shortest distance that the fibre band can cover from one point of the mandrel to another [5, 7].

In simple terms, applying these trajectories results in the absence of lateral forces applied on the fibre band and the remaining forces normal to the mandrel do not create fibre slippage [5]. For a fibre to move laterally while following a geodesic path, it would need to stretch - but as fibres are considered inextensible, this is theoretically impossible [7], meaning that these are the most stable and slip-proof trajectories that can be implemented.

Examples of geodesic curves are the equatorial circles of a sphere and a helix around a cylinder. A simple tube, such as the ones studied along this thesis, can not be wound solely through a geodesic path due to the turn around sections that appear at each end of the mandrel [5, 7]. A geodesic curve on a tube is created by maintaining a constant pitch and winding angle during the process, so there is a need to step away from this ideal path at the extremities [7]. Fortunately, geometric analysis is not the only one that comes into play regarding fibre slippage, and the concept of friction allows a deviation from the geodesic path [7].

Friction between the fibre bands and the surface of the mandrel, or between independently laid bands, creates a strong opposition to fibre slippage, meaning that there is

some positional margin from the geodesic path where fibre placement will still be correct, without any unwanted lateral movement [7]. Many physical aspects can contribute to this friction, such as pure mechanical friction, physical adhesion between the resins and the mandrel, and mechanical interlock due to high fibre tension [7]. It is usually of great importance that friction is taken into account while developing numerical models that predict fibre slippage and associated occurrences.

2.3.2 Axisymmetric Shapes

The rotational symmetry of axisymmetric components facilitates the winding process because only one carriage circuit needs to be defined and repeated in order to fully cover the mandrel - lack of rotational symmetry requires distinct carriage circuits and complicates pattern generation [7]. This justifies the higher popularity of axisymmetric parts, such as cylinders, cones and spheres - which includes the tubes studied along this thesis.

It is possible to calculate the number of circuit repetitions necessary to fully cover a cylindrical mandrel through a basic expression. With B being the real band width, θ representing the winding angle and $\varnothing$ the mandrel's diameter, equation 2.2 returns the value of N_c, the number of circuits that will guarantee a complete coverage of the mandrel [5, 7]. Note that $B/\cos(\theta)$ represents the fibre band width projected on the cross-section of the mandrel. For axisymmetric surfaces with varying diameter, N has to be calculated for every position along the winding path and the highest value is used [5, 7].

$$N_c = \pi \cdot \varnothing \cdot \frac{\cos(\theta)}{B} \tag{2.2}$$

It is very likely that this expression does not produce the necessary integer to define the discrete number of needed repetitions, and two diverging scenarios emerge. If the result is rounded up, overlaps will occur and create uneven surfaces, and if N is rounded down, there will be gaps between the fibre bands filled with resin [7]. The degree at which these problems appear may be controlled by manipulating the fibre band width or even the winding angle to obtain an integer number, or one much closer to it, albeit allowing overlaps is quite common.

Another interesting mathematical property of the helical winding of axisymmetric components is the *Clairault Relation*, presented in equation 2.3. This expression can be applied to any point of a geodesic path traced on an axisymmetric surface, and assumes a virtually null friction factor [7, 9]. Note that r is the radial coordinate of the fibre band and θ is the winding angle.

$$r \cdot \sin(\theta) = Constant \tag{2.3}$$

The main consequence of this relation is that, while following a geodesic path on an axisymmetric surface, if the radius of the mandrel decreases, the winding angle will increase. This is a critical relation for many filament winding processes, but it will not affect winding of constant radii parts, such as tubes.

Chapter 3

Thermal Behaviour of Composite Materials

The first filament wound struts launched into orbit were part of the KU-3 and KU-4 satellites developed by G.E. Astro Space, in 1988. These CFRP tubes, very similar to the ones under the scope of this thesis, showed that filament winding is a valid option for aerospace structures, with a lower cost than previous methods while maintaining appropriate physical and mechanical properties. Again, as the struts manufactured by FHP, these groundbreaking tubes were cured in an oven not subject to additional external pressure, tested at cryogenic conditions and connected by an adhesive joint to titanium end fittings [7].

As satellites orbit the Earth, their temperature can rise while exposed to direct sunlight and cool when in the planet's shadow - this means that the spacecraft is exposed to thermal cycling, which is a phenomenon that can heavily affect the integrity of composite materials [15]. Each material has a different reaction to changes in temperature, made evident by their coefficient of thermal expansion. Due to that, concerns arise regarding the dimensional stability of the assembly comprised by the CFRP struts and the titanium end fittings. Additionally, these temperature variations subject the filament wound component to internal stresses due to the rivalling expansion and contraction of the matrix and the reinforcing fibres, which leads to the progression of damage mechanisms that affect the mechanical and physical properties of the laminate. The end-of-life properties of the filament wound struts are considered to be dominated by the effect of thermal cycling, demanding a deep understanding of its implications on the physical and mechanical properties of the filament wound struts in order for them to be confidently deployed into orbit as part of a structure that requires high dimensional stability throughout its service life.

To understand why the thermal behaviour of composite materials for aerospace applications is so important, section 3.1 provides a brief description of the harsh conditions encountered while in orbit. After establishing the motivation for this work, section 3.2

delves into the parameters that define the thermal behaviour of a composite material and explains why temperature variations easily induce stresses in composite systems. Section 3.3 highlights how the design choices and the adopted production parameters, from the constituent selection to the curing stage, affect the thermal properties and corresponding response to temperature changes. Finally, the effect of thermal cycling on composite materials is assessed in section 3.4, which will serve as a cornerstone for the analysis of the experimental results performed in chapter 5. The description of fatigue damage mechanisms in composites is followed by a review of experimental studies on the effect of thermal cycling on the mechanical properties, coefficient of thermal expansion and glass transition temperature of composite specimens.

3.1 Space Environment

The environmental conditions of space influence not only the behaviour of the spacecrafts, but also the health of the astronauts in manned missions, and are therefore object of detailed characterisation. Space environment can be defined as "the large void which occupies the relatively empty areas of the universe outside the atmosphere or surface of any planet or other celestial body" [16], which in this case is the area just beyond Earth's atmosphere. The studied filament wound struts need to withstand the harsh conditions encountered in low orbit, and that can only be guaranteed if there is an extensive comprehension of this environment. The conditions that the filament wound struts are expected to encounter can be summarised as an ultra-vacuum with low particle density exposed to high energy radiation, micrometeoroids, extreme temperatures and atomic oxygen [16, 17]. The use of composite materials in aerospace applications is highly common and extremely successful, particularly with CFRP components. Vacuum, thermal cycling, the presence of atomic oxygen, particulate radiation and UV radiation can be highlighted as the conditions that affect polymer matrix composites the most.

3.1.1 Ultraviolet and Particulate Radiation

The radiation environment experienced while in orbit is composed of the solar electromagnetic radiation, that contains ultraviolet radiation, and also particulate radiation [16–18]. Materials in low Earth orbit are no longer protected by the atmosphere, and become exposed to ultraviolet radiation, which can damage polymers by leading to excessive degrees of cross-linking or weaken their properties through chain scission. Particulate or ionizing radiation results from the galactic cosmic rays, trapped radiation belts or solar cosmic radiation. When polymers are bombarded by these charged particles, the consequences

can be similar to the ones associated with UV exposure, but their effect is usually not as severe.

The consequences of the radiation environment are not contemplated in this work, but these are definitely points of interest in the qualification of composite components for space flight.

3.1.2 Atomic Oxygen

Generally, when oxygen molecules are split, oxygen atoms are quick to become part of another molecular arrangement. At low Earth orbit, however, the extremely low density of particles allows that these atoms are left alone, in what is usually referred to as atomic oxygen (*AO*). The presence of *AO* in the upper atmosphere is mainly caused by short-wavelength ultraviolet radiation that separates molecular oxygen. The problem of oxidation is well known, even in the presence of O_2 molecules, and it is vastly aggravated in the presence of *AO* [17, 18]. Besides reacting with various metals, atomic oxygen strongly reacts with materials that contain sulfur, nitrogen, carbon, and hydrogen bonds, meaning that it has the capacity to erode polymeric matrices [17].

The development stage that this thesis accompanies does not yet contemplate the influence of exposure of the filament wound struts to atomic oxygen, but this an important parameter to assess in a more advanced phase of maturity of these components.

3.1.3 Vacuum

A pure vacuum is obtained when a volume is not occupied by any material, which in reality is close to unattainable - however, atmospheric density does decrease very significantly with altitude [18]. While atmospheric pressure at sea level is around 10^5Pa, pressure in interplanetary space can reach 10^{-14}Pa. Satellites orbiting the Earth, still under some effect of Earth's atmosphere, already experience hard vacuum conditions with pressure ranging between 10^{-4} and 10^{-7}Pa from 300km to 1000km of altitude [16].

The vacuum of space originates three potential complications for spacecrafts, namely cold welding, limited heat transfer and outgassing [18], with the latter being the most important in the scope of this thesis. Cold welding may occur between metallic parts that are separated by a small space, and consists in the fusion of these parts after the effect of vacuum eliminates this distance between them that allowed relative motion [18] - which is a design problem that is not relevant to the work at hands. Heat transfer into and out of a structure is limited to radiation, as conduction and convection need matter to carry its energy [18] - again, a theme that is not addressed in this study. On the other hand, outgassing is a matter of great concern with composite materials utilised in aerospace

applications.

Outgassing is the release of volatiles from materials exposed to a hard vacuum, and it is a particularly common problem with composite materials, including CFRP. During the impregnation stage at atmospheric pressure, gas bubbles can become trapped in the resin mix. While rising in altitude, the pressure drops and a vacuum condition is originated, which forces these gasses out of the material [17, 18]. Although outgassing does not significantly affect the properties of the material itself, it can have a destructive effect on its surroundings. The released volatiles may deposit on sensitive surfaces, such as lenses, or even cause electronic components to arc [18]. To avoid any influence in the optical properties of the spacecraft's components and its overall performance, the materials known to outgas must be subjected to a thermal vacuum bake, where the vacuum of space is simulated, to guarantee that they will not be a liability after launch [17].

3.1.4 Thermal Cycling

As the antenna or any other satellites revolve around the Earth, they move in and out of direct sunlight, which exposes them to thermal cycling between quite extreme temperatures. The extent of its severity is affected by several factors, among which the following can be highlighted [17]:

- thermal emittance, solar absorptance and thermal mass of the material;
- exposure to the sun and the Earth;
- view of surrounding surfaces;
- time in sunlight and shadow; and
- thermal radiation from the structure it composes;

Objects in low Earth orbit tend to swing between reference temperatures of -120ºC to 120ºC, however, a material with high solar absorptance and low thermal emittance is expected to reach more distanced extremes [16, 17]. While dealing with extreme temperature ranges, the CTE mismatch between the constituents of composite systems and even amongst the different materials that compose the structure is amplified, which leads us to a two-level analysis.

With the struts studied in this thesis, a negative linear longitudinal expansion is expected to compensate the positive expansion of the titanium end fittings bonded to their extremities, guaranteeing the dimensional stability of the structure throughout a wide range of temperatures. At a smaller scale, as composite systems are composed of at least two different materials - a matrix and reinforcing fibre -, the exposure to temperature extremes and thermal cycling poses a grave concern due to the distinct responses of each constituent. The resin matrix and the fibres have different coefficients of thermal expansion, which means that while the composite system sees a variation in temperature, its constituents

are expanding or contracting at a different rate, which induces thermal stresses - a topic developed in section 3.2.3. The cumulative effect of thermal cycling may lead to multiple defects that ultimately cause failure of the component [19].

As this is a theme of paramount importance under the scope of this thesis, section 3.4 delves deeper into the effects of thermal cycling on composite materials and, consequently, the filament wound tubes at hands.

3.2 Defining Thermal Behaviour

Before delving into the particular effect of key parameters on the thermal behaviour of composite components, a clarification is in order about what thermal behaviour represents under the scope of this thesis. As mentioned multiple times up to this point, a crucial factor in the successful implementation of the considered filament wound tubes in a satellite antenna is their response to the extreme temperature variations expected while in orbit. The development phase of these tubes, at the time of this study, is still restrained to a limited number of factors, as the considered indicators are only the glass transition temperature and the coefficient of thermal expansion. Although it is admissible that this is an overly simplistic way of characterising the response of composite systems to temperature changes, these two indicators already permit a rich analysis of the overall performance of the material. Both CTE and T_g are fundamental in guaranteeing that the component will show the necessary dimensional stability under the expected harsh conditions, and maintain its structural integrity for the necessary temperature range. These parameters also play a major role on the effect of thermal cycling - not only contributing to the overall outcome but also undergoing variations from those same events. Additionally, one of the most important consequences of the response to temperature changes are the stresses originated from the disparate characteristic of each constituent or ply that composes a composite laminate. With that in mind, a brief description of how these stresses are originated is also presented, taking into account the multiple scenarios that components such as the studied filament wound tubes are exposed to. The need for clear indicators of the thermal response of composite materials throughout the remainder of this study justifies the lengthened definition of them that follows.

3.2.1 Glass Transition Temperature

For the concept of glass transition temperature, T_g, to be correctly understood, the molecular arrangement of polymers needs to be addressed. Most polymers are either amorphous or semi-crystalline - amorphous materials are characterised by randomly arranged chains, while semi-crystalline polymers present both ordered and random molecular chains.

Simply put, for amorphous polymers, or for the amorphous regions of semi-crystalline polymers, the temperature above which the material goes from a glassy state to a rubbery state is called glass transition temperature [20–22].

The theme of glass transition is still subject of diverging views regarding its underlying physical phenomena, particularly if it is explained by thermodynamics or solely by kinetic constraints [23–27]. Nonetheless, the mechanisms relevant to this study are quite unanimous. The reversible transition from hard and brittle to soft and ductile is explained by the molecular mobility of the material - Wang et al. [28] even state that the "glass transition temperature is the macro-manifestation of polymer chain's mobility". During heating, there is an identifiable range of temperatures where free volume - a space not occupied by molecular chains in a liquid or solid polymer - increases significantly, with molecules distancing themselves. The T_g is usually the midpoint of this interval, and serves as a reference point for the transition in the polymers' behaviour. As the amorphous domain is heated above T_g, the material becomes more prone to flow if forces are applied and its mechanical properties drop, CTE is expected to rise, the polymer becomes more exposed to oxidation reactions, and there are abrupt changes to its heat capacity [21, 27]. Semi-crystalline materials additionally present a melting temperature correspondent to the phase change of its crystalline regions, which is always above T_g, and are able to preserve their mechanical properties and dimensional stability up to that point, at a percentage dependent on their degree of crystallinity [21, 27].

The temperature range where the glass transition occurs is dependent on many factors, but the underlying cause of a shift in its magnitude always comes from the contribution of these parameters to the mobility of the polymeric chain. Young and Lovell [27] consider chain flexibility the most determining factor of a polymer's T_g. The chemical groups that compose the polymeric chains have an intrinsic ability to move, or lack thereof, that affects the overall chain mobility. The presence of more flexible groups leads to lower thresholds for the glass transition to occur than the presence of, for example, large and bulky side groups that prohibit rotations and result in stiffer chains [19, 27, 29, 30]. The polar nature of the molecular groups is also relevant, as polar groups can reduce the free volume by promoting intermolecular attraction, which increases T_g [27, 30]. In similar fashion, a higher molecular mass and longer chains are known to increase the glass transition temperature [30].

Another fundamental factor affecting T_g, particularly under the scope of this thesis, is the degree of cross-linking - which defines the degree of cure. As chemical cross-links are formed, the short covalent bonds reduce the specific volume of the polymer, meaning that the free volume will also be diminished [19, 27, 30]. As it is now clear, reducing mobility results in a higher glass transition temperature, which is the effect of a higher

degree of cure. The influence of the curing stage on thermal behaviour is further elucidated in section 3.3.3.

Many other factors - such as copolymerisation phenomena, water absorption and the addition of plasticisers - contribute to the glass transition under the same principle as the ones described above, that is, if it reduces molecular mobility, it increases T_g. This is because with lower chain mobility the activation energy required for the glass transition to occur is higher, and the necessary thermal energy only comes at higher temperatures [30].

In the study of composite materials, T_g is heavily defined by the polymeric matrix, as fibres maintain a stable behaviour throughout the whole temperature range that these materials are expected to withstand.

3.2.2 Coefficient of Thermal Expansion

While undergoing a temperature variation, materials present a volumetric change defined as thermal expansion. This dimensional response is portrayed by the coefficient of thermal expansion (CTE), which indicates the fractional difference in dimension per unit change in temperature [31–34]. The most common assessment of CTE is done by inspecting the variation in length, as considered in equation 3.1, defined as the linear coefficient of thermal expansion, α_L. In the following expression, L represents the lenght at the reference temperature, while $\frac{dL}{dT}$ stands for the rate of variation in length with the change in temperature. CTE is typically expressed in $\mu m\, m^{-1} K^{-1}$.

$$\alpha_L = \frac{1}{L}\frac{dL}{dT} \tag{3.1}$$

The mechanisms associated with strains induced by temperature changes can be explained by the chemical composition of materials. When the molecular chains experience a rise in temperature, their kinetic energy increases, which is signalled by a larger amplitude of atomic vibration. This excitation leads to a higher average separation between molecules, which generally results in the expansion of the material while heated, and the opposite behaviour while cooled [35–37].

Although an isotropic expansion is the expected behaviour for most materials under increasing temperature, the dispersion of the molecular chains may result in quite distinct responses [37–39]. With amorphous polymers, and knowing that interatomic bonds are stiffer and shorter than intermolecular links, the manifested vibrations are mainly transverse to the alignment of the polymer backbone[1] [37]. Materials that fit into the amorphous category, as thermoset resins do, tend to present a highly scattered atomic

[1]The polymer backbone is defined by a long series of atoms connected by covalent bonds, creating a linear continuous chain that other molecular groups are linked to.

arrangement, which results in an isotropic response. With crystalline solids, on the other hand, the periodicity of the molecular packing may create structural peculiarities that lead to anisotropic responses [38, 39]. Carbon fibres are highly crystalline materials composed by sheets of carbon atoms with very strong bonds - much stronger than the van der Waals forces that connect these planes among themselves. The distance between each carbon sheet is also bigger than the one between the carbon atoms that compose each plane. This particular arrangement favours thermally induced vibrations to occur transversely to the carbon sheets, which are oriented along fibre direction. The predominance of out-of-plane vibrations of the carbon atoms, coupled with the strong covalent bonds between them, leads to an expansion perpendicular to fibre direction, and an axial contraction [37]. The result of the very particular structure of carbon fibres is then a positive transverse CTE and a much smaller and negative longitudinal CTE. When carbon fibres present a higher degree of crystallinity and the carbon basal plans are more sharply oriented with fibre direction, the tensile modulus usually becomes higher and the longitudinal CTE becomes more negative [29] - however, commercially available fibres do not seem to respect this trend at all times, as this is likely a simplistic justification of the value of CTE and elastic modulus.

The technical datasheets of most materials present CTE as an unique value, but this information is often misleading. Materials with physical properties highly dependent on temperature - like polymers - are expected to present a CTE that significantly changes with it [31, 32, 36, 40–42]. If this is the case, predicting the expansion of a component over a temperature range by simplifying equation 3.1 to $\Delta L = \alpha_L \, L \, \Delta T$ may result in substantial design errors. A more correct prediction would call for the integration of $\frac{dL}{dT}$ over the specified temperature range, meaning that the material's CTE as a function of temperature needs to be requested or obtained experimentally.

Amorphous materials, like thermoset resins, experience a significant change in the value of CTE and its rate of change with temperature depending on where they stand relative to T_g [36, 41]. To better explain this dependency, lets recover and expand on the concept of free volume introduced in the previous section. The volumetric domain of a polymer is not perfectly occupied by molecular chains to a point of complete saturation. In fact, a distinction can be made regarding occupied volume - by molecules and their thermally induced vibration - and free volume - allowed by the imperfect packing of the molecular chains [36]. Consider a polymer in a rubbery state, above T_g. As temperature decreases, molecular kinetic energy also lowers, meaning that the volume occupied due to atomic vibration is reduced. At the same time, chain mobility is also inhibited, and the limitation of molecular rotations and translations cause a decrease of free volume. At T_g, the advent of the glassy state is synonym of a critical reduction in free volume, as chain mobility

is heavily obstructed. This way, below T_g, the material's contraction with decreasing temperatures is almost exclusively due to a reduction in atomic vibrations [36]. This entire process justifies why the CTE of polymers quickly rises above the glass transition temperature - the increase in volume is due to, not only the higher kinetic energy of the atomic structure, but also the variation in free volume.

When materials are expected to work under significant temperature variations, such as the filament wound struts under study, thermal expansion becomes a critical design parameter [34, 40]. The study of this subject is an opportune moment to remember that the produced CFRP tubes compose the frame of a large deployable space antenna, from which great dimensional stability is expected while in low Earth orbit. Manipulating the linear and transverse CTE of the CFRP struts in order to compensate the expected positive expansion of the titanium end-fittings is an absolutely fundamental design requirement, thus justifying the importance of this theme under the scope of this thesis. With composite systems, due to the disparate behaviour of each constituent, engineers are able to tailor the response of the laminate to meet the specific needs of the application.

3.2.3 Thermally Induced Stress

The formation of residual stresses in composite materials comes from many factors at different scales, starting with opposing strains between constituents and among plies, further advancing with part-tool interactions, and ending with post-processing [41, 43–47]. This accumulation of stresses in the laminate lower its ability to sustain additional external solicitations, thus jeopardising the expected behaviour of the material. Thermal events are a major contributor to the appearance of residual stresses in composite parts for aerospace applications due to the temperature changes that these materials are exposed to during both the production process and their service life in orbit.

The development of free strains can be identified as the primordial cause of residual stresses in laminates. These free strains are originated by different phenomena, but three main sources can be named - temperature variations, chemical shrinkage through the advance of the degree of cure, and moisture absorption [41, 43–45, 48]. As their designation indicates, free strains are not necessarily associated with any stresses. In fact, in the case of a perfectly homogeneous and unconstrained body, no stresses originate from the development of free strains [41, 43, 49]. However, composite materials are far from homogeneous, and their inherent anisotropy translates to a mismatch of free strains aggravated by external boundary conditions, resulting in the appearance of residual stresses [41, 43–45, 49]. In order to acquire some sensibility regarding thermally induced stresses, a simplistic one-dimensional approach can be utilised to illustrate the impact of free strains in a composite material. Lets consider a case of axial force balance in an

unidirectional ply, where strains and stresses normal to the fibres are ignored.

The total strain in a material under an environment that induces free strains, such as uniform heating, is given by equation 3.2 [41, 43, 49]. The elastic strain associated with mechanical loads, ε_{mech}, and the free strain, ε_{free}, represent the total strain. The value of the elastic strain respects Hooke's Law, while the free strain is the result of any of the conditions mentioned above. As an example, the free strain for a body under temperature variation is equal to $\alpha\Delta T$, where α represents the coefficient of thermal expansion.

$$\varepsilon = \varepsilon_{mech} + \varepsilon_{free} = \frac{\sigma}{E} + \varepsilon_{free} \tag{3.2}$$

This means that stress can be obtained by equation 3.3, which albeit incredibly simple, exposes a crucial idea mentioned before. If free strains are the only ones affecting an homogeneous and unconstrained body ($\varepsilon = \varepsilon_{free}$), the resulting stress is null [41, 43, 49].

$$\sigma = E\left(\varepsilon - \varepsilon_{free}\right) \tag{3.3}$$

For a composite ply, however, residual stresses do emerge from simple phenomena as these. Lets recognise the unidirectional ply as a system composed by fibres in a matrix. For this model, it is common to assume that stresses are distributed between constituents according to the volume fraction that each occupies, and that the matrix and fibres suffer the same amount of strain, as their length should remain equal [43, 49, 50]. Both of these assumptions are expressed below. The subscripts f and m indicate fibre and matrix related properties, respectively.

$$\varepsilon = \varepsilon_f = \varepsilon_m \tag{3.4}$$

$$\sigma = \sigma_f\, V_f + \sigma_m\, V_m \tag{3.5}$$

Combining equations 3.3 and 3.4, the consequences of a mismatch in free strains start to appear. Equation 3.6 shows how a mismatch between the strain experienced by the ply and the free strains in each constituent leads to stresses in that same constituent.

$$\sigma_{f,m} = E_{f,m}\,\left(\varepsilon_{f,m} - \varepsilon_{free_{f,m}}\right) = E_{f,m}\,\left(\varepsilon - \varepsilon_{free_{f,m}}\right) \tag{3.6}$$

This idea can be clearly interpreted through a particular case where a ply is uniformly heated without any other solicitations. As mentioned before, the free strain related to this environment is given by the product of the coefficient of thermal expansion and the temperature variation. With the fibre and matrix presenting a different coefficient of thermal expansion, the ply's coefficient will naturally be distinct from both, and as equation 3.7

clearly states, thermal stresses will arise in each constituent due to this discrepancy.

$$\sigma_{f,m} = E_{f,m}\ \left(\varepsilon - \varepsilon_{f,m}\right) = E_{f,m}\ \left(\alpha - \alpha_{f,m}\right)\ \Delta T \tag{3.7}$$

This influence of the mismatch of free strains in the formation of residual stresses can also be expressed in more general terms under the adopted model. In a case where only free strain inducing solicitations are present, the equilibrium equation (3.5) can be equalled to zero ($\sigma = 0$) [41, 43, 49]. Furthermore, equation 3.4 can be expanded taking into account the definition of strain in equation 3.2. The resulting expressions are presented in the system of equations below.

$$V_m\ \sigma_m + V_f\ \sigma_f = 0 \tag{3.8}$$

$$\varepsilon = \frac{\sigma_f}{E_f} + \varepsilon_{free_f} = \frac{\sigma_m}{E_m} + \varepsilon_{free_m} \tag{3.9}$$

To obtain the residual stresses in the matrix, equation 3.9 can be presented as follows.

$$\sigma_m = \frac{E_m}{E_f}\ \sigma_f + E_m \left(\varepsilon_{free_f} - \varepsilon_{free_m}\right) \tag{3.10}$$

Considering the expression for σ_f attainable from equation 3.8, expression 3.10 can be further manipulated to highlight the influence of the free strains in the resulting residual stresses.

$$\sigma_m = \frac{E_m}{E_f}\ \left(-\frac{V_m}{V_f}\right)\ \sigma_m + E_m \left(\varepsilon_{free_f} - \varepsilon_{free_m}\right) \Leftrightarrow$$

$$\Leftrightarrow \sigma_m\ \left(1 + \frac{E_m V_m}{E_f V_f}\right) = E_m \left(\varepsilon_{free_f} - \varepsilon_{free_m}\right) \Leftrightarrow$$

$$\Leftrightarrow \sigma_m = \frac{V_f\ E_f\ E_m\ \left(\varepsilon_{free_f} - \varepsilon_{free_m}\right)}{E_m\ V_m + E_f\ V_f} \tag{3.11}$$

It is now clear that the the residual stresses in each constituent are a function of the mismatch of free strains, their elastic modulus and the respective volume fractions. As initially stated, these expressions result from an extremely simplified one-dimensional model, however, the fundamental ideas transmitted by equations 3.2 and 3.3 can be presented in a broader way through expressions 3.12 and 3.13, where $[S]$ and $[C]$ represent

the compliance and stiffness matrices, respectively.

$$\{\varepsilon\} = [S]\{\sigma\} + \{\varepsilon\}_{free} \tag{3.12}$$

$$\{\sigma\} = [C]\left(\{\varepsilon\} - \{\varepsilon\}_{free}\right) = [C]\{\varepsilon\}_{mech} \tag{3.13}$$

These equations hold the same consequences exposed by the simplified model above. Nonetheless, considering additional through-thickness discrepancies and even taking into account the viscoelastic behaviour of the polymeric matrix is bound to result in a closer approximation to reality, with a more complete assessment of how residual stresses accumulate in each ply.

The interactions between constituents at the ply level are far from being the only cause of residual stresses in composite parts. Laminates are composed of multiple plies, commonly stacked under different orientations, which results in deformations along different directions among plies and numerous additional constraints that lead to further development of residual stresses. At the laminate level, the stress strain relations can be presented as in expression 3.14, where $[A]$, $[B]$ and $[D]$ are the extension, bending/extension coupling and bending matrices, respectively. $[N]$ and $[M]$ are the stress resultants and bending moments, $\{\varepsilon_0\}$ are the mid-plane strains and $\{k\}$ represents the curvature. $\{N_{free}\}$ and $\{M_{free}\}$ refer to the non-mechanical loads, related to free strains.

$$\begin{Bmatrix} N \\ M \end{Bmatrix} = \begin{bmatrix} A & B \\ B & D \end{bmatrix} \begin{Bmatrix} \varepsilon_0 \\ K \end{Bmatrix} - \begin{Bmatrix} N_{free} \\ M_{free} \end{Bmatrix} \tag{3.14}$$

This relationship bares a striking resemblance with expression 3.13, implying similar consequences. In fact, as $[N]$ and $[M]$ come from integrating $\{\sigma\}$ along the thickness of the laminate, the overall conclusions extracted above regarding the influence of free strains remain true. The cause of additional stresses at the laminate level is not the presence of free strains in itself, but the mismatch of its magnitude and direction between plies.

It also serves as an opportunity to highlight how the lay-up selection and the thickness of each ply influence the stiffness tensors of the laminate (3.15) and, consequently, the development of residual stresses. The thickness of the laminate is presented as h, the distance from the top of the layer to the centre of the laminate is z, and $[C']$ is the off-axis stiffness matrix of each ply. The superscript i refers to the i^{th} layer among the total m plies

of the laminate.

$$[A] = \int_{-h/2}^{h/2} [C]\, dz = \sum_{i=1}^{m} [C']^i \left[z^i - z^{i-1}\right]$$

$$[B] = \int_{-h/2}^{h/2} [C]\, z\, dz = \frac{1}{2} \sum_{i=1}^{m} [C']^i \left[\left(z^i\right)^2 - \left(z^{i-1}\right)^2\right]$$

$$[D] = \int_{-h/2}^{h/2} [C]\, z^2\, dz = \frac{1}{3} \sum_{i=1}^{m} [C']^i \left[\left(z^i\right)^3 - \left(z^{i-1}\right)^3\right] \tag{3.15}$$

Besides the free strains that originate at the ply or laminate level due to thermal variations, cure shrinkage or moisture absorption, the production process and finishing operations can also lead to additional residual stresses [41, 43, 44, 47]. In filament winding, part-tool interaction is particularly important as the impregnated fibre tows are wound around a mandrel and cured while still on it. The strains experienced by the tool and part during the entire process are coupled due to friction between both. This constraint causes stresses in the part, and although some are relieved through interply slippage, a stress gradient is created, which can result in warpage and compressive residual stresses after demolding. Finishing processes such as trimming, cutting and drilling may relieve some stresses in the component, sometimes causing unwanted additional geometrical changes [41, 43, 44, 47].

3.3 Parameters Affecting Thermal Behaviour

The multiple decisions made in the design stage and relative to the production process define the thermal behaviour of the composite component. As chapter 2 delves into the specificities of the filament winding process, and how its various stages can affect the final part, this section paints a broader picture of how customisable the thermal properties of composite systems are, and how they can be manipulated to better fit the intended application.

3.3.1 Constituent Selection and Fibre Volume Fraction

The constituents of a composite system are the most critical factor in its characterisation. Defining the matrix and reinforcing fibres is naturally a very important step in obtaining the expected thermal response, as well as any other property. Each constituent has a different intrinsic weight in the response of composites, and their influence is further altered by the

volume fraction that each one occupies.

When it comes to the glass transition temperature, as discussed in section 3.2.1, the matrix definitely holds the most weight. Even though, for example, the presence of fibres difficults the measurement of T_g via the detection of changes in heat capacity, the glass transition temperature of the polymer matrix is a good approximation of the composite's response, even if it represents less than half of its volume. Both thermoset and thermoplastic matrices present choices for high temperature applications, with a high attainable T_g. The polymeric matrices suffer from critical failure due to extreme temperatures much sooner than the fibres do, which justifies the lower influence of the latter.

In regard to the thermal expansion behaviour, the weight of each constituent is dramatically changed. As fibres present a much higher stiffness than the polymer matrices, especially in the longitudinal fibre axis, they dominate the resulting coefficient of thermal expansion in the fibre direction. Considering an unidirectional ply of CFRP, the longitudinal CTE is typically small and negative due to the high influence of the carbon fibres. Oppositely, the transverse CTE of the composite is positive and tends to be an order of magnitude higher, which is the result of the combined positive CTE of both fibre and matrix in that direction. To better grasp the distinct influence of each constituent in the thermal expansion of a composite, lets continue to consider an unidirectional ply with parallel fibre reinforcements. Myiano and Nakada [51] present equations 3.16 and 3.17 to predict the longitudinal and transverse coefficient of thermal expansion of an unidirectional laminate, based on the rule of mixtures. Subscripts L and T represent the longitudinal and transverse directions, while f and m refer to properties of the fibre and matrix, respectively. The fibre volume fraction is V_f, E is the elastic modulus, ν is the Poisson's ratio, and α is the coefficient of thermal expansion.

$$\alpha_L = \frac{\alpha_{L_f} V_f E_{L_f} + \alpha_m (1 - V_f) E_m}{V_f E_{L_f} + (1 - V_f) E_m} \tag{3.16}$$

$$\alpha_T = \alpha_{T_f} V_f (1 + \nu_{23_f}) + \alpha_m (1 - V_f)(1 + \nu_m) - \alpha_L \nu_{12} \tag{3.17}$$

The impact of fibre volume fraction on the CTE of unidirectional laminates can be better comprehended by graphically representing the expressions above. To do that, lets consider three hypothetical composite systems composed of the same epoxy resin but distinct fibres. Table 3.1 shows the properties of a glass fibre, low modulus and high modulus carbon fibres, and an epoxy resin, based on real commercially available products. By applying the rule of mixtures to find the properties of the corresponding laminates, figure 3.1 shows the evolution of the CTE of these unidirectional laminates with fibre volume fraction.

Table 3.1: Properties of generic fibres and epoxy resin.

Constituent	$\alpha_L \left[10^{-6}\, K^{-1}\right]$	$\alpha_T \left[10^{-6}\, K^{-1}\right]$	E_L [GPa]	E_T [GPa]
Glass Fibre	5.6	5.6	73	73
Low Mod. Carbon Fibre	-0.5	15	235	20
High Mod. Carbon Fibre	-0.5	15	500	20
Epoxy Resin	58	58	3	3

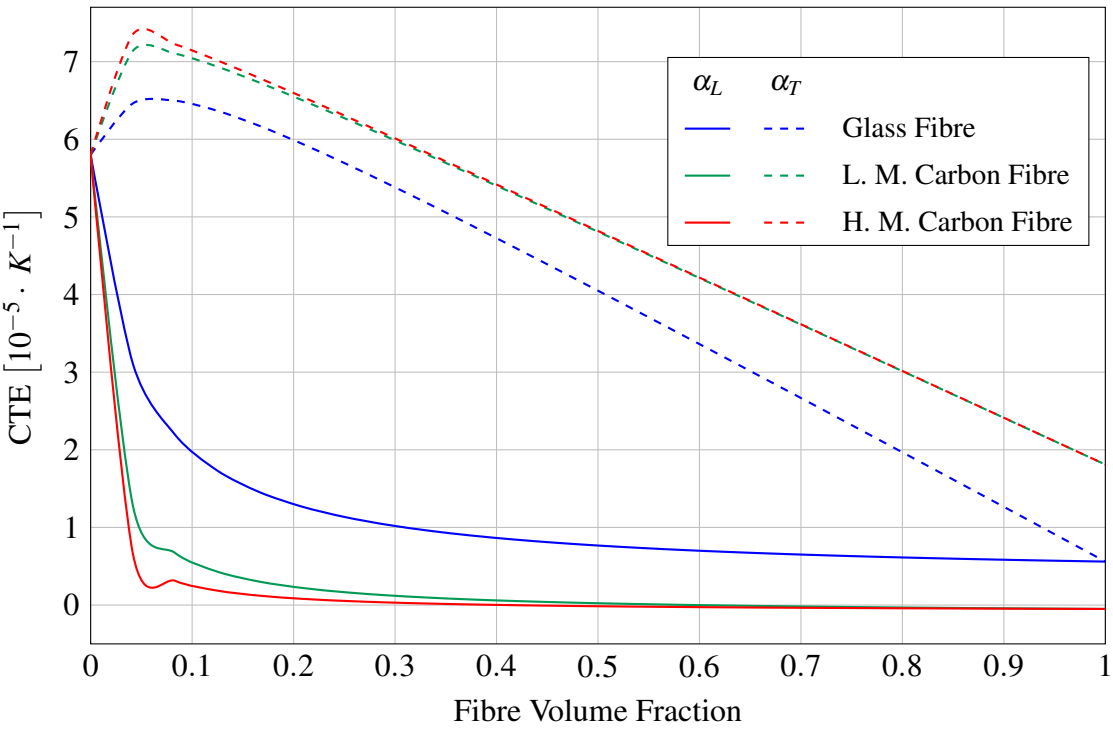


Figure 3.1: Evolution of the coefficient of thermal expansion with the fibre volume fraction of composite systems composed by different fibres, based on the rule of mixtures.

The analysis of figure 3.1, inspired by the works in [40, 52], confirms that the fibres have a higher power in the definition of the laminate's CTE, and that predominance grows with stiffer fibres. With glass fibres, the longitudinal CTE stabilises around a FVF of 0.6. With carbon fibres, this happens at much lower values of FVF - around 0.5 for low modulus fibres and 0.3 for higher modulus fibres. The epoxy resin is much less rigid than the fibres, which explains its lower impact. However, transverse CTE is much more sensible to variations in FVF throughout the entire domain of the plot, as this property is not dependent on the longitudinal elastic modulus, and only on the transverse properties, which are not as disparate between constituents.

As discussed before, the formation of thermally induced stresses is heavily defined by the disparate behaviour of the fibres and matrix while undergoing temperature changes,

and this should be a topic to pay attention to while defining the composition of a laminate. Utilising resins and fibres with more extreme values of CTE tends to result in a higher density of damage after thermal cycling [29, 53, 54].

3.3.2 Layup and Fibre Orientation

Composite systems can be tailored to meet specific needs, not only by defining the ratio of its constituents, but also by the arrangement of its plies. The thickness and fibre orientation of each ply, along with the stacking sequence of the laminate, can radically alter the physical and mechanical properties of a composite part.

The thermal expansion behaviour of composite laminates is heavily influenced by the defined layup and respective fibre orientation of each ply [19, 40, 55]. Ply orientation has great consequences in the mechanical properties of laminates - composites have the ability to withstand higher loads in the fibre direction than others, and this behaviour is aggravated if anisotropic fibres, such as carbon fibres, are used. Similar consequences are true for the thermal expansion of the laminate, as the layup sequence affects the weight of each constituent in the thermal behaviour, and the directional arrangements for the reinforcing fibres of each ply are endless. Fibre alignment defines in which direction a CFRP part will tend to contract under heating, and the various stacking sequences possible will affect the resulting CTE in each direction. This complexity is actually helpful in the design of composite components, as they add another factor that can help achieve the desired response.

Some configurations, however, are more helpful than others in the reduction of thermally induced stress, and achieving lamina symmetry is one of the most important. A laminate is considered symmetric when the stacking sequence is mirrored on the mid-plane. For example, $[0/45/45/0]$ and $[0/90/45/45/90/0]$ are symmetric laminates. Adopting this type of configuration eliminates bending-extension coupling - contemplated as $[B]$ in section 3.2.3 - which prevents bending and warping during temperature changes, such as the ones experienced during cure or thermal cycling [7, 40, 43]. For a plane symmetric laminate, this means that temperature changes will not induce curvature, which is quite important. Tubular components, such as the filament wound struts under study, have a particular advantage in this topic, as they are intrinsically symmetric even if the winding sequence is not. Even though the closed geometry of tubes always appears to meet the criteria for symmetry, precise applications - such as the case in hands - require caution regarding this assumption. In unsymmetric tubular laminates, while bending-extension coupling goes generally unnoticed, the consequences of its lack of in-plane symmetry can cause some tubular twisting [7, 40]. As the result of this twist is mainly noticeable at the edges, this is not likely to be problematic in most applications, as is the case with

tubular test specimens where the ends are under the grip-influenced regions [7]. However, Johnson [40] specifically states that for the support of antenna frames - which is precisely the application of the produced tubes - the thermal shear strain induced by the lack of symmetry can eventually cause issues in such a thermally sensitive design. It should be noted that bending-extension coupling can also be greatly reduced by sub-laminate repetition, since this results in laminate homogenisation. For example, a $[0/90]_{8S}$ laminate has a much higher degree of dispersion than a $[0_8/90_8]_S$ sequence, which leads to a higher decay of every term in $[B]$, thus also mitigating bending and warping.

The adopted lamina thickness and layup also have consequences in the damage resulting from thermal changes. Decreasing the thickness of the plies and increasing the sub-laminate repetition, while maintaining the laminate thickness, has shown to increase the necessary stress for the initiation of damage mechanisms [37, 56, 57]. However, this does not seem to be a consequence of the thickness reduction in itself, but from the higher number of constraints between adjacent plies with significantly different fibre orientations. Tompkins et al. [58] exposed $[0/90]_S$ and $[0/90]_{10S}$ CFRP laminates to thermal cycling between -156ºC and 121ºC. The thick ply laminate experienced microcracking in the very first cycles and reached saturation around 400 cycles, while the thin ply laminate only showed microcracks after around 200 cycles, but after 200 cycles more already presented a crack density two times higher than the other laminate, with no signs of saturation even after 1600 cycles. Brown [56] presents similar results for $[0/90]_S$ CFRP laminates of distinct ply thickness. Adopting thicker plies resulted in microcrack saturation at 500 cycles between -160ºC and 120ºC, while the thinner plies laminate only showed damage around 1500 cycles, with no saturation after 5000 cycles. It appears that adopting thinner plies delays the appearance of damage mechanisms in composites under thermal cycling, but the higher level of constraints present in the laminate causes more severe damage when the necessary stress threshold for crack initiation is surpassed. The same behaviour is verified in specimens under mechanical static and fatigue loading [37, 57]. Depending on the expected work environment of the composite part, the degree of repetition of the laminates and the correspondent ply thickness should be a matter of concern regarding damage progression, taking into consideration that the constraining effect is mainly due to the disparities in the orientation of adjacent plies.

3.3.3 Curing Stage

The role of the curing stage in the production of a filament wound part is discussed in section 2.2.6, where it is presented as the phase where the composite system obtains its expected mechanical and physical properties through polymerisation of the matrix. This definition leads to the correct assumption that the curing stage has a crucial role in the

definition of the thermal response of the material, as the cure parameters define, to a great extent, the resulting glass transition temperature, T_g.

As described in section 3.2.1, the density of cross-links is determinant in the definition of the resin's T_g. As the progression of cross-linking is heavily defined by the duration and temperature of the curing cycle, and most of the other factors affecting T_g are already inherent to the chosen material system, it becomes clear why the curing stage is so important in obtaining the desired glass transition temperature. This analysis focuses on thermoset matrices, but it should be noted that crystallisation in semi-amorphous materials also affects the curing progress.

The linear epoxy resin used for the production of the filament wound tubes under study transforms into a three-dimensional cross-linked thermoset during cure through complex chemical interactions and physical processes. Figure 3.2 shows a typical representation of a time-temperature transformation diagram for an isothermal cure of a thermoset resin, which presents the required time of cure to reach the different states of a material at a given cure temperature, T_{cure}. The curves that mark the gelation and vitrification transformations, along with the one that represents a full cure, divide the diagram in the different attainable states of the material - liquid, sol/gel rubber, gel rubber, sol glass, sol/gel glass, gel glass and char [30, 59]. The gel fraction of the polymer is insoluble and cross-linked, while the sol portion is still solluble. Three different temperatures are represented in the vertical axis of the applied curing temperature. The initial glass transition temperature of the unreacted resin mix is represented by T_{g0}, the temperature at which gelation and vitrification ideally occur simultaneously is ${}_{gel}T_g$, and the theoretical glass transition temperature of the fully cured material is $T_{g\infty}$ [30, 59, 60].

The rate at which the curing reactions occur is dependent on the region of the diagram where the material is encountered. Previous to gelation and vitrification, the reactions are of chemical nature and thus kinetically controlled. In the rubbery regions that come after gelation, curing proceeds mainly through the same mechanisms, but some diffusion phenomena start to appear. Finally, after vitrification, diffusion assumes control of the reaction process, and the curing rate decreases immensely, between two and three orders of magnitude [59, 60]. This is why resins should be stored around 20ºC below the T_{g0}, or at even lower temperatures, since in its initial glassy state the reactions in the epoxy-hardener mix are hardly significant due to their extremely slow rate [60].

The chosen curing temperature is usually between ${}_{gel}T_g$ and $T_{g\infty}$. The first transformation to occur at this interval is gelation, which marks the irreversible passage of viscuous liquid to insoluble cross-linked material - the gel fraction. At this point, the macroscopic properties of the resin are significantly altered, but a portion of the rubbery resin mix remains soluble. As curing progresses and the cross-link density increases, vitrification

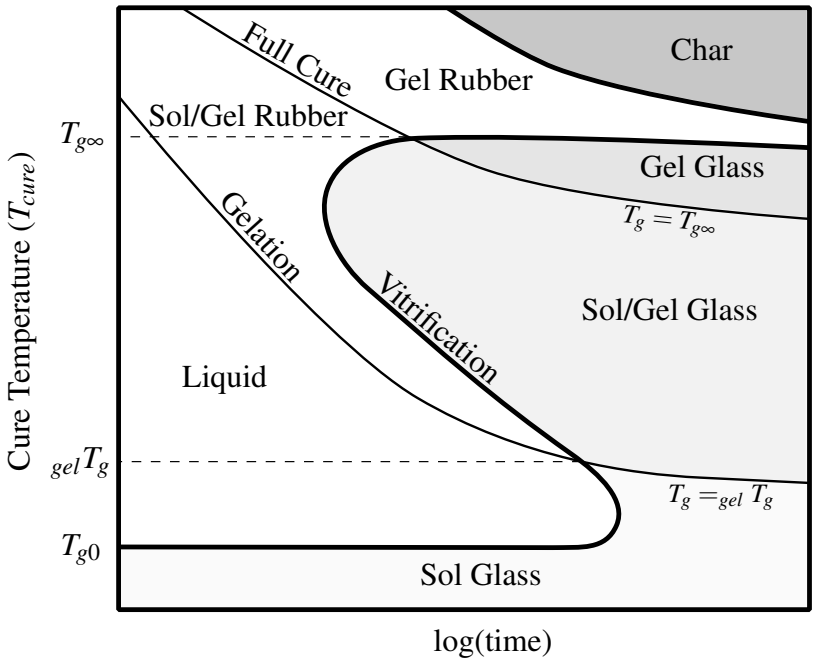


Figure 3.2: Generalised time-temperature transformation (TTT) isothermal cure diagram for a thermoset resin, adapted from [30, 59, 60].

occurs and the rubbery material enters a glass state. From this point on, the diffusion-controlled reaction mechanisms are responsible for the curing process and thus heavily decrease the reaction rate [59, 60]. The resin system only reaches full cure when every monomer is included in the molecular chain that constitutes the polymer, eliminating the soluble portion of the mix [60]. If this were to happen, the material's T_g becomes equal to $T_{g\infty}$. Reaching this perfect degree of conversion has proved to be borderline impossible due to how slowly further cross-linking occurs when the material is well into a region where diffusion mechanisms are responsible for it [59]. However, there are clear signs of saturation in the value of T_g when the cure temperature is close to, or even above $T_{g\infty}$ [30, 61].

With curing temperatures below $T_{g\infty}$, some additional cross-linking still occurs after vitrification - at the point of this transformation, T_g becomes equal to T_{cure}, and if curing continues, T_g can still increase steadily for around 20ºC before a definite reduction in the curing rate [41, 62–64]. Besides the slow advance of cross-linking under diffusion mechanisms, Wu [61] justifies this T_g above T_{cure} also due to the exothermic nature of the curing reaction, which increases the temperature of the samples. On the other hand, with curing temperatures equal to or above $T_{g\infty}$, the glass transition temperature no longer goes above T_{cure}, since the epoxy network is already at a very high degree of conversion at that temperature [30, 61, 63, 64]. Adopting a T_{cure} significantly above $T_{g\infty}$ can result in thermal degradation of the polymeric chains and oxidative cross-linking that can actually lower the

component's T_g [30, 61, 65].

The curing stage is generally comprised of an initial isothermal cure phase and one, or more, temperature dwells. Figure 3.3 represents a generic curing stage for a thermoset resin along with the correspondent evolution of the glass transition temperature and viscosity of the resin system, showing the consequences of the phenomena described up to this point.

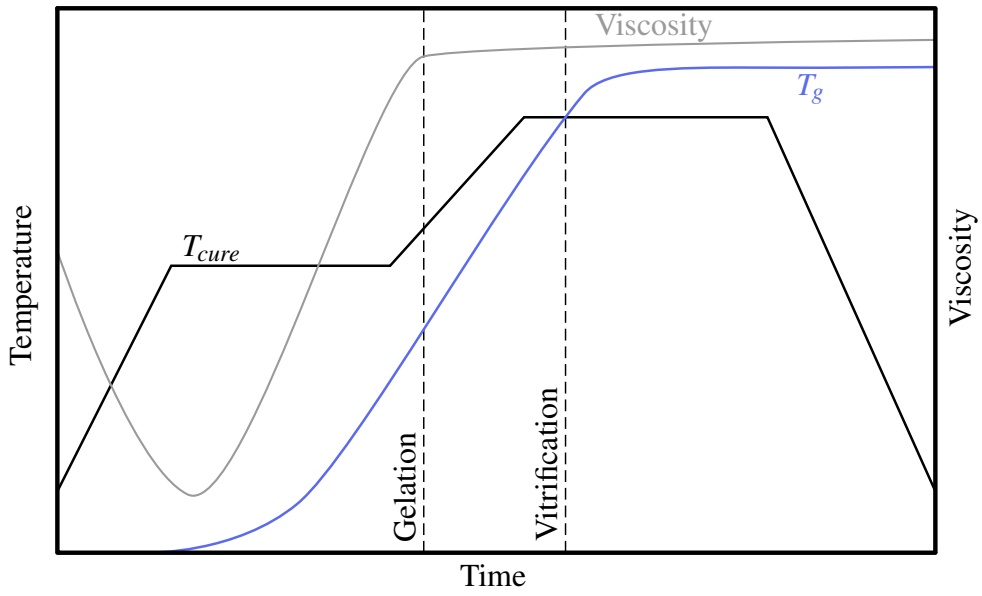


Figure 3.3: Simplified representation of the curing stage of a thermoset resin, based on the illustrations in [41, 47, 62].

As temperature increases, viscosity drops rapidly until curing reactions start to take place, which is signalled by the increase of T_g - in fact, if the degree of cure were to be represented in this scheme, its evolution would mimic the climb of the glass transition temperature, as both are closely connected. Reaching a low viscosity is crucial to correctly fill the fibre tows, as resin fluidity helps eliminating any entrapped volatiles. When gelation occurs, the resin transforms in a rubbery solid that already presents some strength. The microstructure of the laminate is heavily defined by what happens up to this point, since its development is mainly stopped during gelation. At this phase, the increase of T_g remains steady as curing is still kinetically controlled. Curing progresses to vitrification ($T_g = T_{cure}$), and as diffusion begins to dominate molecular cross-linking, T_g inevitably stabilises - note that if the cure temperature is close to or above $T_{g\infty}$, the glass transition temperature remains equal to or below T_{cure}, reaching a maximum degree of conversion [41, 47, 62].

The implications of the complex described phenomena surrounding the curing stage and its influence on T_g are deserving of a summary. The TTT diagram (figure 3.2) makes clear that choosing a higher curing temperature allows faster cures - the inflexion of the vitrification curve is due to higher rates of conversion at higher temperatures - and results in a higher T_g, because when the material reaches a glassy state and T_g equals T_{cure}, the

advance of cross-linking is limited and tends to stagnate. To guarantee a maximum degree of cure, exposing the material to temperatures close to $T_{g\infty}$ is recommended, due to the high density of cross-links already formed before entering the glassy region.

Searching for the highest T_g attainable for the resin system is a common demand, particularly for aerospace applications where materials need to withstand extreme temperatures, as is the case with the filament wound tubes under study. There are, however, other factors to take into consideration while defining the curing stage. The cure cycle should actually be performed at the lowest possible temperatures to limit the development of residual stresses [41, 47, 62].

The thermal cure of a thermoset resin leads to changes in its volume for two distinct reasons. The most obvious one is the practical consequence of the polymer's coefficient of thermal expansion that creates thermal deformation as a result of temperature variation - a recurring subject along this thesis. The second justification for this volumetric change is the curing shrinkage phenomenon, which results from the progress in the degree of cure, turning this into a particular effect of the curing stage [28, 41, 47, 66–68]. The advancement of cross-linking is responsible for the reduction in volume, and its magnitude is heavily dependent on the chemical properties of each thermoset resin, namely its density before curing, molecular release during cure, and proximity of the molecular chains after cure. The volumetric shrinkage of epoxy is one of the lowest - around 1% to 2% - precisely because it presents an uncured high density, it does not release small molecules while it is cured and the cured polymeric structure is relatively distant, particularly when compared to polyester and phenolic resins, which present a curing shrinkage around 5% and 9%, respectively [28]. All of these processes are naturally magnified by the application of a higher cure temperature because it increases the temperature range that the resin is exposed to - thus increasing volumetric change due to its CTE - and also furthers the degree of cure, which is related to an increasing chemical shrinkage [41, 47, 62, 69, 70].

In composite materials, this resin shrinkage is especially problematic because the matrix deformation is restrained by the fibres, leading to significant residual stresses [41, 47, 56, 66]. At gelation, the rubbery matrix still presents a low modulus of elasticity, meaning that at this phase volumetric contractions do not contribute greatly to the accumulation of residual stresses, as these are quickly relieved due to the viscoelastic response. With vitrification, the material develops a higher modulus of elasticity and, consequently, thermal stresses now rise significantly. During cooldown, stresses are again multiplied by the distinct expansion coefficient of the constituents [41, 47]. These stresses are associated, at a macro level, with geometrical distortions [41, 47, 66, 67] and, at a micro scale, with the nucleation of transverse matrix cracks and fibre-matrix debonding [28, 56, 66–68, 71]. The appearance of defects in the microstructure due to the curing process alone is particularly

relevant to this study, as their presence in the filament wound tubes is assessed. A detailed description of damage modes in composites exposed to thermal variations is presented in section 3.4.1.

The way in which the design choices affect the thermal behaviour of composite systems, illustrated along the last sections, shows how the behaviour of every constituent and the configuration of the laminate can be manipulated to meet the necessary requirements. As a summary of the information collected up to this point, it is clear that the coefficient of thermal expansion, along fibre direction, is heavily defined by the reinforcing fibres, while T_g is intrinsically connected to the polymeric matrix. The development of residual stresses is strongly connected with the layup, particularly in how it accommodates the disparate responses of each constituent. Reaching a perfect balance between every parameter is certainly a complex task, and demands a widespread knowledge of how every decision affects a multitude of variables.

3.4 Effect of Thermal Cycling

With composite materials, such as filament wound struts, the disparities in the response to temperature variations from each constituent lead to internal stresses. The relief of the stresses caused by the mismatch in thermal expansion coefficients of the fibres and matrix is reached mainly through microcracking and tends to progress in the form of more severe damage mechanisms that affect the structural integrity of the laminate. Through thermal cycling, materials are also exposed to extreme temperatures, which can alter its properties through various physical and chemical phenomena. The combined consequences of exposure to thermal cycling are known to affect the underlying micromechanics of composite materials, with macro scale consequences. Keeping in mind the information presented in the previous sections, the effect of thermal cycling on the mechanical properties, coefficient of thermal expansion and glass transition temperature of composite specimens is assessed, after a thorough depiction of how damage mechanisms affect laminates under fatigue environments.

3.4.1 Fatigue Damage Mechanisms

With homogeneous materials, such as metallic alloys, the analysis of the damage mechanism is quite straightforward - a dominant crack propagates and ultimately leads to rupture. Composite systems require a more complex study, as a wide array of damage modes can contribute in varying scale through time up to the moment of failure [72]. The complex underlying micromechanics and lamina interactions that constitute the response of the laminate are hard to predict during a fatigue-inducing event with cumulative consequences,

such as thermal cycling. As a result, the comprehension of fatigue damage mechanisms in composite materials remains as a contemporary problematic for the implementation of fatigue design methodologies that are not either too conservative or too optimistic, both being a result of oversimplified models [73].

Despite the described complexity, damage propagation tends to follow the same path in energetic terms. Interface and matrix failure generally occur first, as they require a lower energy consumption than the final stages of failure, such as fibre rupture. However, the different damage stages, and the moment they occur at, are also heavily dependent on the constituents, the layup selection, the loading scenario, and even the environmental conditions [73–75]. With this in mind, a generalised description of fatigue-induced damage in composites follows, ending with special remarks regarding the particular consequences of thermal cycling.

The damage accumulation of composite systems under fatigue can be summarised in three distinct stages [72–74, 76, 76–78], represented in figure 3.4. This illustration shows the damage progression with an increasing number of fatigue cycles applied to a generic composite system. Contrary to what happens with metallic alloys, damage in composites appears quite early and at a rapid rate. This first stage of deterioration is followed by a long period of slower degradation, with more damage mechanisms contributing to a slight drop in the mechanical properties. Lastly, more severe damage modes quickly reduce the strength of the material, leading to its ultimate failure.

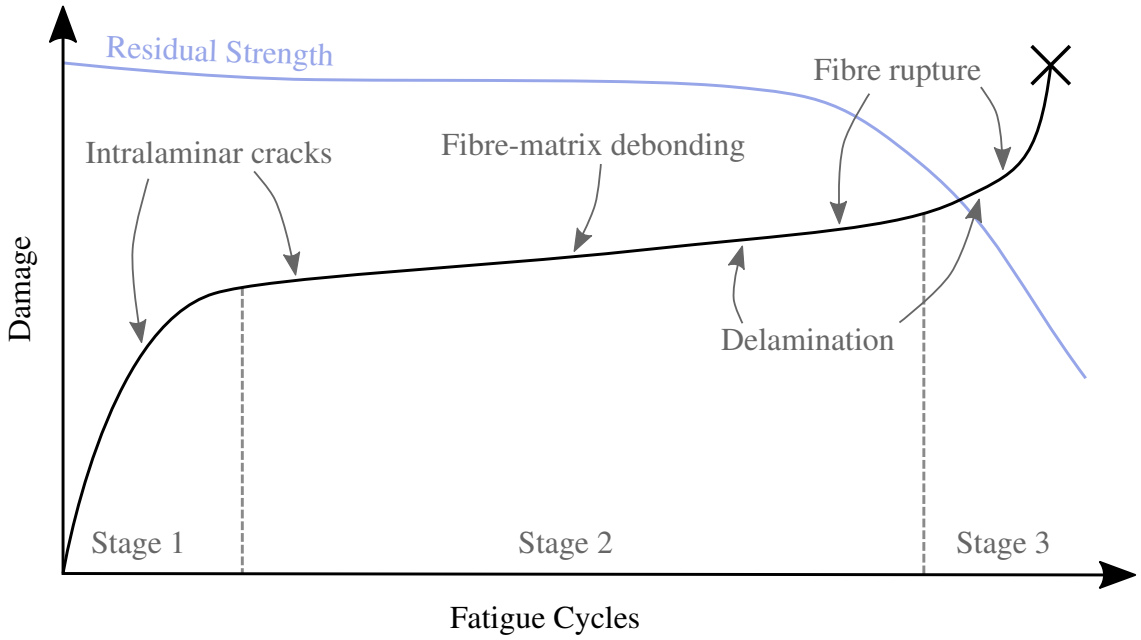


Figure 3.4: Damage progression in composite systems, inspired by illustrations in [72, 73].

The areas that are the most exposed to the initiation of damage are naturally the ones with the least strength, which leads us to the previous statement where the matrix and fibre-

matrix interfaces are designated as the first to experience failure. The degradation of the composite starts mainly with transverse matrix cracking - often referred to as intralaminar cracking -, which consists on the initiation of multiple microscopic cracks that propagate into the polymeric matrix, similar to the process observed in metals [74, 79]. Intralaminar cracks occur when the transverse stress that a lamina is subjected to surpasses the tensile strength of the polymeric matrix [37, 79]. The visual inspection of samples subjected to cyclic loading has shown that these transverse matrix cracks are often oriented in the fibre direction and perpendicular to the ply interfaces. This diffuse deterioration of the matrix progresses quite quickly, reaching the interfaces between fibres and matrix or adjacent plies [37, 73, 74, 79].

Areas where the reinforcing fibres are not oriented along the loading direction are more prone to damage, as that exposes the matrix even further. The influence on the ultimate strength of the laminate, and on its mechanical properties in general, is usually very small while this is the only damage mechanism in play, but a noticeable drop in stiffness may be observed [72–74].

This initial stage of intralaminar damage may advance up to the point where crack density - often identified as λ, representing the number of cracks per unit of length - reaches a saturation level that signals the arrival of the lamina to an equilibrium condition referred to as *Characteristic Damage State* (CDS) [73, 77, 79, 80]. The point at which this condition is achieved is dependent on the constituents, layup, and thickness of the composite system [79]. When the plies reach CDS, a second major stage begins, with other damage mechanisms being commonly observed, namely fibre-matrix debonding, delamination and fibre rupture [73].

The progress of intralaminar cracks in a ply often stops at the interface with reinforcing fibres or an adjacent lamina. If a high density of cracks is generated along the fibres, fibre-matrix debonding is likely to occur [79]. In a similar way, as the tip of an intralaminar crack reaches the interface with adjacent plies, the stress concentration on that region may lead to its propagation along the interface, resulting in delamination. In laminates with off-axis plies, delamination may also start solely due to the distinct behaviour of each lamina in response to a given loading scenario [74, 80]. These damage mechanisms are illustrated in figure 3.5.

This second stage is usually the one encountered during a larger amount of loading cycles. The drop in the mechanical properties becomes noticeable, but still quite minimal [73]. As the solicitation of the laminate continues, a third and final stage emerges. At this point, the matrix is usually widely damaged, delamination becomes more critical and, most importantly, fibre rupture assumes a dominant role in the degradation of the composite system - which sees its properties drop considerably until collapsing [73]. Fibre

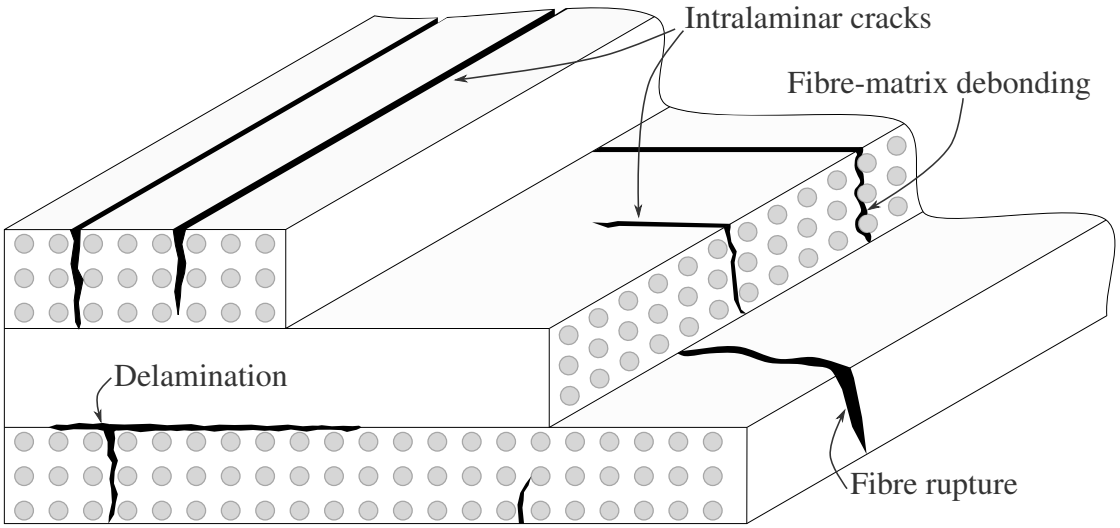


Figure 3.5: Illustration of damage in a cross-ply laminate.

fracture can occur along the entire fatigue-inducing event, but it is only when a significant amount of fibres suffers from rupture - particularly in areas exposed to high stress and where the reinforcements are more closely aligned with the loading direction - that the laminate reaches ultimate failure [74, 79]. Fibre rupture is also illustrated in figure 3.5, propagating closely perpendicular to the fibres.

Even though fibre rupture tends to appear only after other damage mechanisms come into play, all of the described mechanisms can emerge in different order and in varying combinations [73, 74, 79]. The uncertainty brought by this simultaneous effect of the different damage modes comes in line with the comments made before regarding how hard it is to predict the response of composite materials to fatigue environments, particularly due to the numerous parameters that contribute to this process - such as the loading scenario. In fact, although mechanical equivalences can be performed regarding stress levels, thermal cycling exerts specific consequences on composite systems that are not precisely the same as the ones that come with mechanical loading, due to the different nature of these solicitations.

With cyclic uniaxial tensile loading - a common mechanical fatigue environment - a given loading direction acts on the sample. With laminate composites, off-axis plies, particularly those closer to 90º, will become more damaged than those with a fibre orientation closer, or even equal to the loading axis [79, 81]. This is a general conclusion of multiple investigations on the effect of mechanical fatigue in composites, where laminas reinforced with fibres disoriented with the loading axis present the highest density of intralaminar cracks, while on-axis plies may not suffer from these transverse matrix cracks at all for a given number of fatigue cycles [76, 80, 82–84]. This distinct progression of damage between plies based on their fibre orientation marks a very clear difference to a thermal

fatigue environment - while mechanical cycling induces axial loading, and can thus create very different responses from each ply, thermal fatigue leads to biaxial in-plane stresses in every lamina [57, 81].

With thermal fatigue, composite systems are exposed to cyclic changes between extreme temperatures, which originates thermal stresses for two main reasons, already indicated in section 3.2.3. Firstly, the distinct coefficient of thermal expansion of the matrix and fibre reinforcement leads to a rivalling contraction or expansion of each constituent when under temperature variations. Secondly, as the deformation of each ply is heavily influenced by its fibre orientation, cross-ply laminates will suffer from a directional mismatch among its layers that also introduces stresses. Due to the latter, some plies may be more damaged than others because of the layup selection and resultant lamina interactions. However, as temperature changes act globally - and not according to a specific direction - thermal cycling tends to induce damage in a more equally distributed amount throughout the thickness than mechanical cycling, with every ply usually showing approximate levels of strain. This statement is corroborated by the observation of transverse matrix cracks in every lamina of cross-ply laminates [29, 75, 79, 81, 85] - and not only in off-axis plies, as is the case with mechanical cycling. The distinct responses from the constituents to thermal variations potentiate the nucleation of microcracks and accelerate debonding phenomena between constituents and plies [19, 79, 86, 87]. The outcome of thermal cycling also differs from mechanical cycling due to the aggregated consequences of exposure to extreme temperatures, with emphasis on the matrix embrittlement at cryogenic temperatures, and physical ageing at high temperatures [57, 69].

Besides this differences in how mechanical and thermal cycling affect composite systems, the generic description of fatigue damage mechanisms presented above can be applied to both cases, as the energetic pathways that lead to their appearance are similar [57, 79]. Numerous studies on the effect of thermal cycling on composite systems confirm the behaviour illustrated in figure 3.4 and described earlier in this section. The appearance of damage in the form of intralaminar cracks usually occurs in the very first cycles [53, 70, 81, 88], although some studies point to its delay from 50 to 300 cycles [75, 89, 90], showing that the use of some material systems under specific conditions can delay damage initiation. No clear pattern seems to justify this difference between experiments, but as mentioned multiple times up to this point, the order and time at which the described damage mechanisms occur is dependent on a multitude of parameters, and that naturally creates disparities on the encountered experimental studies. Nonetheless, in some cases, the delay in matrix cracking might be credited to the use of laminates with a high degree of dispersion through sub-laminate repetition, as discussed in section 3.3.2. A more unanimous conclusion is the saturation of crack density after a certain number

of cycles, followed by a longer stable period of damage where new damage modes develop [53, 70, 75, 77, 78, 88, 89]. The propagation of tranverse matrix cracks and the appearance of delamination with an increasing number of cycles is also evident in micrographs presented in [19, 29, 53, 70, 88, 89].

It is also important to be aware that the presence of defects resulting from the manufacturing process - such as voids, foreign inclusions and local fibre-matrix debonding - can accelerate the appearance or propagation of the described damage modes [74, 79, 80].

A fundamental detail should be noted in this analysis. Thermal cycling can be performed under various environments, with different pressures and reactive atmospheres. If a composite is exposed to vacuum thermal cycling, the matrix loss will be accelerated due to outgassing, which potentiates the nucleation of matrix defects [86]. Furthermore, thermal cycling can be performed in oxidative environments, such as air or even more oxygen-rich atmospheres. Oxidation reactions becomes quite significant above 120ºC, causing matrix shrinkage, which leads to a high stress concentration in the fibre-matrix interface and thus potentiates debonding and crack initiation. This particular situation is virtually nonexistent in nitrogen environments. Lafarie-Frenot [75] showed that an oxidative environment accelerates the progression of damage substantially when in comparison with inert atmospheres, showing evidence of coupling between matrix cracking and high oxygen concentrations during thermal cycling. Those experiments made clear that oxidation increases the degradation rates of the laminate, resulting in a higher density of cracks, which present wider and deeper profiles than the superficial and narrow failures observed with nitrogen environments. A study carried out by González *et al.* [91] confirmed this behaviour, with samples exposed to oxidative environments showing more signs of damage than the ones engulfed in an inert gas. This means that the definition of the thermal cycling environment has a strong effect on the damage mechanisms involved in this fatigue scenario. The tubes considered in this thesis were cycled in a nitrogen environment, with some cycles at atmospheric pressure and others under high vacuum, meaning that the observed damage should be lower than what would be encountered in the presence of oxygen.

3.4.2 Mechanical Properties

When materials are exposed to thermal cycling, an important outcome of the thermally induced stresses and other phenomena caused by thermal fatigue is the variation of its mechanical properties. In the previous section, as the different stages of damage that composite materials go through during thermal cycling are described, there are brief references to the correspondent changes to its mechanical properties during those phases. As mentioned above, the mechanical properties are not catastrophically altered during the

first two stages of damage. With growing occurrences of fibre rupture and more severe delamination in the final phase of fatigue, mechanical failure occurs rapidly. It is relevant to perform a more detailed assessment of how the mechanical behaviour is expected to vary under these conditions. The CFRP tubes under the scope of this thesis were tested under compression and four point bending, so the focus of this section will not deviate significantly from strength and stiffness assessments of composite exposed to thermal cycling.

Meng et al. [85] inspected the mechanical properties of unidirectional and quasi-isotropic CFRP laminates after 150 cycles between -196ºC and 25ºC. Uniaxial tensile tests showed that the tensile strength dropped around 1.4% for the quasi-isotropic specimen and 2.4% for the unidirectional sample. The tensile modulus did not show any noticeable change. The drop in flexural properties was more severe, with both laminates having its flexural strenght decline by 10%.

Asai et al. [88] followed the evolution of the tensile modulus with the exposure to thermal cycling of $[0/30/90/-30/0]_{4S}$ CFRP laminates. After 20 cycles between -170ºC and 120ºC the specimens already presented a degradation that remained constant until 100 cycles, showing signs of saturation in the decay of the tensile modulus after a 3% loss. Crack density stabilised after 50 cycles, and at 100 cycles delamination was present in some ply interfaces.

Kobayashi et al. [53] performed three point bending tests on $[0/30/90/-30/0]_{4S}$ CFRP samples after thermal cycling between -170ºC and 120ºC. The bending modulus decayed around 3% after 100 cycles, and a drop was already noticed after 20 cycles. Through the visual inspection of this sample after intervals of 20 cycles, the authors concluded that delamination had a much higher influence in the decrease of the bending modulus than transverse matrix cracks. Crack density stabilised at 70 cycles.

Yeh and Won [90] assessed the tensile properties of multiple quasi-isotropic CFRP laminates along 400 cycles between -196ºC and 120ºC. This extreme temperature interval lead to losses in tensile strength from 4% to 8.5%, however, the tensile modulus appeared to be unaffected. The adopted laminates had a very high sub-laminate repetition, which might explain why microcracking was only observed after 100 to 200 cycles.

Brown [56] found that the tensile modulus of $[0/45/90/-45]_S$ CFRP specimens suffered minimal variation even after 3000 cycles between -160ºC and 120ºC, in a point where crack density was well into the saturation stage.

Park et al. [54] studied the influence of thermal cycling between -175ºC and 120ºC in unidirectional CFRP samples with three distinct fibres. After 2000 cycles, the flexural strength of two of the lamintes decreased more than 10%, while a third composition only decreased around 1%. The flexural modulus decreased by 22%, 13% and 0.4%. The

laminates with the smaller variation in these two properties were not the same, and these unexpected results were justified by the analysis of the failure modes that were more peculiar in the samples with smaller variation. Tensile strength decreased from 7% to 11%, while the tensile modulus was reduced between 2% and 7%. The decrease of compressive strength and modulus fell in the same intervals that the tensile properties, but for laminates with the same fibre, the compressive properties showed a higher decay.

Cuong et al. [92] encountered a decrease in the tensile modulus of 12% in $[0/90]_S$ CFRP laminates cycled 120 times between -195ºC and 80ºC. After 40 cycles, the decrease in modulus was already established, but tensile strength showed the same value after 120 cycles, with some significant variations along this period. This study is based on the results for 40 different samples that showed a particularly high variance in the results for tensile strength, which was not the case in the assessment of the elastic modulus, advising caution in any conclusions drawn from the results for tensile strength.

Yu et a. [86] exposed carbon/bismaleimide unidirectional samples to vacuum thermal cycling between -140ºC and 140ºC for 283 cycles. The transverse tensile strength dropped 9% in 95 cycles, and became stable onward. The flexural strength showed a particularly interesting evolution, as it rose around 8% in the first 48 cycles, and decreased back to its initial value after 98 cycles. The explanation of the authors for these results is perfectly aligned with most studies and adds some relevant details that are coherent with the characterisation of thermal behaviour of composites performed along this chapter. In this study, the T_g of the laminate was also assessed along the various cycles, and it was found that the material was not completely cured in the beginning, as its T_g rose around 10ºC after 48 cycles, and 20ºC after 283 cycles. This means that the laminate underwent further cross-linking, improving the properties of the bismaleimide matrix. On the other hand, vacuum thermal cycling aggravates matrix loss, which accelerates the progression of damage. This means that the matrix was under two competing factors - one enhanced its properties, and the other increased damage. Transverse tensile strength in an unidirectional laminate is a matrix-dominated property, and the effect of post-cure can not compensate the damage created by vacuum thermal cycling in a critical transverse loading scenario, which justifies the rapid drop verified in this property. Bending tests are not so dependent on the matrix, although they still rely on it. The damage induced by flexural tests is dependent on the tensile strength of the fibres in the area under extension, and on the compression resistance of the matrix in the upper zone. Additional cross-linking improves the elastic modulus of the polymeric matrix, which might explain the initial rise in the flexural strength of the laminate. However, as cross-linking reaches saturation and damage progresses further, defects in the matrix such as fibre-matrix debonding can overpower any advantage of post curing and reduce flexural strength.

In the previous section, the description of fatigue induced damage makes clear that the matrix is the target of most damage mechanisms, especially in the first stages of fatigue, and when fibres start to become significantly affected, the laminate quickly reaches failure. The composite specimens considered in the studies above were far from reaching failure, meaning that fibre-dominated properties are not expected to show notorious decreases, and properties that rely more on the matrix properties, albeit still immensely dependent on fibre-matrix bonding, are not expected to fail catastrophically either. Tensile properties are mainly fibre-dominated, so it is no surprise that decreases in the tensile strength and modulus are minimal and probably most affected by fibre-matrix debonding. Flexural properties have a less biased influence of each constituent, while still mainly defined by the tensile strength of the fibre - nonetheless, flexural strength and modulus do appear to present slightly higher losses. Properties that rely more substantially on the matrix characteristics and fibre-matrix bonding, such as torsional and compressive response, are not popularly characterised in the literature, but are expected to suffer more significantly than fibre-dominated properties.

3.4.3 Glass Transition Temperature

The glass transition temperature, T_g, establishes a reference above which the resin properties can change drastically - making this a crucial point in the characterisation of a composite system that must withstand extreme temperatures. Composite components expected to withstand the severe conditions of the space environment need to show a degree of thermal stability that guarantees a preservation of its properties throughout its life cycle, so it is recommendable that the glass transition temperature does not lower when exposed to temperature variations. A summary of experimental studies carried out on this topic follows.

The T_g of CFRP samples studied by Brown [56] increased from 156ºC to 160ºC after 3000 cycles between -160ºC and 120ºC, matching the T_g indicated by the manufactured for the utilised epoxy resin.

Yu et al. [86] verified a significant increase of T_g in carbon/bismaleimide specimens exposed to vacuum thermal cycling from -140ºC to 140ºC. After 283 cycles, T_g rose from 233ºC to 250ºC. The authors indicate that additional cross-linking must have occurred to justify this higher glass transition temperature. However, they also warn that excessive cross-linking might lead to a degradation phase that worsens the mechanical properties of the matrix while appearing to increase T_g.

Park et al. [54] assessed the evolution of T_g in three unidirectional laminates with different fibres along 2000 cycles between -175ºC and 120ºC. Only one of the composite systems showed a significant alteration in T_g, going from 218ºC to about 200ºC after 500

cycles, maintaining a steady value up to 2000 cycles. The authors justify this behaviour by pointing out that exposure to thermal fatigue can lead to chain scissioning which causes structural changes to the polymeric chains and affects the glass transition temperature.

Mahdavi [19] reported the behaviour of an unidirectional and a woven CFRP laminate along 350 cycles between -196ºC and 140ºC. The unidirectional laminate presented a small rise of 1.6% in T_g after 150 cycles, followed by a significant decline of 7.4% with additional 200 cycles - which translates to a 13ºC drop in T_g, that ends at 207ºC. Mahdavi credits the initial rise in T_g to additional cross-linking of the resin matrix. The initial degree of cure of the laminates was assessed, and the unidirectional specimens showed that they were 92% cured, which is coherent with the hypothesis raised by the author regarding post-curing during thermal cycling. These specimens did not show any signs of microcracks in the first cycles, and their presence was only significant at observations after 350 cycles. The author credits matrix damage as the reason for a drop in T_g after its early rise. The results for the cross-ply laminate are quite divergent, but the author refers to the same mechanisms as causes for changes. The T_g of the cross-ply specimen dropped 3.6% after 30 cycles, but increased again up to the initial value after 200 cycles. The initial degree of cure of these laminates was of 97%, and microcraks were found after just one thermal cyle. Mahdavi justifies the early drop in T_g with the early progression of damage in the matrix, and credits the following rise to the effect of post-curing. TMA analysis was performed for both laminates, and it was found that the elastic behaviour of the polymer gained prominence over the the viscous phase along the 350 cycles, which indicates that further cross-linking occurred throughout the entire thermal fatigue event, as this is a consequence of lower chain mobility - the same was reported in [86, 93]. Curiously, this indication of additional cross-linking through the observation of the storage and loss modulus did not always result in a higher T_g.

As T_g is a property so intrinsically connected to the molecular structure of the polymeric matrix, it is understandable that changes in its values are open to subjectivity when it comes to the justifying its alteration. However, there appears to be a consensus on the two competing factors that result in changes of the glass transition temperature - post-curing caused by additional cross-linking and matrix degradation. The studies presented on this matter agree that, if the initial degree of cure is not of 100%, additional cross-linking may occur in the first cycles, leading to higher T_g and, eventually, an increase in matrix-dependent mechanical properties. This is coherent with the information found in section 3.3.3, where higher temperatures are confirmed to potentiate curing reactions by the correspondent higher molecular mobility. Nonetheless, the overall expectancy is that, after hundreds or thousands of thermal cycles, the eventual increase in the degree of cure can be overshadowed by the damages originated from thermal cycling which degrade T_g.

After this analysis, it is appropriate to highlight that although it looks certain that thermal cycling can improve T_g by further cross-linking, the point at which degradation occurs and what mechanisms are behind it seem to be still under some uncertainty.

3.4.4 Coefficient of Thermal Expansion

If the coefficient of thermal expansion of the filament wound struts under study were to change while in orbit as part of the frame of a satellite antenna, the whole structure could be compromised by the unexpected strains of those components. This application is one of endless cases where the dimensional stability of the composite components needs to be guaranteed during its entire exposure to the extreme conditions encountered in low Earth orbit. To better understand the changes in the coefficient of thermal expansion that thermal cycling can provoke, one can delve into the studies that tackle that problematic.

The transverse and longitudinal CTE of carbon/bismaleimide unidirectional laminates as a function of temperature after exposure to a different number of thermal cycles between -140ºC and 140ºC was interpreted by Yu et al. [86]. The authors strongly believe that the state of the fibre-matrix interface bond is a decisive factor in the thermal expansion of composites, and credit changes in that property to the debonding phenomena. Both transverse and longitudinal CTE were unaltered after 48 cycles. The advance of thermal cycling is expected to be associated with the progression of damage mechanisms such as fibre-matrix debonding, meaning that fibre-dominant behaviour can become more influenced by the matrix. The variation of transverse CTE with temperature did become much higher with further thermal cycling, which approximated the behaviour of the composite to the observed response of the neat resin system. This is due to interfacial debonding, which decreases the degree of constraint that the fibres place the matrix under. The longitudinal CTE is much more dominated by fibre behaviour than transverse CTE - as it is explained in section 3.3.1. This is coherent with the results encountered in [86], where the longitudinal CTE suffered a much more extreme variation with thermal cycling than the out-of-plane expansion. Yu et al. highlight that in a fibre-dominated property, freeing the matrix through debonding mechanisms will naturally result in higher changes than the ones observed in properties where the matrix originally has a more significant weight.

Gao et al. [93] reached similar conclusions to the study above. Unidirectional CFRP specimens were thermal cycled between -140ºC and 140ºC for 351 cycles. Changes in the transverse CTE were very small, but still indicative of some fibre-matrix debonding. The longitudinal CTE presented extreme changes in its behaviour over a temperature range after 351 cycles - the laminate went from expansion during cooling, which is the expected behaviour for CFRP composites, to significant contraction. This means that the expected fibre-matrix debonding during thermal cycling has massively increased the influence of

the matrix behaviour in the resultant longitudinal CTE.

Others experiments have found completely opposite results. Shin et al. [94] encountered that the longitudinal and transverse CTE of unidirectional CFRP specimens decreased significantly after exposure to vacuum thermal cycling, particularly at higher temperatures. The authors credit this behaviour to the matrix loss that occurs during thermal cycling, which increases the fibre volume fraction and thus enhances its weight in the resultant thermal expansion. Brown [56] and Asai et al. [88] performed similar studies and also found that the longitudinal CTE became more negative in CFRP samples, which confirms that the influence of the fibres grew larger.

The complexity of the degradation phenomena that composite materials undergo during thermal cycling is still very present in the study of its effect on the thermal expansion coefficient. Regardless, two competing mechanisms emerge in most studies. The damage progression in composites can lead to fibre-matrix debonding, which is expected to lift the constraints imposed on the matrix by the reinforcing fibres and thus concedes a higher influence of the matrix behaviour in the overall expansion of the laminate. However, if the working environment leads to a significant amount of matrix loss, the opposite can occur, with the increase in fibre volume fraction highlighting the fibre response even further.

The review performed up to this point on the effect of thermal cycling on composite materials showcases, once again, their highly complex behaviour. The progression of damage in composite systems is a particularly interesting topic, as it is quite unique to this field, posing exciting challenges in the characterisation of these materials. The main ideas that can be extracted from the last sections start with an awareness of how damage progression is delicately intertwined with losses in mechanical properties. Although transverse matrix cracks propagate quickly with a few number of cycles, the mechanical properties do not tend to present a catastrophic drop. The mechanical behaviour is immensely dominated by the fibres and the fibre-matrix bonds. It is only when debonding phenomena start to occur that significant mechanical losses are registered. The same seems to apply to the coefficient of thermal expansion, although matrix loss may influence this behaviour as well. The glass transition temperature is, out of the studied properties, the one which seems to be less connected with damage itself, as it is dependent on the chemical reactions induced by thermal cycling.

Chapter 4

Experimental Characterisation

Every choice made during the manufacturing stage of the filament wound struts, which is concisely described in section 4.1, defines the obtained physical and mechanical properties for those composite components. Furthermore, it is crucial to comprehend if the produced tubes are capable of withstanding the conditions encountered while in Earth's orbit. The best way to evaluate the influence of the production stage in the component's behaviour, and assess if it is capable of preserving those same properties while exposed to operational conditions, is by conducting comprehensive experimental studies.

At this stage of development, the simulation of the space environment is reduced to the exposure to thermal cycling - one of the critical conditions encountered while in orbit, whose effects in polymer matrix composites are significant. Some tubes were then exposed to thermal cycling procedures, reported in section 4.2, as a mean of examining the consequences of this environment on the properties of the CFRP tubes. Section 4.3 outlines the non-destructive inspection methodologies employed to grasp a detailed look into the microstructure of the tubular specimens - microscopic observation - and the techniques selected to identify damage progression due to thermal cycling - x-ray radiography and thermography. Another important indicator of the effect of thermal cycling is the alteration of its mechanical properties. Taking into consideration the role of these tubes in the frame of a large deployable antenna, the compression and flexural properties are evaluated, and the procedures for the adopted tests are presented in section 4.4. In this study, the thermal behaviour is mainly evaluated by the coefficient of thermal expansion and the glass transition temperature - the methods utilised to measure those properties are indicated in section 4.5, and the results can offer evidence of the influence of the production parameters and the resistance of these properties to thermal fatigue.

4.1 Manufactured Struts

Before delving into the experimental characterisation of the filament wound tubes, it is important to know its constituents, the selected layup and the chosen curing stage. The CFRP tubes are part of the frame of a deployable space antenna, where they are mounted in titanium end-fittings. These metallic end-fittings suffer a positive expansion while heated, which means that, to maintain an excellent dimensional stability, the composite struts must compensate that response with a longitudinal contraction. Besides that, due to the geometry of the deployable frame, compression and flexural behaviour of the struts are identified as its most important mechanical properties. The tubes and end-fittings are open on both ends, allowing air to circulate freely inside of them, which means that there is no pressure differential between the inside and outside of the tubes, and thus no concerns regarding bursting strength are applicable.

Due to design impositions, the struts need to present very high longitudinal strength and equally large elastic modulus. Depending on their production process, carbon fibres can present very high strength or very high elastic modulus, but usually they do not present both. When carbon fibres have an elevated degree of crystallinity - which is typically the case of graphite fibres with around 99% of carbon in its composition - its highly oriented structure leads to a very high tensile modulus. However, stress concentration occurs at the grain boundaries, and promotes crack propagation. On the other hand, fibres with a more irregular dispersion of its crystals, which is the case of carbon fibres with lower carbon contents, obstruct crack progression and present a higher strength. The irregularity of its crystalline structure, however, does not allow for a tensile modulus as high as the one verified in graphite fibres. Taking into account this limitation in fibre selection, the requirements of this project lead to an hybrid proposition where high strength (T1100) and high modulus (MJ55) fibres are combined at an equal percentage. The chosen epoxy matrix system is composed of Araldite® LY556 epoxy resin, Aradur® 906 anhydride hardener and DY070 imidazole accelerator. The selection of the matrix, besides providing excellent adhesion properties with the carbon fibres, was based on its flight heritage. The resulting laminate is expected to present a fibre volume fraction around 65%. The main properties of the chosen fibres and matrix system are presented in tables 4.1 and 4.2.

Table 4.1: Properties of the adopted carbon fibres from Torayca®.

Fibre	Tensile Strength	Tensile Modulus	CTE	Carbon Fraction
T1100	7000 MPa	324 GPa	-0.5·$10^{-6}K^{-1}$	>96%
M55J	4020 MPa	540 GPa	-1.1·$10^{-6}K^{-1}$	>99%

Table 4.2: Properties of the hot curing epoxy matrix system from Huntsman®.

Matrix System	Tensile Strength	Tensile Modulus	CTE[1]
Araldite® LY556 Aradur® 906 DY070	45 - 60 MPa	2.7 - 3 GPa	$\approx 60 \cdot 10^{-6} K^{-1}$

[1] Collected from experimental studies on similar matrix systems.

The tubes are obtained by wet filament winding in a helical horizontal filament winding machine. Again, taking into consideration the project requirements, the defined layup favours low winding angles, so that a slightly negative linear coefficient of thermal expansion is obtained, and mechanical properties in the axial direction are maximised. The adopted layup starts with two $\pm 10^{\circ}$ layers, followed by one $+85^{\circ}$ layer, four additional $\pm 10^{\circ}$ layers and one final sacrificial -85° layer. The $\pm 10^{\circ}$ ply is referred here as one layer because, recovering the ideas transmitted in section 2.3, when the carriage moves to one end, it lays a fibre band on the mandrel in a 10° angle, and when it moves to the other end, a band covers the mandrel at -10º, meaning that every pair of 10° and -10º plies are interwoven and created simultaneously. The 85° layers, which fit in the category of hoop winding, can be performed in one single carriage movement. The hoop layers help compacting the laminate and aid in the demolding step by promoting some transverse expansion during cooling. In fact, initial iterations of the tubes could only be demolded with specialised accessories, but by manipulating the order at which the hoop layers are wound, it became possible to extract the struts by hand, without exerting significant pressure. This was an important breakthrough because the forced removal of the tubes from the mandrel lead to cracks and warping. The role of the hoop layers will be a point of higher interest in future development stages, as the transverse coefficient of thermal expansion also needs to fit into strict requirements. The final -85° layer is sacrificial because the tubes go through a centerless grinding process to achieve a better superficial finish after curing and meet the dimensional tolerances. The concern with surface roughness is related to additional components that should slide along the exterior surface of the struts.

After the winding process is complete, and before curing, the tubes are wrapped in a shrink tape that contracts during cure, promoting compaction of the laminate. By doing so, this tape potentiates the expulsion of volatiles and excesses of resin, which contributes to a saner microstructure. The adopted curing stage aims at achieving the highest possible glass transition temperature. The curing cycle recommended by the manufacturer to achieve the largest T_g is composed by an initial dwell at 120ºC for 2 hours, followed by an intermediate step at 160ºC for another 2 hours, and ending with a 2 hours stage at 180ºC, which should

result in a T_g between 165ºC and 180ºC. The tubes are cured in an oven at room pressure, counting on the compression exerted by the tension of the wounded layers and the help of the shrink tape to obtain a compact structure. The use of autoclaves is not very common for filament wound components, even though it is expected to result in a lower percentage of voids. These matters are discussed along section 2.2.6, where another crucial detail is noted - the composite tubes need to be slowly rotated while in the oven so that there is no resin accumulation and dripping at the bottom.

The obtained tubes are 1.80 meters long, with a 16mm external diameter and 1mm thickness, which represents a very thin geometry. As the description of the layup selection implies, the tube's walls are not symmetric, however, as thoroughly discussed along section 3.3.2, tubular components tend to mitigate the effect of bending-extension coupling as geometrical symmetry is inherent to a closed geometry of this kind. Although some authors believe that caution is advised in the adoption of unsymmetric laminates in composite tubes [40], Peters [7] states that, not only are unsymmetric layups not problematic in tubular laminates, but they also create advantages in filament wound components. This author specifically recalls the cases where exterior hoop layers aid compaction and lower the resin fraction of cylindrical parts, which is similar to what happens with the filament wound tubes under study. It should be noted that if portions of the tube's wall are cut to resemble flat specimens for test procedures, the mitigation of the bending-extension coupling will not occur and warping forces will affect the specimen, especially one with such thin walls.

4.2 Thermal Cycling

Artificial satellites and other spacecrafts encountered in Earth's orbit go through, among other things, a cyclic rise and fall in temperature as their exposure to the Sun changes - a topic covered in section 3.1. Thermal cycling has a very dominant effect in the degradation of composite materials in the space environment, and at this stage of development of the studied CFRP tubes, its consequences are the ones under the spotlight. To simulate the conditions encountered while in orbit, the filament wound struts can be exposed to thermal cycling and thermal vacuum cycling in thermal chambers. From this point onward, samples not exposed to this procedure are referred to as BOL (beginning-of-life) and the ones that went through it are designated as EOL (end-of-life). In the aerospace industry, specimens that were thermal cycled, but not exposed to any other environmental simulations, are not usually designated as EOL - however, to promote clarity throughout this work, this is the adopted nomenclature.

Two distinct procedures - thermal cycling (TC) and thermal vacuum cycling (TVC) -

were performed at ISQ in Abrantes, Portugal. The general conditions for these stages are covered in table 4.3, where the main difference between them is evident - the pressure at which each procedure is performed. The different atmosphere in each stage has natural consequences in the heat transfer mechanisms that take place. Thermal cycling is performed in an ambient pressure chamber where temperature changes are obtained through forced convection of the inner N_2 atmosphere. While heating phases are mainly controlled by manipulating the temperature of the circulating gas, cooling results from the insertion of liquid nitrogen. Both phases need to respect the predefined average temperature change rate of $\leq$ 5ºC/min.

Table 4.3: Conditions defined for the thermal cycling (TC) and thermal vacuum cycling (TVC) stages.

Stage	Cycles	Pressure	Temperature		Dwell time
			T_{min}	T_{max}	
TC	90	Room pressure	-160ºC (+0/-5ºC)	150ºC (+5/-0ºC)	$\geq$ 10min
TVC	10	$\leq 1 \cdot 10^{-5}$mbar	-150ºC (+0/-5ºC)	150ºC (-5/+5ºC)	$\geq$ 10min

Convection is no longer a significant heat transfer mechanism during thermal vacuum cycling, where conduction and radiation are responsible for temperature variations. The vacuum chamber is equipped with thermal plates controlled by an inner liquid nitrogen system and electrical heating. The defined thresholds for the average temperature change rates are the following: $\leq$ 3ºC/min during heating and from T_{max} to -100ºC, $\leq$ 1.5ºC/min from -100ºC to -140ºC, and $\leq$ 0.5ºC/min from -140ºC to T_{min}. In both procedures, the temperature of the specimens is monitored by thermocouples in contact with various tubes inside the chamber. Before thermal cycling, the tubes are cleaned with IPA lint-free wipes to remove any contaminants.

It should be noted that thermal vacuum cycling is expected to cause more severe consequences to the filament wound tubes as it leads to outgassing. Only 10 thermal vacuum cycles were performed due to scheduling constraints and under the assumption that the first cycles are the most decisive in the particular consequences of a vacuum environment. The aggravating effect of a vacuum environment in damage progression is quite unpredictable, and as section 3.4 shows, although damage does tend to advance at a higher rate in the first stages, it is uncertain at how many cycles a saturation level is reached. With this in mind, it is not possible to state that the consequences for the CFRP tubes would be the same if a higher percentage of the thermal cycles were under vacuum conditions. Nonetheless, composite systems exposed to 100 thermal cycles at room pressure commonly

show signs of clear degradation, and often reach crack density saturation, meaning that the adopted procedure is expected to be a meaningful representation of the specimen's resistance to temperature variations. The temperature range for these cycles was initially defined according to typical survival temperatures for applications of this kind (+160ºC to -160ºC) and later adjusted due to observed constraints. The maximum temperature was too close to values obtained for the glass transition temperature of the CFRP tubes meaning that some overshoot during heating could have nefarious effects. The minimum temperature for TVC was increased because going below -150ºC with the available equipment took multiple hours and the effect of this change is expected to be negligible.

Table 4.4 shows the number of samples extracted from tubes that underwent thermal cycling stages destined to different testing procedures. The EOL specimens for the assessment of CTE only went through thermal vacuum cycling and not thermal cycling at room pressure due to scheduling issues - this aspect is taken into account in the analysis of CTE. The results obtained for EOL samples are compared to the ones from BOL samples along chapter 5 to comprehend the effect of thermal cycling.

Table 4.4: Number of specimens cut from tube sections exposed to TC and TVC stages, designated as EOL (end-of-life) samples.

Procedure	No. of samples	TC	TVC
Compression Test	20	Yes	Yes
Four-Point Bending	10	Yes	Yes
TMA (CTE)	9	No	Yes
DSC (T_g)	2	Yes	Yes

4.3 Non-Destructive Inspection

For the composite struts studied along this thesis, non-destructive inspection can play an important role at two different moments - after the production stage, and after simulation of space environment conditions. The components produced by wet filament winding are especially prone to the appearance of voids, as they are often cured in ovens at room pressure. Defects of this kind must be a cause of concern because they can have an important influence in the physical and mechanical properties of composite systems. Identifying them facilitates the understanding of what production parameters should be altered so that the properties of the composite component are improved, as a result of a saner microstructure. A similar premise applies to parts exposed to ageing

processes. The progression of damage mechanisms in composite systems is identified in section 3.4.1 as an expected result of exposure to thermal cycling. Evaluating the state of the material after these procedures allows a deeper understanding of the phenomena associated with the conditions encountered in the space environment. Assessing the progression of damage can even be correlated with consequences in the properties of the material without any destructive methodologies being employed. In this work, the microstructure of the composite struts is inspected by microscopic observation, and the presence of damage resulting from thermal cycling is further investigated by two methodologies: x-ray radiography and thermography.

4.3.1 Microscopic Observation

To obtain a detailed look into the microstructure of the composite struts, optical microscopy was performed at FEUP, which fits into the category of visual inspection. Although microscopy demands some material removal for better results, it is still acceptable to catalogue it as a non-destructive inspection technique.

For the cross-sectional area of the tubular specimens to clearly show the different layers and constituents, polishing operations were performed. Due to scheduling constraints, only one BOL and one EOL sample were studied, and surface preparation was not ideal. Embedding the specimens in resin blocks is a recommendable method before polishing operations, as it allows a better positioning of the samples during material removal, resulting in less unwanted marks and a clearer image. In this case, 5mm long tubular specimens were cut and directly grinded and polished with pads of increasingly fine abrasive particles. The cross-sectional cuts of each specimen were then inspected in an optical microscope. Although not ideal, surface preparation still resulted in lustrous surfaces for the CFRP samples, which allowed the capture of detailed images.

4.3.2 X-Ray Radiography

The radiolucency of carbon fibres turns CFRP components into good candidates for x-ray radiography in search of damage such as transverse matrix cracks. The available equipment at FEUP was a Satelec X-Mind Intraoral X-Ray for dental applications, which although unorthodox, represents a highly capable choice. Each sample is soaked in diiodomethane for at least 30 minutes. This is a high capillarity liquid that penetrates on the cracks of the composite laminate and has a high attenuation effect on x-rays, meaning that during image acquisition the areas infiltrated by this liquid will show a very different colour from the rest of the material. The samples are placed on top of a Kodak RVG 5100 digital sensor that captures the radiation and transmits the resulting image to a computer.

The captured radiograph is completely dependent of the small acquisition cell - about 3cm long - so the length of the samples is not very important, as long as it can be placed on top of the acquisition sensor. Tubular specimens can be used as the width of the digital sensor is larger than the tube's diameter. After being soaked on diiodomethane, the specimens need to be thoroughly cleaned, inside and out, so that no liquid remains on the surface and alters the resulting image. This penetrating liquid is an excellent choice for this application due to its high opacity to x-rays and ease of penetration, but caution is advised while handling it as it can lead to severe skin burns.

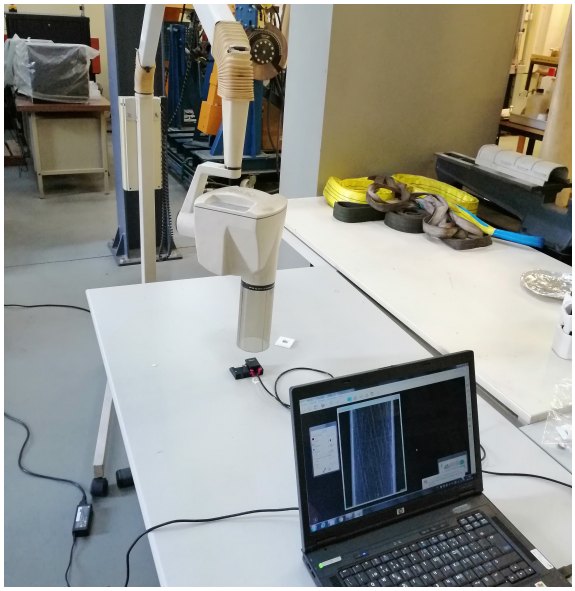


Figure 4.1: X-ray radiography setup.

Figure 4.1 shows the adopted setup, and table 4.5 shows the number of samples considered for this study. To eliminate any effect of variability along the length of the tubes, five specimens about 5mm long were cut from each one.

Table 4.5: Summary of the number of tubes and sections per tube analysed by x-ray radiography.

Group	No. of tubes	Samples per tube
BOL	2	5
EOL	2	5

4.3.3 Thermography

During heating or cooling, areas with cracks will be at a different temperature because the presence of defects alters their thermal conductivity. As thermography captures the

temperature of every surface in frame, it is a possible way of discovering damage in composite materials. For this experiment, a FLIR E60 infrared camera was used at FEUP. The tubular specimens were coupled with heat shrink tubes on both extremities, and forced convection was introduced by an hot air blower. Without an extension of length, it would never be possible to promote uniform heatig throughout the tubular specimen, as the areas closer to the heat source would always be hotter than the opposing ones. Heating takes place until the sample is at an uniform temperature along its length, and cooling occurs naturally by turning off the hot air blower. Images are acquired during both heating and cooling to assess different behaviour along the tubular specimens. The samples prepared for x-ray radiography, presented in table 4.5, are the same available for thermography. Connecting each end of the sample to heat shrink tubes around 100mm long should be enough to promote an uniform temperature along its length.

4.4 Mechanical Properties

The critical mechanical properties of the CFRP tubes are defined by their role in the frame of the deployable space antenna. As mentioned in section 4.1, compressive and flexural behaviour are undoubtedly important design considerations, and the following sections describe the procedures adopted for the inspection of the strength and elastic modulus under those solicitations. Considering the scope of this thesis, the focus of this evaluation falls on comparing the results obtained for specimens exposed to thermal cycling and samples that did not go through any ageing process, correlating any differences with the observed damage mechanisms. Both compression and flexural tests were performed at Applus+, in Spain.

4.4.1 Compression Test

The procedure for the compression test is defined following ASTM D 695-15, which recommends a test specimen length of 25.4mm for tubes with a wall thickness of 1mm. The cut samples are 65.4mm long to compensate for the regions that are bonded to the end-fittings. To avoid crushing, metallic pins with the same diameter as the inner dimension of the tube are also inserted in the extremities of the tubular specimens.

The compression tests are performed at an universal testing machine that controls the crosshead displacement with uniform constant velocity and includes a load cell. Two plates are responsible for the compression load - a fixed lower plate and a spherically seated upper plate. This setup, presented in figure 4.2, is expected to apply an uniformly distributed load to the test specimen, assuring that it remains aligned with the machine axis. The estimated

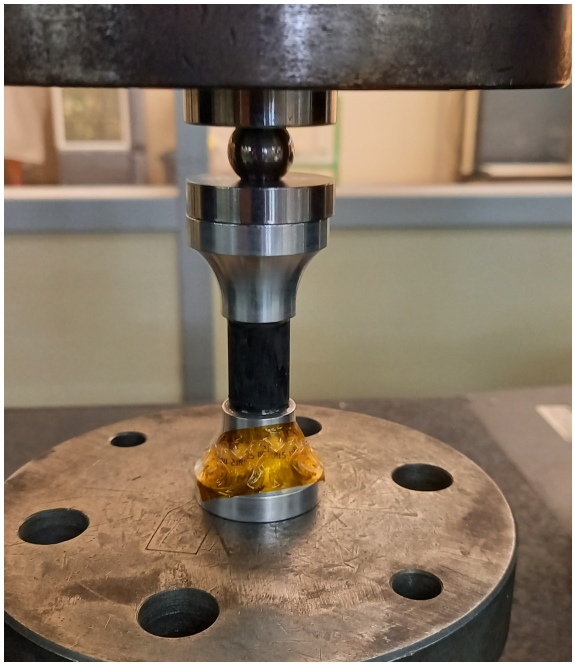


Figure 4.2: Compression test setup.

failure loads of the specimens are expected to be under 100kN, even with a safety factor of 50%. The defined testing parameters are the following:

- 100kN load cell;
- 100N preload;
- test speed of 0.5mm/min;
- data acquisition rate $\geq$ 50Hz;
- test ends when load drops by 40%.

The compressive stress (σ_C) applied to each specimen is obtained through equation 4.1. To achieve more precise results, the inner and outer diameter of every test specimen is measured to calculate its cross-sectional area (A). Some specimens are fitted with strain gauges to assess the compressive modulus (E_C), given by Hooke's Law - equation 4.2. To calculate E_C, two points of the linear elastic domain of the stress-strain curve should be considered, which is expected to be easily attainable given the highly elastic behaviour of CFRP. The amount of BOL and EOL specimens considered for this study are presented in table 4.6. It should be noted that every sample is extracted from a different tube, meaning that any repeatability issues in the production stage will affect the variance of the results.

$$\sigma_C = \frac{F_C}{A} \tag{4.1}$$

$$E_C = \frac{\sigma_C}{\varepsilon_C} \tag{4.2}$$

Table 4.6: Specimens for compression tests.

Tubes	No. of samples	Samples with strain gauge
BOL	20	4
EOL	20	5

4.4.2 Four-Point Bending

In order to evaluate the flexural behaviour of the composite struts, a four-point bending procedure was adopted. This test was defined following the main guidelines in ASTM 6272, but as this standard does not make any particular considerations in regard to tubular specimens, many adaptations had to be performed. Much like the compression tests, the bending tests are performed at an universal testing machine that controls crosshead displacement with uniform velocity and incorporates a load cell. In four-point bending, the specimen lays on two supports and it is loaded at two points, with the latter defining the centre section where the applied bending moment is uniform. In this case, the distance between the two loading points is equal to one half of the support span to maximise the length where axial fibre stress is expected to be uniform. While the lower supports are fixed, the test machine crosshead that holds the loading accessories advances at a constant rate and applies load to the tubular specimen. The test specimens are 300mm in length, falling within the recommendations in ASTM 6272. Longer tubular samples allow higher span-to-depth ratios, which is recommendable in materials of such rigidity. The adopted testing parameters are the following:

- 5, 25 or 50kN load cell;
- 25N preload;
- test speed of 0.5mm/min;
- support span of 260mm;
- load span of 130mm (one half of the support span);
- data acquisition rate $\geq$ 50Hz;
- test ends when load drops by 40% or excessive indentation occurs.

The high rigidity of CFRP coupled with the geometrical particularities of a tubular specimen lead to severe indentation at the loading points if the usual cylindrical punches are used - this was confirmed through numerical simulations and experimental runs, and can be explained by the stress concentration that occurs in the small contact area between two cylindrical components. To reach valid results, new support and loading accessories were designed, which guarantee a higher contact area and perpendicularity between the

specimen's axis and the crosshead displacement. Figure 4.3 shows the test setup with concave supports and loading punches, with the latter presenting a degree of freedom that allows a better adjustment with the tubular specimen throughout the entire test. The implementation of these accessories was successful, as it avoided crushing and indentation at the contact points with the sample.

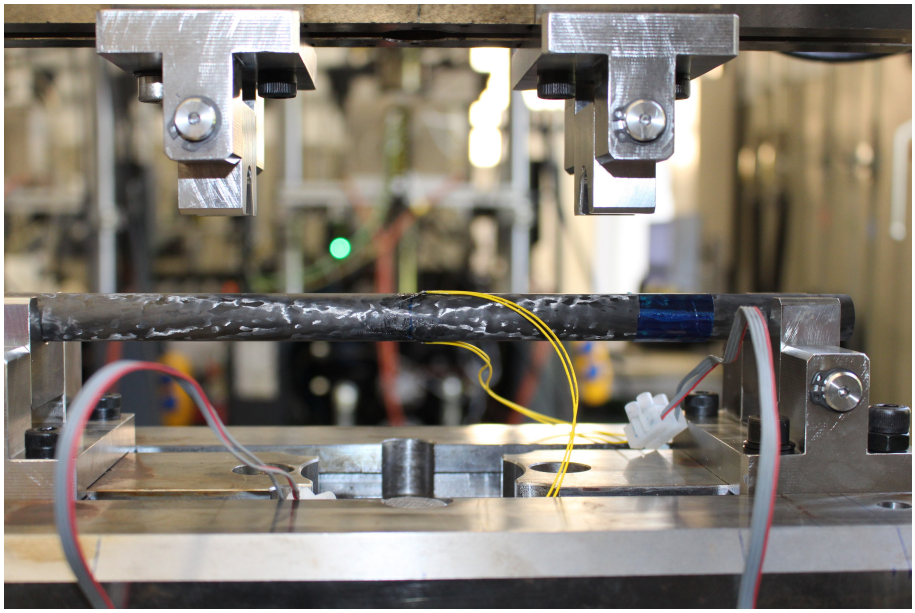


Figure 4.3: Four-point bending test setup.

In bending tests, the deflection is typically measured by a LVDT at the centre point of the loading span, however, due to the high rigidity of the CFRP samples, the maximum displacement is expected to be very small - an hypothesis confirmed during trial runs. This means that calculating the flexural modulus following the methods presented in ASTM 6272, where the value of deflection is considered, can result in quite inaccurate estimations. With that in mind, and given the importance of the flexural modulus in the design, two strain gauges are fitted in the tubular specimens - one at the top, and one at the bottom of the centre of the loading span. This way, the strain in the axial direction of the outside surface is measured with a high accuracy and can be directly utilised to obtain the flexural modulus.

The flexural stress (σ_F) is obtained by equation 4.3, where L is the support span, R is the radius of the tubular specimen and t is its thickness. Similarly to the compression modulus, the flexural modulus (E_F) is obtained by Hooke's Law, considering the strain registered by the strain gauges and considering two points of the elastic domain of the

stress-strain curve.

$$\sigma_F = \frac{F_F \, L \, R}{8 \, \pi \, R^3 \, t} \tag{4.3}$$

$$E_F = \frac{\sigma_F}{\varepsilon_F} \tag{4.4}$$

The number of BOL and EOL specimens considered for this work are presented in table 4.7. Just like in the case of the compression tests, every specimen is extracted from a different tube, which might increase the variance in the results if the production stage lacks repeatability.

Table 4.7: Specimens for four-point bending.

Tubes	No. of samples	Samples with strain gauges
BOL	10	10
EOL	10	10

4.5 Thermal Properties

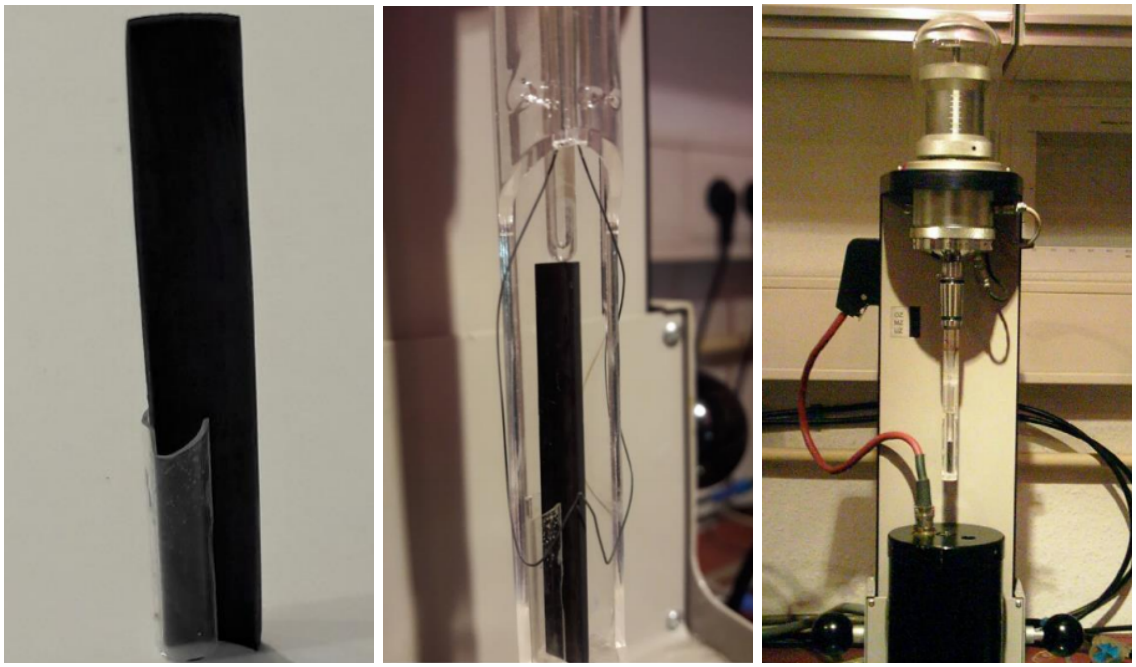
In the study of the thermal behaviour of a composite system, inspecting thermal properties is an evident path to follow. Section 3.2 explores the importance of two factors in particular - the glass transition temperature and the coefficient of thermal expansion. The composite struts will be exposed to extreme temperatures while in orbit, meaning that their T_g must be high enough to avoid any significant loss of mechanical properties at elevated temperatures. Additionally, the deployable antenna represents a high sensitivity structure that should preserve an excellent dimensional stability in a wide range of temperatures, which stresses the importance of the struts' coefficient of thermal expansion. Both of these properties are inspected via the procedures described below to understand if the production choices are pointing in the right direction and to assess if the exposure to thermal cycling jeopardises the value of these properties. Note that, although T_g might not be considered a thermal property by some authors, its pairing with the coefficient of thermal expansion allows thematic coherence, as it is strongly related to thermal events and heavily influences other thermal properties.

4.5.1 Coefficient of Thermal Expansion

The typical operational temperature for the deployable satellite antenna goes from -78ºC to 91ºC, and at this stage of development it is necessary to evaluate the average linear coefficient of thermal expansion in that range. In future phases, the transverse CTE will also be assessed. Thermomechanical analysis (TMA) was the chosen test procedure, performed at WSK, in Germany, in compliance with ASTM E831-6. It consists on the measurement of the length change as a function of temperature. In this test, the specimen is placed in a quartz glass measuring device - of very low thermal expansion - and the strain of the sample is transmitted by a quartz rod placed in a measuring head fitted with a high sensitivity encoder.

The test specimens were not tubular - a 52º section of the CFRP tubes was cut with a 49mm length so that the samples could fit in the quartz holding device. The specimens must stand vertically by themselves without wobbling, which was not verified. For that reason, quartz supports were prepared to stabilise the samples, enabling a vertical stand. The samples are placed in the quartz glass holding device, where a quartz pushrod is lowered until it touches the surface of the sample. The contact area between the hemispherical tip and the top of the specimen is around $1mm^2$, and during the test a 10cN force is applied on the sample. To avoid free fibres and other imperfections at the extremities, the cut samples are carefully sanded, conserving the parallelism between the edges. Figure 4.4 shows the adopted test setup, including a detailed view of the quartz sample support and holding device.

After the specimen is correctly positioned, the low-temperature furnace (appearing in black at the bottom of figure 4.4c) is placed over the holding device. For each sample, one conditioning run and three measurement runs are performed. In the conditioning run, the sample is heated to 100ºC, and remains at that temperature during 10 minutes to remove superficial impurities, exclude structural settling effects and, mainly, remove absorbed moisture. To discard the influence of any run-in and run-out effects, the adopted temperature range was higher than the one considered for the measurements, and goes from -100ºC to 100ºC. With the conditioning run complete, the sample is then cooled to -100ºC at a rate of less than 20ºC/min, and the measurement run consists on the heating phase up to 100ºC at a rate of 5ºC/min. The cooling and heating phases are repeated until the three measurement runs are completed. There are two important corrections made to the measurements: the sample holder correction and the baseline correction. The quartz holding device slightly expands downwards, which influences the strain detected by the quartz rod that is pushed against the sample, mandating that the software adjusts the registered expansion to accommodate that behaviour. The baseline correction comes from the measurement of a flawless piece of quartz glass that should reproduce a straight line



(a) Sample with quartz support. (b) Quartz holding device. (c) TMA dilatometer.

Figure 4.4: Test setup for thermomechanical analysis.

parallel to the horizontal axis. Any fluctuations during this measurement are expected to result from the TMA equipment, and are then eliminated from the measurements of the actual samples.

The linear coefficient of thermal expansion is given by equation 4.5. The results provided by the test house responsible for this procedure are the plot of the length-corrected expansion $\left(\frac{dL}{L}\right)$ with temperature, meaning that the average α_L can be calculated by simply dividing the total strain between -78ºC and 91ºC by the temperature range.

$$\alpha_L = \frac{1}{L}\frac{dL}{dT} \tag{4.5}$$

The samples cut for CTE tests come from only three different tubes. Three BOL samples and three EOL samples were cut from each tube, at different positions - naturally, EOL samples originate from tube sections exposed to thermal cycling procedures. An analysis of the results for samples cut from the same tube might eliminate some variance derived from the production stage and help encounter trends. Table 4.8 summarises the number of samples cut for thermomechanical analysis. It must be reminded that, due to scheduling issues, the EOL samples for the determination of CTE were only exposed to 10 vacuum thermal cycles, and did not go through 90 thermal cycles at room pressure.

An important detail mentioned above regarding the geometry of the test specimens is also worthy of reflection. As mentioned in section 4.1, these filament wound tubes

Table 4.8: Specimens considered for thermomechanical analysis and the correspondent number of measuring runs.

Tube Ref.	No. of samples		Measuring runs per sample
	BOL	EOL	
J	3	3	3
K	3	3	3
L	3	3	3

do not have a symmetric layup, and bending-extension coupling is only mitigated by the closed geometry of the tubular specimens. As these specimens are cut from the tube's wall, they do not present any kind of laminate symmetry, which will result in warping during temperature changes. This additional source of deformation of the test specimens is expected to affect the measurements of the longitudinal coefficient of thermal expansion, as bending will tamper the registered linear strain. This hypothesis was confirmed by FEM analysis performed in Abaqus®, where models with this exact geometry and approximate mechanical and thermal properties showed a linear contraction between its extremities after heating about 10% higher than a model with the same properties and a closed geometry due to warping phenomena. This means that the obtained coefficient of thermal expansion is expected to be more negative than the actual CTE of the tubular components.

4.5.2 Glass Transition Temperature

Following ASTM E 1356, differential scanning calorimetry (DSC) was the chosen method to determine T_g, performed at INEGI. In this procedure, the sample and a reference material are placed in distinct microfurnaces, and the difference in the amount of heat required to increase the temperature of both of them is measured and plotted as a function of temperature. The glass transition is indicated by a step change in the plot, and T_g is extracted as the middle point of that variation. A TA Instruments Q20 DSC module was coupled with a RCS90 cooling system and the samples were heated from 30ºC to 200ºC at a rate of 10ºC/min. The samples are cut into very small 2x2x1mm shapes, so that they are encapsulated and then placed on the DSC module.

In this case, the amount of EOL samples is extremely reduced. Table 4.9 shows that 26 BOL samples were analysed, in contrast with only 2 EOL samples. The EOL samples were cut from the same tube as 3 BOL samples, which might serve as an additional indicator of any substantial change in the value of T_g. Nonetheless, the value of the comparison between BOL and EOL tubes is substantially diminished by the limited analysis of EOL

specimens.

Table 4.9: Number of samples for DSC procedure.

Group	Tube Ref.	No. of Samples
BOL	All available	26
	W	3
EOL	W	2

Chapter 5

Results and Discussion

Experimental results are an indispensable tool in the rigorous characterisation of any material, and their importance is exponentially elevated in the case of composite systems, whose complex micromechanics are particularly hard to fully grasp by numerical simulations. This chapter aims at providing a comprehensive portrayal of the studied filament wound struts by dissecting the information collected in the employment of the experimental procedures described in chapter 4.

This depiction starts with the graphic displays attained by the non-destructive inspection methods available for this work. Section 5.1 presents a detailed look into the microstructure of the laminate via optical microscopy, followed by radiographs that illustrate the consequences of thermal cycling, and ending with a report on the viability of thermography for the case at hands. Section 5.2 scrutinises the behaviour of the tubular specimens under compression and four-point bending, with a special emphasis on the effects of thermal cycling on the material response. The coefficient of thermal expansion and glass transition temperature are then investigated along section 5.3, with brief assessments on the impact of the production parameters on those properties, and a particular focus on the preservation of those characteristics after thermal fatigue. Lastly, section 5.4 provides the ground for a generalised discussion of the most relevant discoveries emerging from the performed analysis.

Just as explained in section 4.2, specimens exposed to thermal cycling procedures are identified as EOL (end-of-life), while samples that did not go through any thermal fatigue are designated as BOL (beginning-of-life).

5.1 Non-Destructive Inspection

This section collects the images captured by microscopic observation, x-ray radiography and thermography in the search for defects corrupting the microstructure and damage resulting from the thermal cycling procedure.

5.1.1 Microscopic Observation

As it is indicated in section 4.3.1, the cross-section of one BOL and one EOL sample were observed under an optical microscope. Figures 5.1 and 5.2 show the results for the BOL specimens, while figures 5.3, 5.4 and 5.5 present the micrographs captured from the edge of an EOL sample. The analysis of both samples clearly evidences the presence of defects that must stem from the filament winding process employed. Figures 5.1a, 5.1b, 5.2e are stellar examples of void presence in the BOL specimen, while the same is verified for the EOL sample in figure 5.3f and every image in figure 5.4. These results show that there are clear improvements to be made in order to avoid such a noticeable presence of voids in the microstructure. Before delving into why voids can have nefarious consequences in composite laminates, other defects can be identified. Figures 5.1a, 5.1b and 5.2a make clear that, in some areas, the outermost layer becomes detached. A highly likely reason for this is the centerless grinding process that the tubes go through to achieve a better surface finish and meet the dimensional requirements. This finishing process was supposed to only affect the sacrificial -85º layer wound as the last ply in the tube, but it is clearly removing plies with axial orientation, as not every ± 10º defined in the layup is visible in the micrographs. Figures 5.1c to 5.1f show a similar problem in the innermost layer. This seems to be a result of demolding from the mandrel. Although demolding is reportedly done smoothly, various scratches are visible in the inside of the CFRP tubes, with some areas showing significant damage. As figure 5.1f shows, a signification portion of the laminate is ripped off in some sections, resulting in a thickness more than 10% smaller than it should be, which can have significant implications on the mechanical properties of these struts.

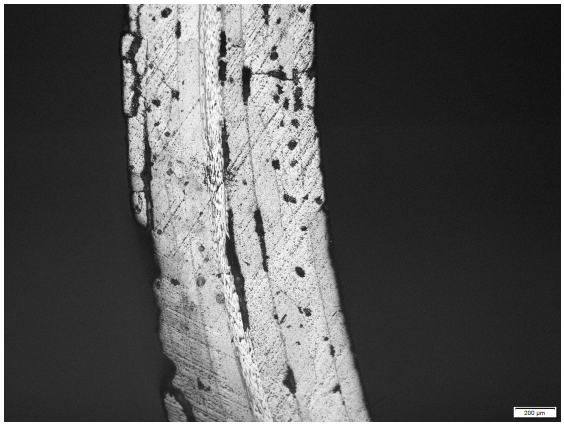
Going back to the presence of voids, the micrographs in figure 5.2 are a testament to the importance of keeping the void volume fraction as low as possible. Even tough not many cracks appear in the BOL sample, there is an undeniable trend among them - the vast majority propagates through voids. The observed transverse cracks are likely to have occurred during cooling at the end of the curing stage. The thermal stresses originated at that point, coupled with the stress concentration potential of the voids, lead to the appearance of cracks before any type of exposure to simulated space environments. The cracks encountered in the BOL specimen that were connected to voids, besides being found

in much higher number, typically displayed larger openings and longer paths than the few cracks that did not pass through any void - like the one in figure 5.2f. This definitely signals the importance of porosity in the propagation of cracks. Reducing the amount of voids in the microstructure is expected to reduce the amount of cracks, or at least shorten their paths and severity.

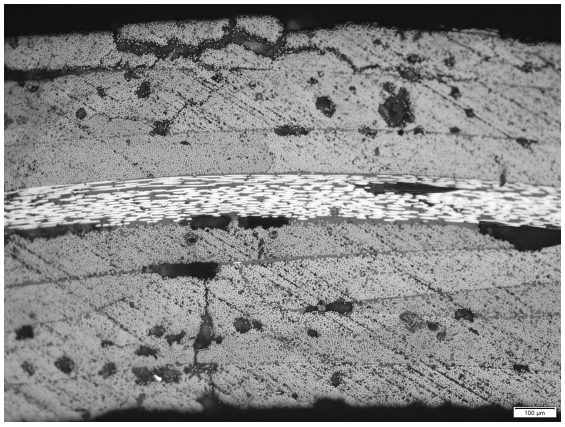
The number and gravity of the intralaminar cracks found in the EOL specimen confirm the vertiginous advance of damage that can occur due to exposure to thermal cycling. In this case, although still identifiable, the propagation of cracks through voids does not occupy such a high percentage of damage found as in the BOL sample. The harsh conditions presented during thermal fatigue lead to multiple cracks that easily pass various layers. The multiple images presented in figures 5.3, 5.4 and 5.5 show a vast combination of damage paths, varying in length, width and degree of attraction to voids. Areas riddled with voids, as the ones depicted in figures 5.4a to 5.4d, have a tendency to show a higher density of cracks, which corroborates the comments made regarding the influence of voids in crack formation in the BOL specimen. This is coherent with the hypothesis of voids acting as stress concentration regions, as thermal stresses resulting from thermal fatigue are also expected to favour relief through these porous areas.

Figures 5.3a, 5.3b and 5.5a show clear examples of how the progression of transverse matrix cracks is often obstructed at the interface between adjacent layers, with damage fully stopping or advancing through the interface before continuing into the next ply. It is also interesting to confirm the appearance of cracks in every layer of the laminate, although the majority of them appears to start at the outermost or innermost layers. Damage in the -85º layer can not be visualised by a cross-sectional cut - a transverse cut, in the direction of the tube axis, is necessary to assess any damage in that ply. Figures 5.5d to 5.5f show the width of different cracks in the EOL specimen, ranging from 10μm to 44μm. While the opening in figure 5.5d is an extreme case of damage likely resultant from previous defects in that region, the vast majority of cracks present a width close to 10μm, like the one in figure 5.5e.

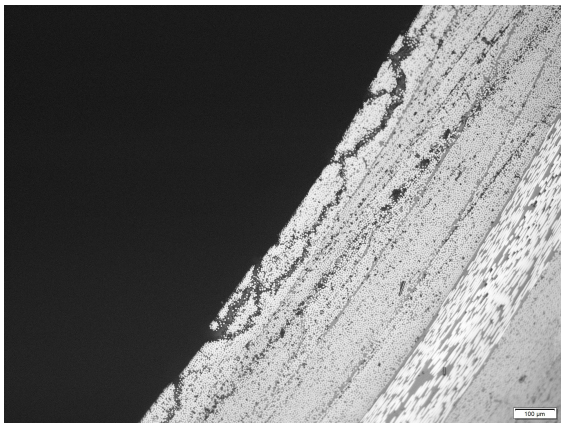
The conditions for this microscopic observations are worthy of some critical comments. As it is mentioned above, only one BOL sample and one EOL sample were observed, which evidently tampers any attempt at finding trends for crack propagation from the images presented in this study. Nonetheless, as the extracted conclusions are completely aligned with findings in literature, particularly the ones presented along section 3.4.1, it is expected that the ideas presented above can be extrapolated to every tube produced under the same conditions.



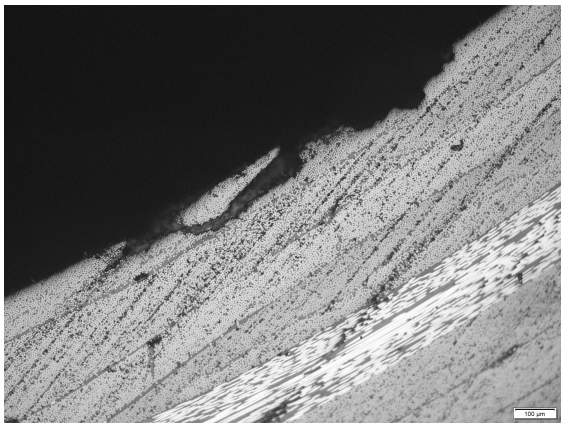
(a) 5x magnification.



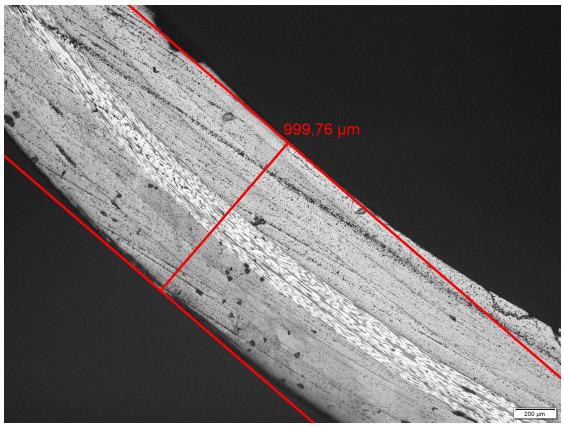
(b) 10x magnification.



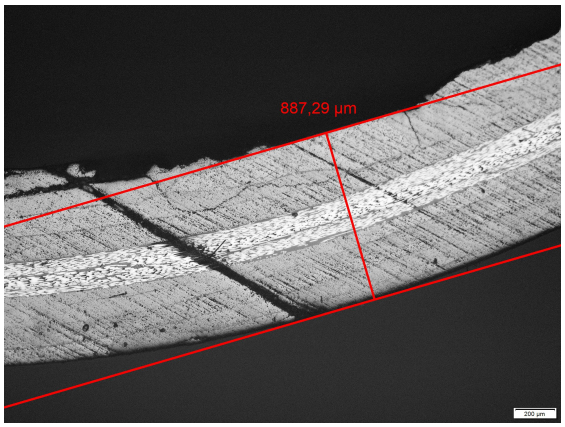
(c) 10x magnification.



(d) 10x magnification.



(e) 5x magnification.

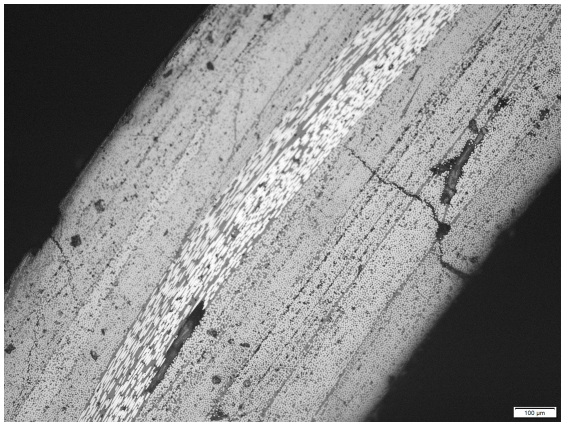


(f) 5x magnification.

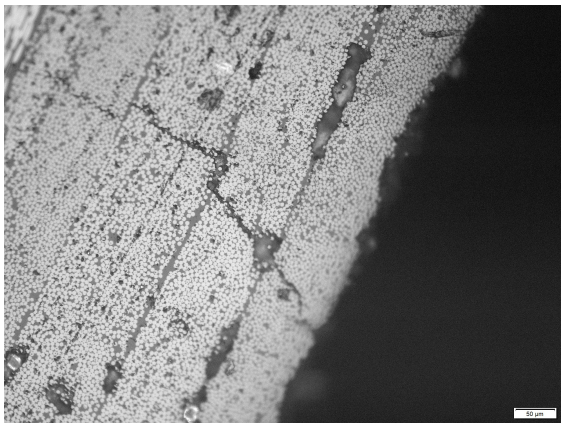
Figure 5.1: Micrographs of one BOL specimen highlighting defects resulting from the manufacturing stage.



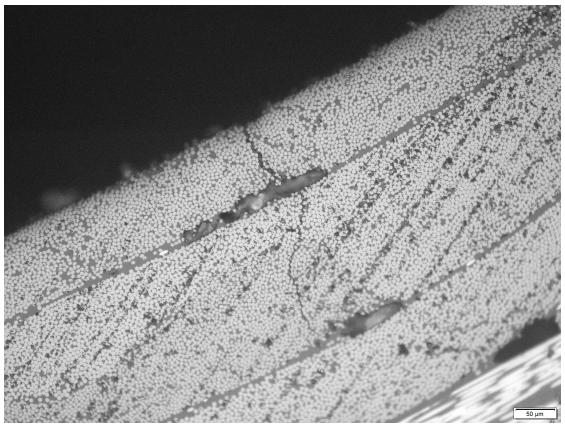
(a) 5x magnification.



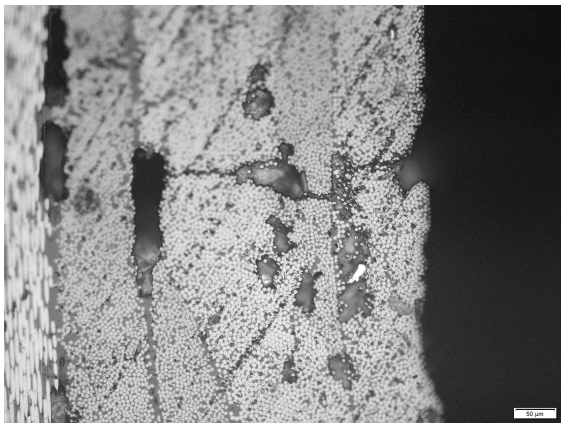
(b) 10x magnification.



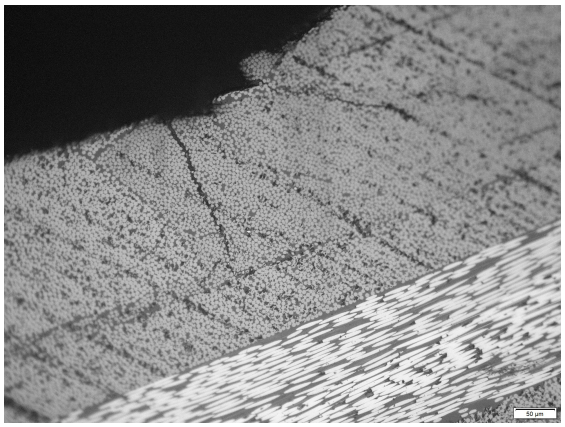
(c) 20x magnification.



(d) 20x magnification.

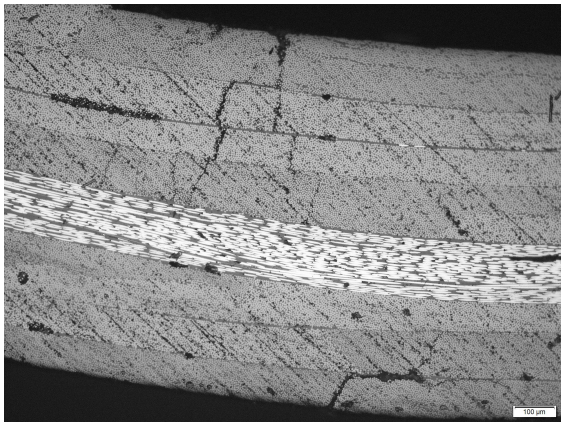


(e) 20x magnification.

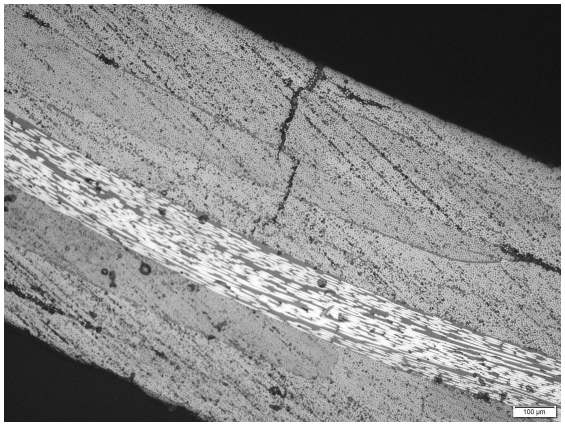


(f) 20x magnification.

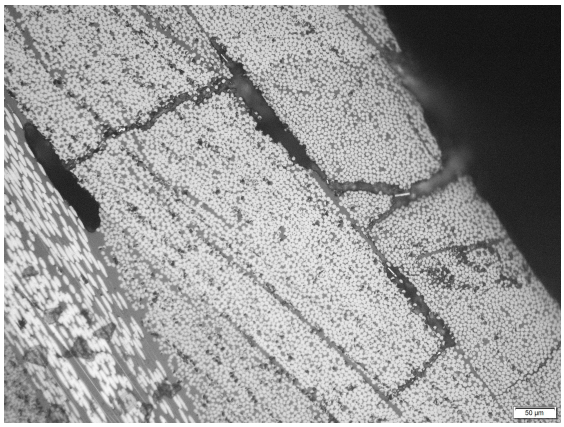
Figure 5.2: Micrographs of one BOL sample showing the presence of cracks before thermal cycling.



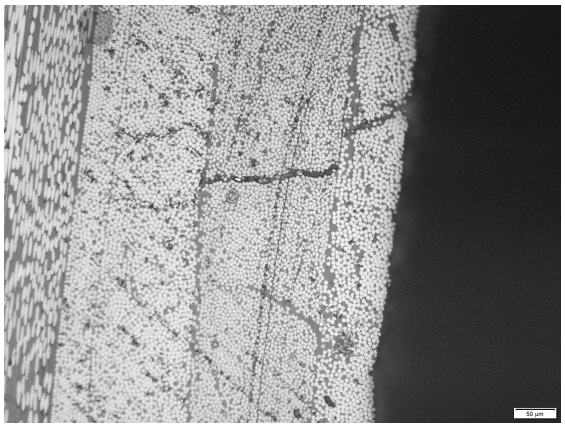
(a) 10x magnification.



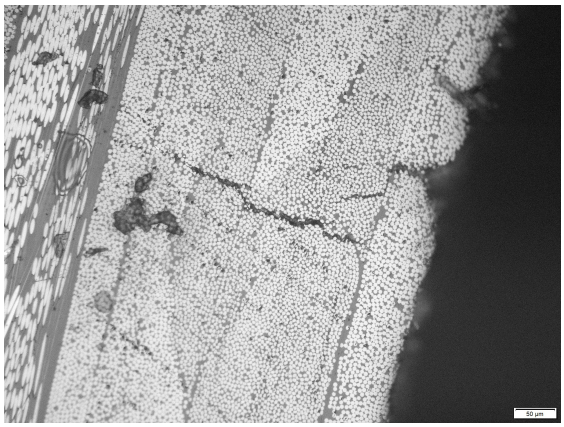
(b) 10x magnification.



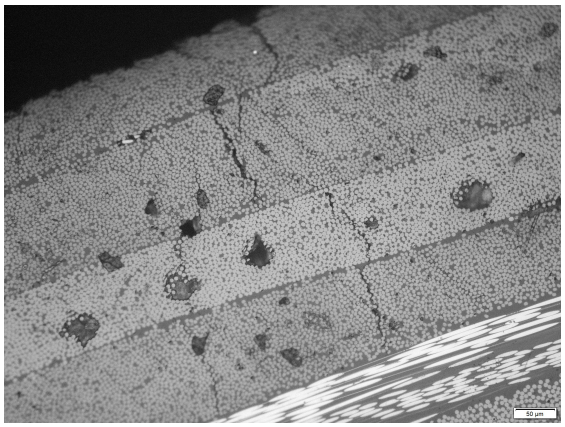
(c) 20x magnification.



(d) 20x magnification.

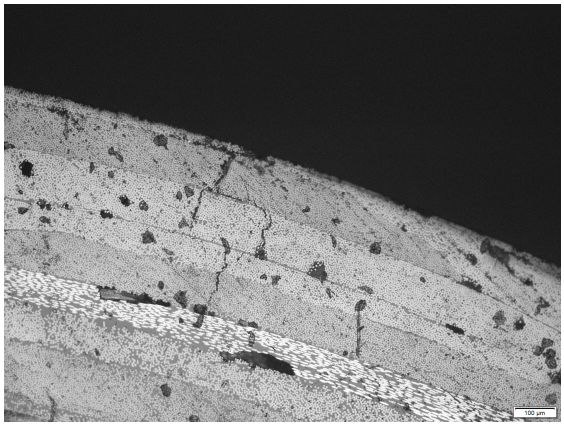


(e) 20x magnification.

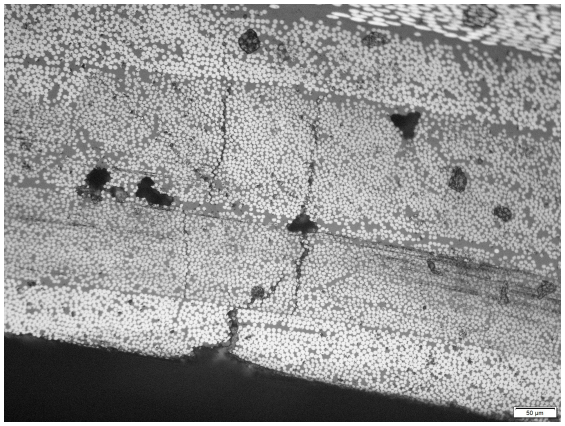


(f) 20x magnification.

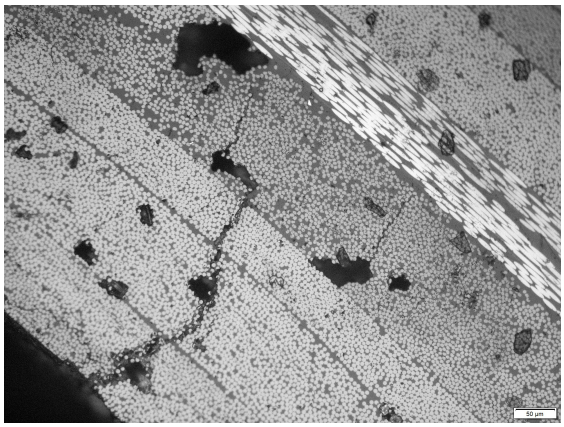
Figure 5.3: Micrographs of one EOL specimen showing multiple intralaminar cracks.



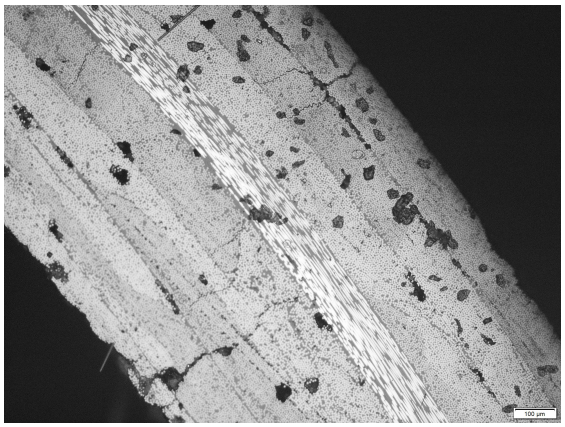
(a) 10x magnification.



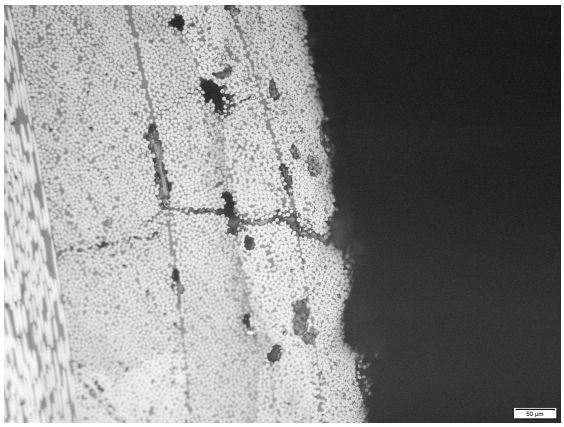
(b) 20x magnification.



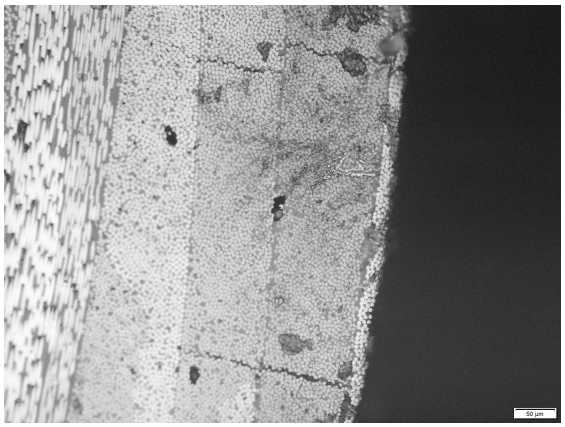
(c) 20x magnification.



(d) 10x magnification.

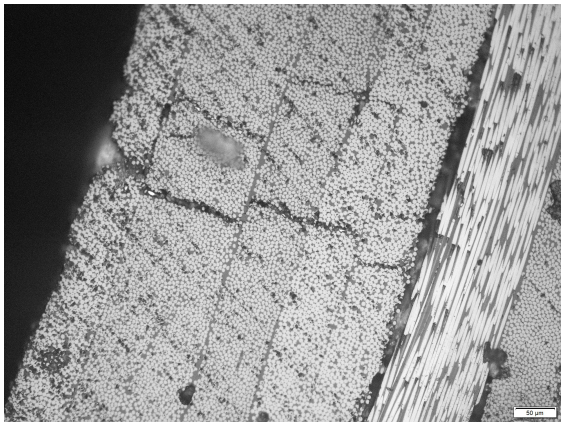


(e) 20x magnification.

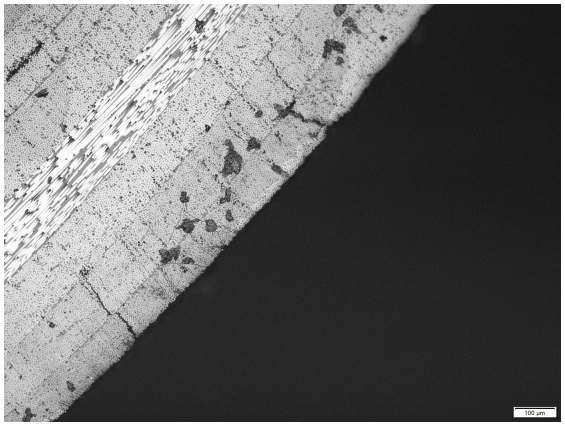


(f) 20x magnification.

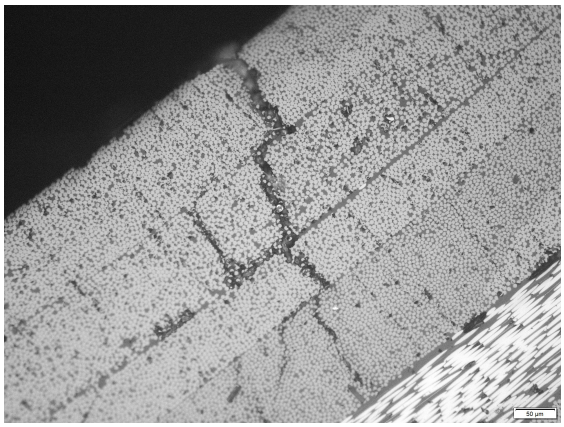
Figure 5.4: Micrographs of an EOL sample revealing how voids attract the growth path of cracks.



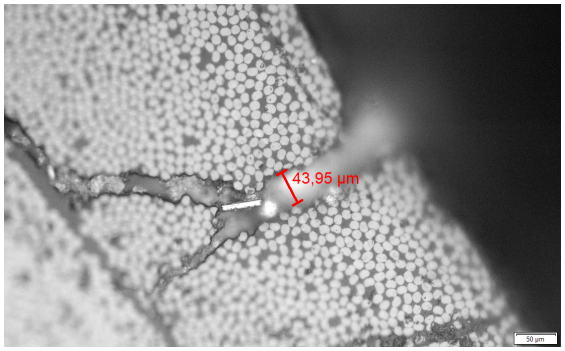
(a) 20x magnification.



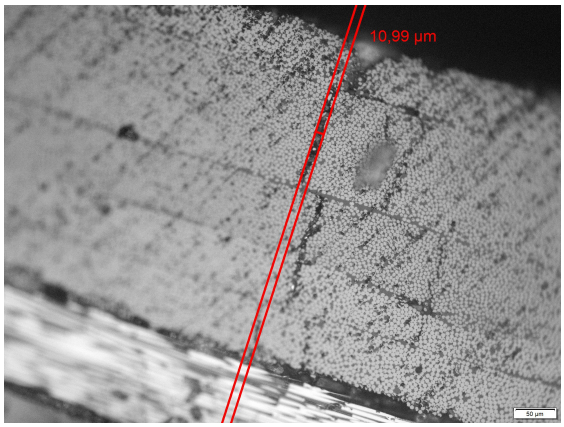
(b) 10x magnification.



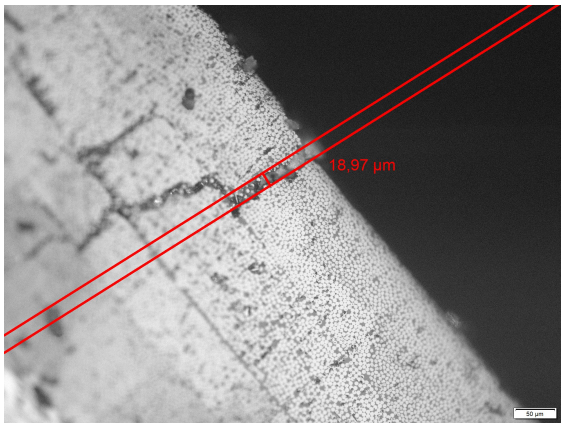
(c) 20x magnification.



(d) 50x magnification.



(e) 20x magnification.



(f) 20x magnification.

Figure 5.5: Micrographs of one EOL sample showing cracks with varying dimensions.

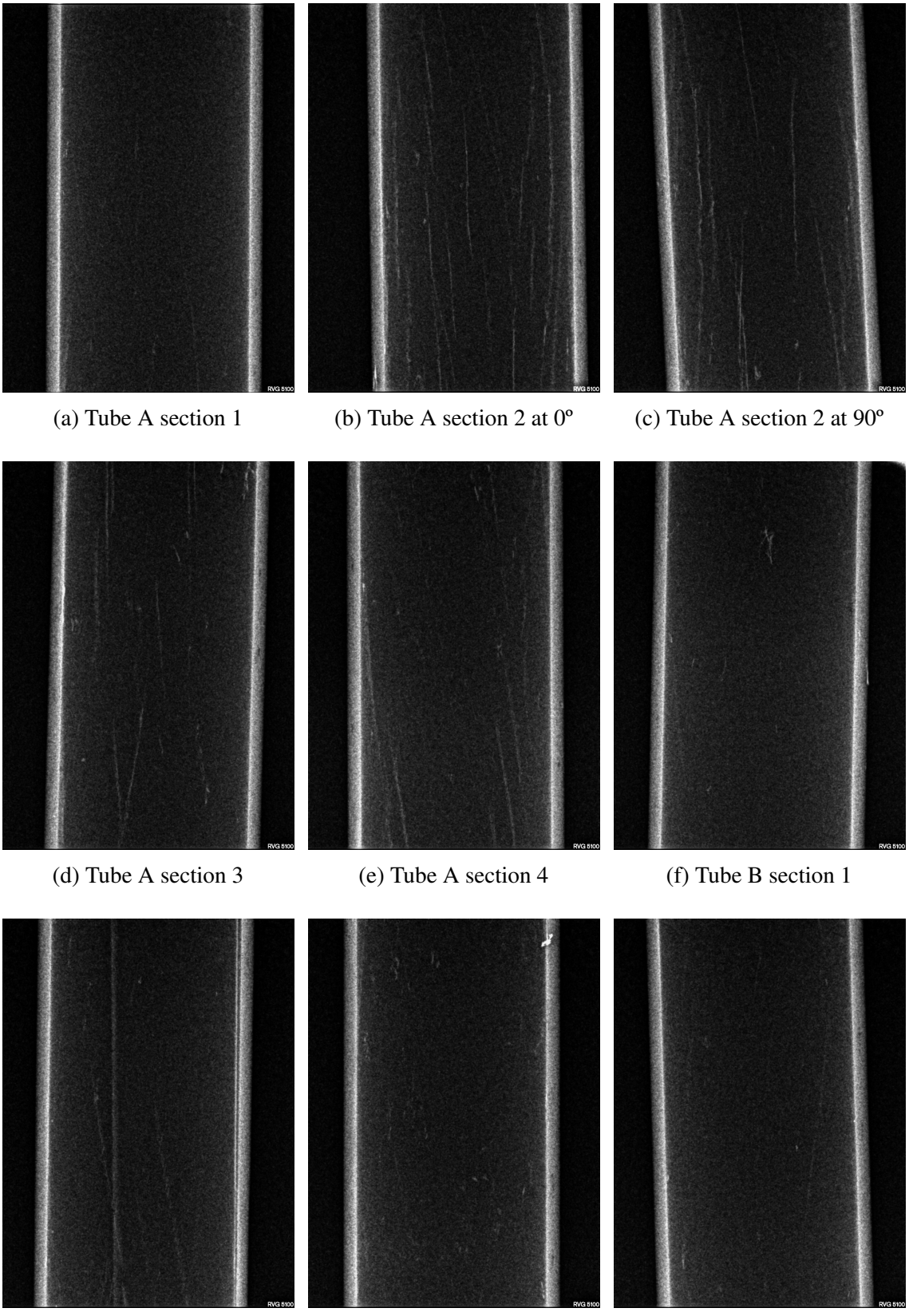
5.1.2 X-Ray Radiography

While exploring the damage mechanisms resulting from fatigue-inducing events such as thermal cycling along section 3.4.1, transverse matrix cracks - the first type of damage

to typically appear - are reported to propagate not only perpendicularly to the plies, but also in the fibre direction. This statement is fully corroborated by the images produced by x-ray radiography, where EOL samples show a high density of cracks - identifiable by lightly coloured lines - aligned with the fibres at 10º and -10º. The difference encountered between BOL samples (figure 5.6) and EOL samples (figure 5.7) is striking, and leaves no doubts regarding the role of thermal cycling in the propagation of intralaminar cracks. Some BOL samples also show signs of cracks, which is coherent with the micrographs of a BOL specimen presented in the previous section. However, the number of cracks is incomparable to the one identified in EOL samples, leading to the conclusion that thermal cycling is responsible for the observed crack density in the EOL specimens. This study was performed on multiple samples of two BOL and two EOL tubes, holding a higher statistical weight than the microscopic observations, and confirming its results regarding crack density before and after thermal cycling.

It is interesting to note that the there are no signs of damage in the -85º hoop layer, but it is not possible to state that they do not exist, by any mean. Recovering the procedure described in section 4.3.2, the lighter coloured lines that signal the presence of cracks are a result of the infiltration of a high capillarity liquid in those same cavities. As the samples are soaked in diiodomethane, this liquid will only reach the cracks that are accessible from the exterior. The micrographs in the previous section show that cracks often stop at the interface between layers, and this obstruction to crack growth is known to be aggravated if adjacent plies have very different fibre orientations. This means that the cracks in the -85º might not appear in the radiographs not because they do not exist, but because they are not accessible by the penetrating liquid. Naturally, this also means that the cracks revealed by this process are not necessarily an accurate representation of the entire crack density of the specimen, or even for every ± 10º layer. At the outermost and innermost surface, the liquid can penetrate through the entire length of the specimen, as well as the edges. For the intermediate ± 10º layers, the cracks are only revealed if they reach the edges or if they are a continuation of cracks in the superficial layers. Cracks in the -85º layer are not accessible by the edges as fibres are aligned almost perpendicularly to them, which further hinders their visualisation.

Radiography produced extremely interesting results, and although it faces some limitations, it appears to be a viable method to assess the progression of damage in the filament wound tubes under study. The equipment utilised to obtain these results is relatively affordable considering the scale of this project, but there are definitely some practicality issues surrounding the use of dangerous chemicals (diiodomethane) and the small dimensions of the acquired images. These disadvantages can be mitigated by the use of more expensive equipment.

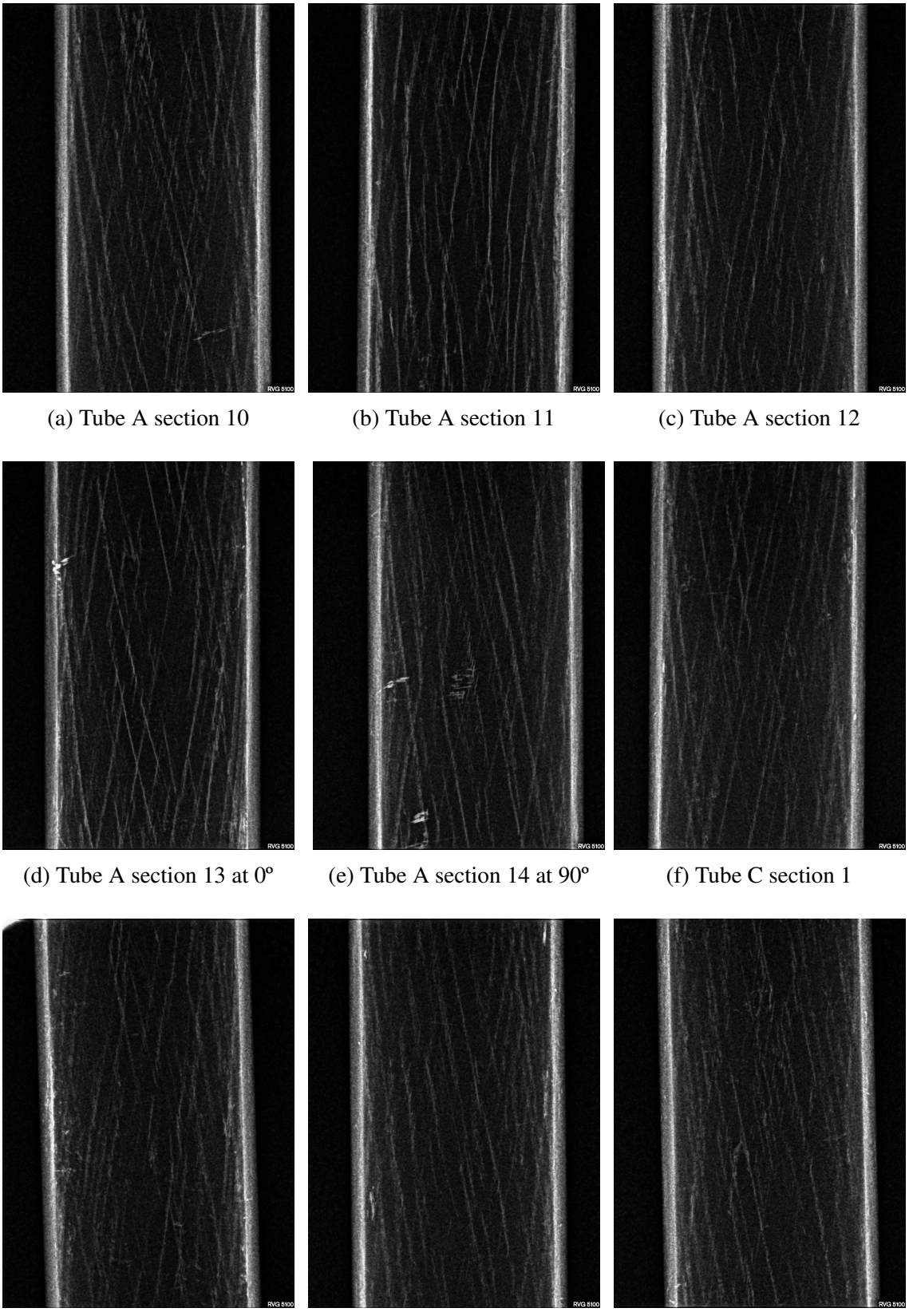


(a) Tube A section 1 (b) Tube A section 2 at 0º (c) Tube A section 2 at 90º

(d) Tube A section 3 (e) Tube A section 4 (f) Tube B section 1

(g) Tube B section 2 (h) Tube B section 3 (i) Tube B section 4

Figure 5.6: Radiographs of BOL specimens.



(a) Tube A section 10 (b) Tube A section 11 (c) Tube A section 12

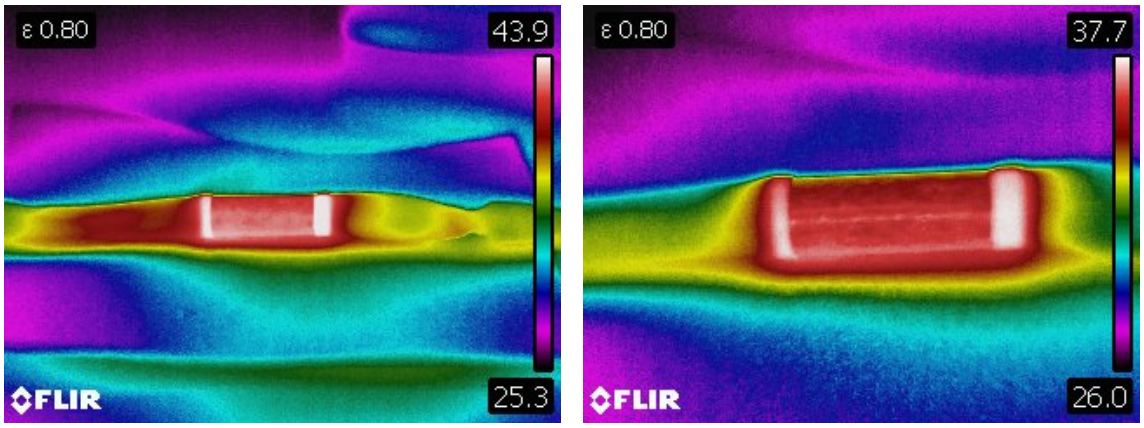
(d) Tube A section 13 at 0º (e) Tube A section 14 at 90º (f) Tube C section 1

(g) Tube C section 2 (h) Tube C section 3 (i) Tube C section 4

Figure 5.7: Radiographs of EOL specimens.

5.1.3 Thermography

The hypothesis of resorting to thermography in search of defects was completely unsuccessful. The utilised camera needs to stand at a 40cm distance to correctly focus on the samples, which coupled with the relatively low resolution of this infrared camera (320x240 pixels) does not seem to allow a detailed view of the samples. As shown in section 5.1.1, the transverse matrix cracks have a width of around 10μm, making it very unlikely to observe changes in the temperature of those small areas with such resolution. The FLIR E60 camera, although not top of the line, certainly presents highly competent characteristics based on what the market offers at this moment, meaning that utilising a more advanced camera would not necessarily solve the issues encountered during this experiment.



(a) Sample during heating. (b) Sample during cooling.

Figure 5.8: Thermograms of EOL sample.

In fact, the low resolution of the camera in comparison with the dimension of defects that affect the composite struts is not the only problem that complicates the application of thermography - the geometry and dimensions of these tubes does so as well. There are two main issues with the studied samples: the tubular geometry and the small thickness. Cylindrical geometries favour the appearance of reflection phenomena that affect the capture of infrared wavelengths by the cameras - this is clearly seen in figure 5.8b, where a lighter stripe appears along the middle of the sample. This problem can be mitigated by a proper positioning of the external lights surrounding the test setup, but the circular geometry will always have a tendency to affect the information captured by the camera at such a detailed scale. The possibility of applying microscopic lenses to the infrared cameras, allowing a much higher level of detail, is also made very difficult by this curved geometry, as the focused area would only be a very small stripe of the sample. This last hypothesis could only work if a complex rotating setup were to be assembled. Lastly,

the thickness of these tubes (1mm) hinders the application of thermography because this procedure depends on the different thermal conductivity among areas of the specimen. The temperature gradient created by the presence of cracks is unknown, but given the thin geometry of the specimen and the fact that the transverse cracks observed only spanned for one or two layers at most times, the difference in temperature between sane areas and cracked areas is expected to be extremely small, in such a way that it might not be captured by the infrared cameras commercially available at the moment.

Due to its practicality, thermography is definitely an inspection method worthy of exploring, and it already plays a significant role in the evaluation of composite materials in the aerospace industry. However, for the tubes at hands, it does not seem likely that this method is capable of finding defects of such dimension at this point in time, at least with a low cost setup. The use of thermography appears to be more indicated for defects of larger dimensions, such as widespread delamination.

5.2 Mechanical Properties

The procedures described in section 4.4 for compression tests and four-point bending see their results grouped in the following section, in the attempt of encountering changes in the mechanical behaviour of the filament wound struts due to thermal fatigue.

5.2.1 Compression Properties

The stress-strain curves for a small selection of the BOL and EOL specimens utilised in the compression tests are presented in figure 5.9 to easily transmit the awareness that every sample showed the typical elastic behaviour of CFRP laminates, and to highlight that thermal cycling did not catastrophically alter the behaviour of the tubular specimens.

The box plots in figure 5.10 show the median (vertical line), average (diamond mark), interquartile range (coloured box), minimum and maximum values (whiskers), and outlier values (dots) of every sample extracted from BOL and EOL tubes. These were chosen over bar plots as the differences encountered are quite small, and box plots provide a look into the dispersion of the collected data, which is relevant in this case. This plot shows that the mean value for the compression strength of EOL specimens is slightly lower than the one of BOL samples. However, the average value for the compression modulus actually increased after thermal cycling. This unexpected result obtained for the elastic modulus might be credited to the very reduced amount of samples that were fitted with a strain gauge - 4 BOL and 5 EOL specimens. The results for the compression strength are aligned with the literature, and lay on a more solid statistical base.

Table 5.1 summarises the results obtained, and highlights the number of samples available for each test. The high variance of the EOL results for compression modulus, coupled with the small pool size, does not advise the extraction of meaningful conclusions regarding that property. In reality, given the information presented in table 5.1 for both properties, the most secure indication is that the applied thermal cycling procedure did not induce drastic changes to the compression properties of the filament wound tubes.

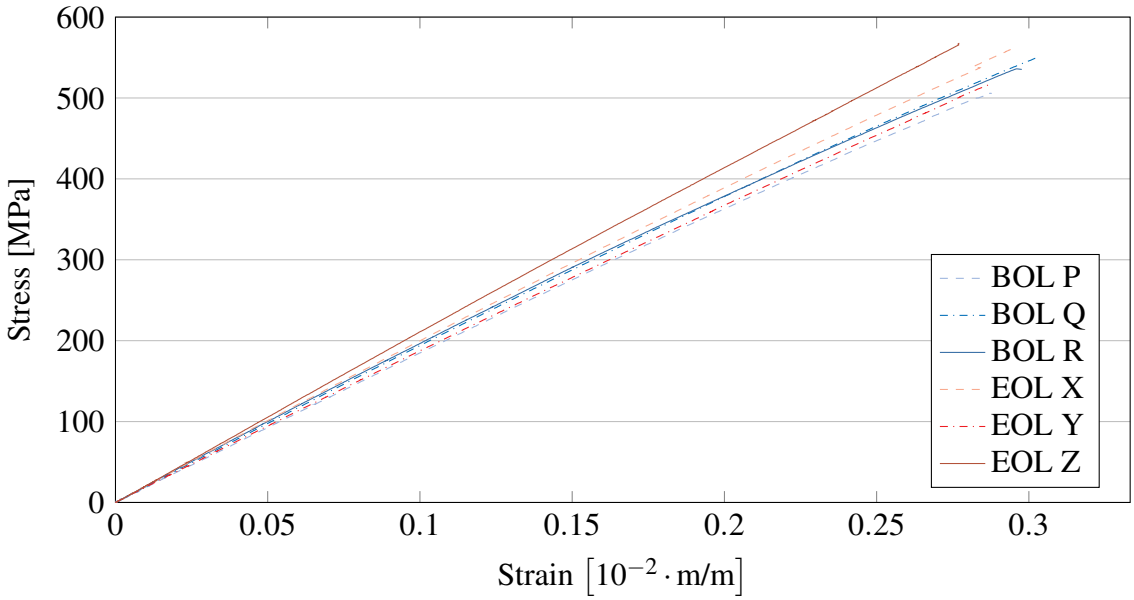


Figure 5.9: Stress-strain curves of multiple BOL and EOL specimens under compression.

Table 5.1: Summary of the compression properties of BOL and EOL specimens, with indication of the mean percentage difference taking BOL value as the baseline.

Property	Sample (Pool Size)	Mean ± s	Mean Difference
Compression Strenght [MPa]	BOL (20)	555.76±27.60	− 2.47%
	EOL (20)	542.19±18.75	
Compression Modulus [GPa]	BOL (4)	188.07±7.60	+ 4.05%
	EOL (5)	195.85±9.40	

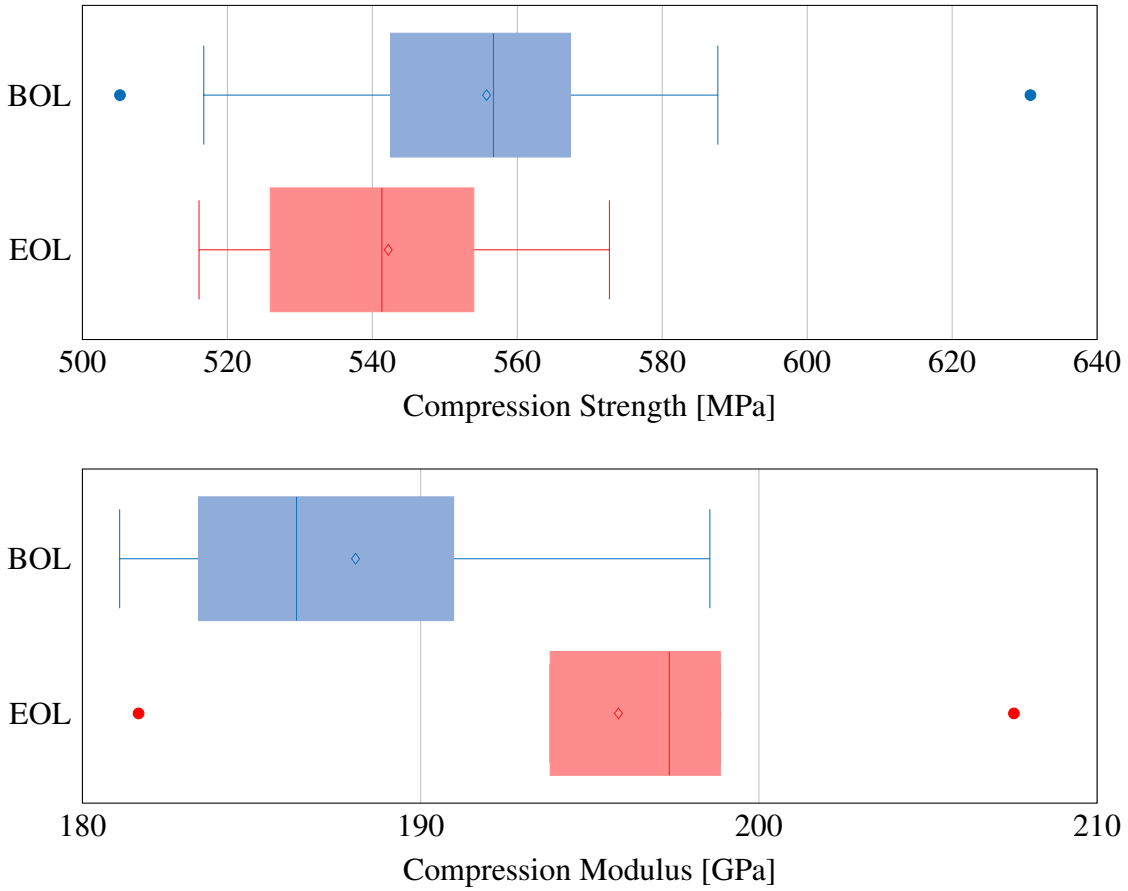


Figure 5.10: Compression properties of BOL and EOL specimens.

5.2.2 Flexural Properties

The analysis of the flexural behaviour follows a similar structure to the one adopted above for the evaluation of the compression properties. Figure 5.11 shows a plot of the stress-strain curves obtained for a small number of the samples utilised in the four-point bending tests. Again, the tubular specimens do not present a significantly different response due to the exposure to thermal fatigue, much like what is verified for the compression tests.

In this case, however, specimens exposed to thermal cycling present a noticeable reduction of the mean value for both flexural strength and modulus, at a magnitude that is aligned with what is described in the literature review. The box plots in figure 5.12 illustrate a more meaningful reduction of strength and elastic modulus than the one observed in the case of compression. Nonetheless, as table 5.2 establishes, the drop of the flexural properties between BOL and EOL specimens is still quite low - close to 3% for both properties.

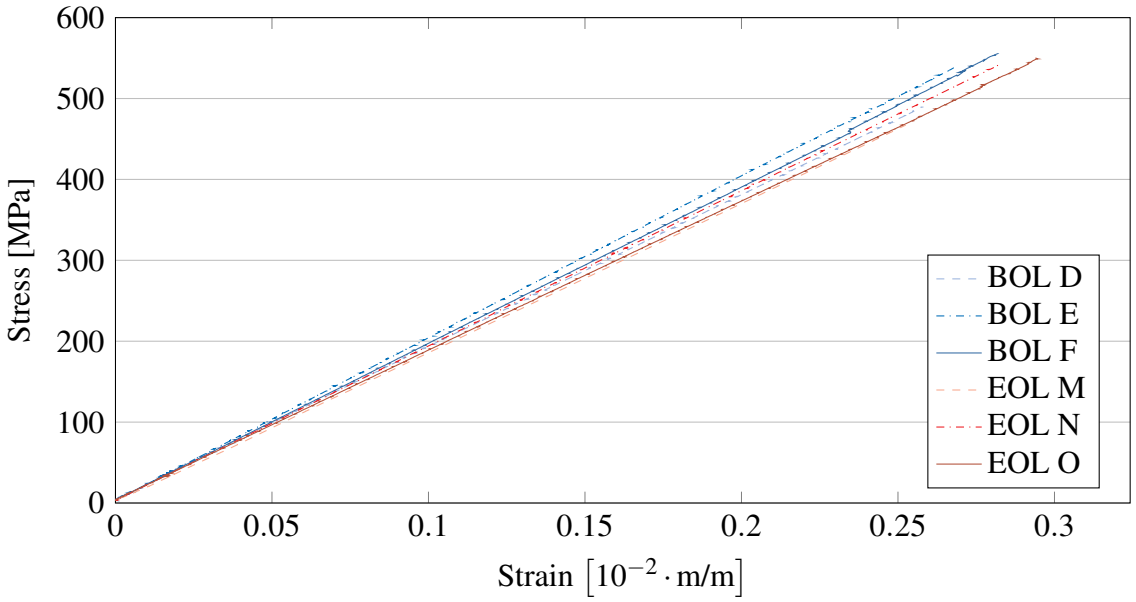


Figure 5.11: Stress-strain curves of multiple BOL and EOL specimens under four-point bending.

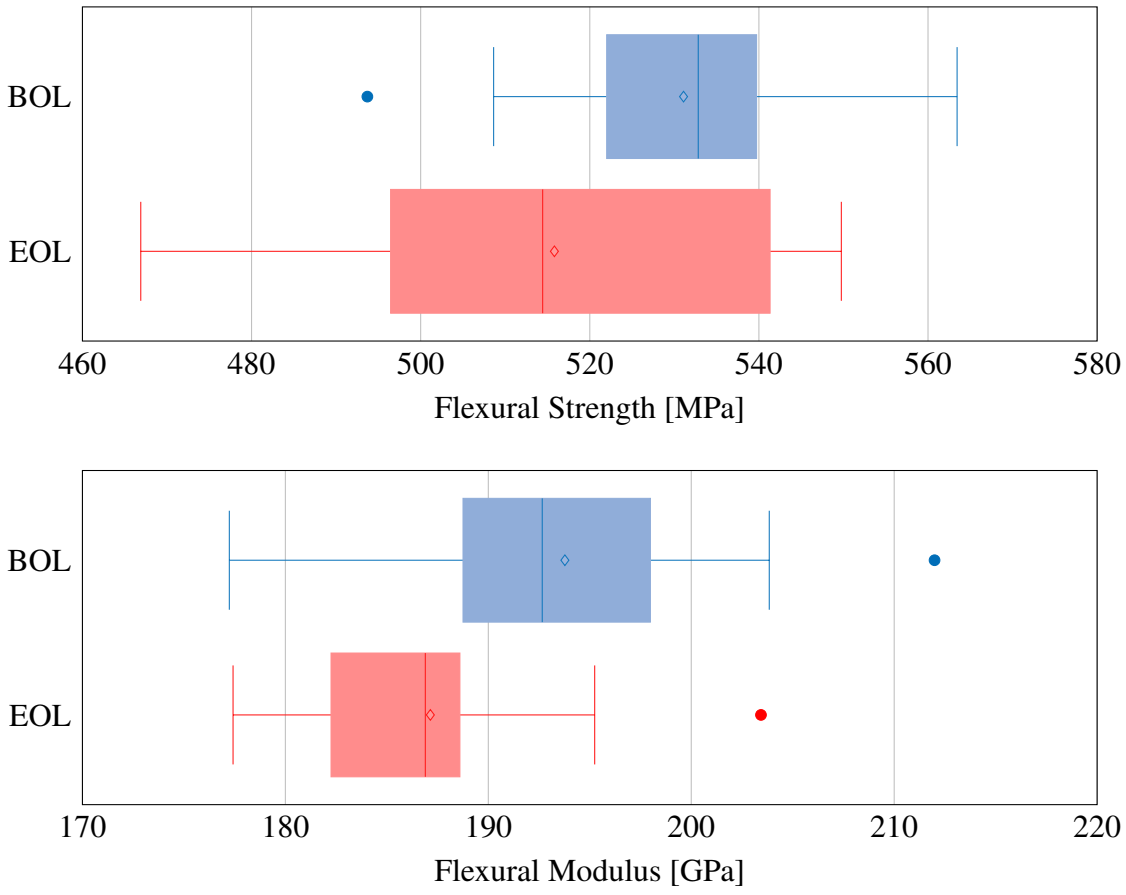


Figure 5.12: Flexural properties of BOL and EOL specimens.

Table 5.2: Summary of the flexural properties of BOL and EOL specimens, with indication of the mean percentage difference taking BOL value as the baseline.

Property	Sample (Pool Size)	Mean ± s	Mean Difference
Flexural Strenght [MPa]	BOL (10)	531.09±20.61	− 2.92%
	EOL (10)	515.82±27.91	
Flexural Modulus [GPa]	BOL (10)	193.77±9.69	− 3.48%
	EOL (10)	187.14±7.76	

5.3 Thermal Properties

In this study, the thermal behaviour of the CFRP tubes is mainly indicated by their linear coefficient of thermal expansion, as well as their glass transition temperature. These properties are heavily defined by the choices made during the production stage, but there are reports on significant variations of those characteristics due to thermal fatigue. These perceptions are evaluated in the following analysis.

5.3.1 Coefficient of Thermal Expansion

Section 4.5.1 describes the adopted procedure for the obtainment of the linear coefficient of thermal expansion, and states that three measurement runs are performed for each sample. Figure 5.13 shows the evolution of the length-corrected thermal strain with temperature during the three measurement runs of one BOL sample and one EOL sample, showing once again that the exposure to thermal cycling might not have drastic effects on some properties, at least at the number of cycles performed. It should be stressed that the EOL samples utilised for thermomechanical analysis were not exposed to 90 thermal cycles at room pressure, but only to 10 vacuum thermal cycles. It is possible that an additional exposure to the thermal cycle procedure at room pressure for 90 cycles could lead to different results. Furthermore, as thoroughly described in section 4.5.1, the specimens utilised are 52º sections of the filament wound tubes, which exposes them to warping due to laminate asymmetry - this is expected to result in a more negative CTE than the actual value for the tubular specimens.

There are two additional noteworthy details regarding figure 5.13. The value for expansion is zero at 20ºC since the specimens are measured at that temperature, and if the room is not at 20ºC a correction is performed. Furthermore, the expansion does not

follow a completely linear path throughout the whole temperature range. While the thermal expansion of the fibres is quite linear at these temperatures, the instantaneous CTE of the matrix is expected to rise significantly at higher temperatures. This reported behaviour is coherent with the evolution of the length-corrected strain of the CFRP specimens, as it is visible that the expansion rate lowers at higher temperatures - in practical terms, if the specimen is cooled by 60º, it suffers a higher strain than if it is heated by 60º. As justified in section 3.3.1, the coefficient of thermal expansion on the main fibre direction is a fibre-dominated property, nonetheless, the rise of the positive expansion rate of the matrix appears to affect the instantaneous CTE of the laminate.

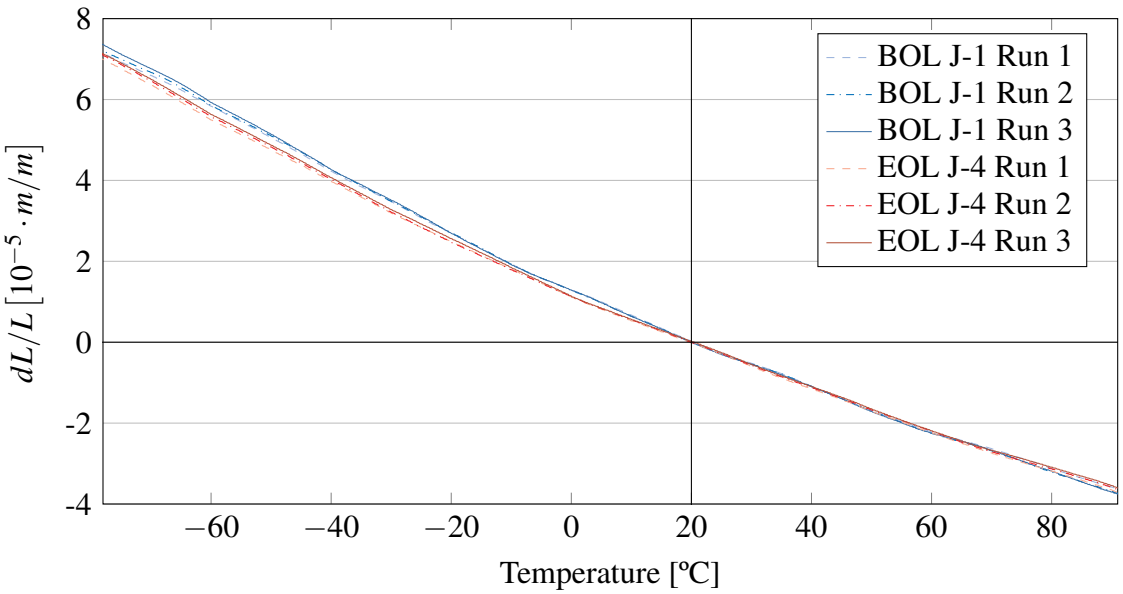


Figure 5.13: Evolution of the length-corrected strain with temperature during three runs of one EOL and one BOL sample from the same tube.

The box plot in figure 5.14 confirms that the average value for the mean longitudinal CTE between -78º and 91º was not significantly affected by the exposure to thermal cycling. Table 5.3 stresses that even further, showing that the mean value obtained for every EOL run is only 1% lower than the one obtained for every BOL measurement. As explained in section 4.5.1, the samples for this procedure come from only three different tubes, with EOL specimens being cut from sections of those tubes that were exposed to thermal cycling. An analysis of the average values obtained for sample of the same tube can help eliminate some variance resulting from the lack of repeatability of the filament winding process. However, even by comparing the mean values for BOL and EOL samples from the same tube, no evident trend emerges - there is a 6% reduction for tube J, a 6% increase for tube K, and a 3% decrease for tube L.

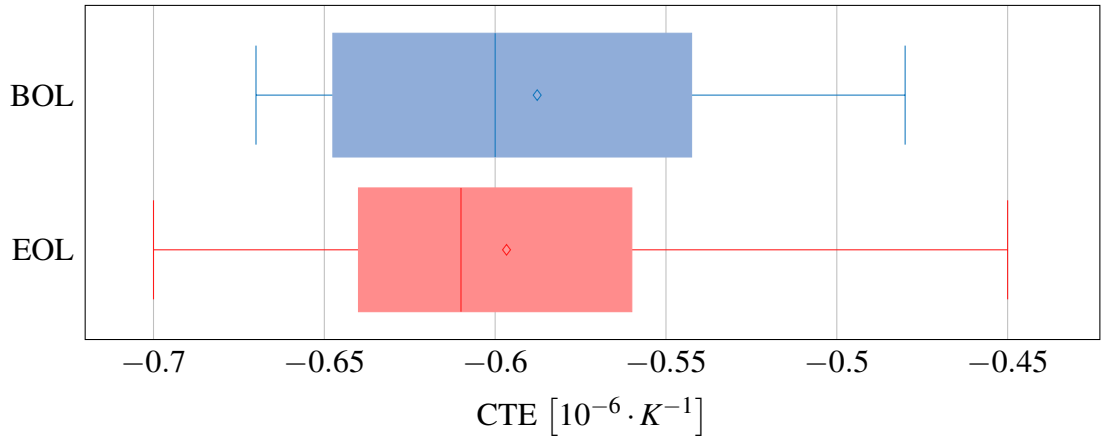


Figure 5.14: Average longitudinal coefficient of thermal expansion of BOL and EOL specimens between -78ºC and 91ºC.

Table 5.3: Summary of the mean longitudinal CTE ($\overline{\alpha_L}$) between -78ºC and 91ºC for BOL and EOL specimens, with indication of the mean percentage difference taking BOL value as the baseline.

Group	Tube (Samples)	Tube $\overline{\alpha_L}$ $\left[10^{-6} \cdot K^{-1}\right]$	Group $\overline{\alpha_L} \pm$ s $\left[10^{-6} \cdot K^{-1}\right]$	Mean Difference
BOL	J (3)	-0.621	-0.591±0.049	−1,03%
	K (3)	-0.617		
	L (3)	-0.534		
EOL	J (3)	-0.586	-0.597±0.051	
	K (3)	-0.652		
	L (3)	-0.552		

5.3.2 Glass Transition Temperature

Figure 5.15 shows the curves resulting from differential scanning calorimetry of three BOL samples, with T_g identified as the middle point of the small step change verified around 170ºC. Before delving into the analysis of the results, it is important to remember that, in this study, only two EOL samples were considered, which weakens any conclusions drawn for the effect of thermal cycling in the glass transition temperature of these filament wound tubes. However, there are measurements for BOL samples extracted from the same

tube as the EOL samples. The comparison between samples extracted from the same tube can serve as a good indicator of any influence of thermal fatigue in T_g.

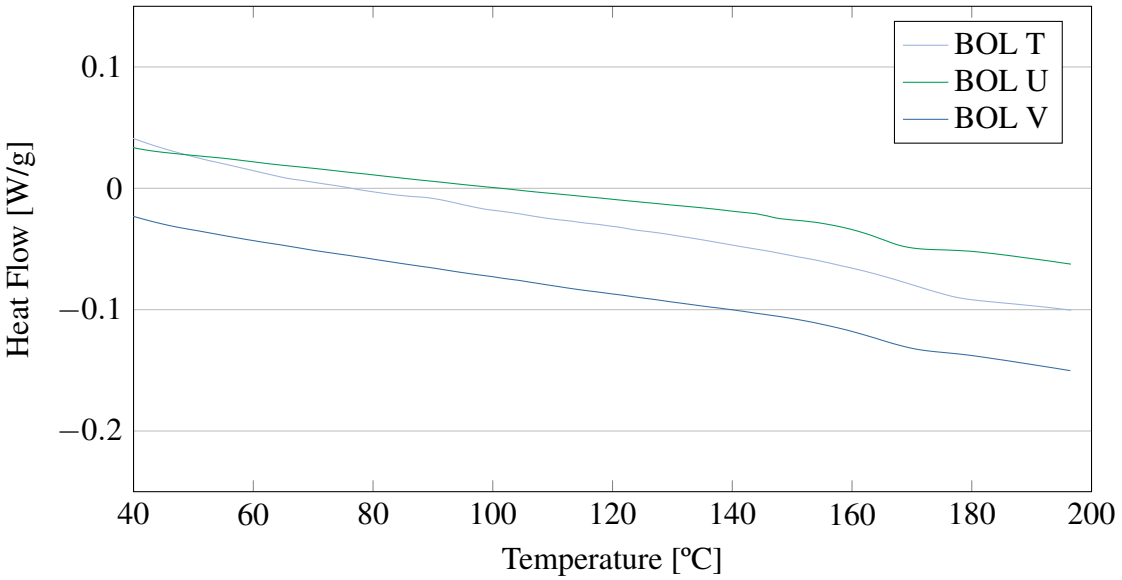


Figure 5.15: Curves obtained from differential scanning calorimetery (DSC) to determine T_g.

The box plot in figure 5.16 shows the dispersion of data for every BOL sample tested, and separately represents the results obtained for three samples extracted from tube W. This allows a more direct comparison with the two EOL samples that were also extracted from a section of tube W, although exposed to thermal cycling. The glass transition temperature of samples from tube W does not seem to change significantly after exposure to thermal fatigue, with every result very close to 170ºC. As mentioned above, caution is advised in this analysis, as the number of EOL samples is extremely reduced, nonetheless, this is a strong indicator that it is unlikely to observe a dramatic change in the value of T_g after the adopted thermal cycling procedure.

Concentrating on the bigger picture transmitted by figure 5.16, it is clear that despite some considerable dispersion, most values are close or even completely inside of the window indicated by the manufacturer for the glass transition temperature resulting from the chosen curing cycle - 165ºC to 180ºC. Additionally, every DSC curve presents a similar behaviour to the one observed for the samples represented in figure 5.15, with a small inflexion in the glass transition region, indicative of no significant exothermic or endothermic reactions. These are signs that the material has plausibly reached a very high degree of cure during the performed curing stage.

Table 5.4 indicates the mean values for the glass transition temperature of every BOL sample, as well as the samples extracted from tube W. The information found in this tests leads to the assumption that no further cross-linking took place, which is coherent with the

idea that the cure degree must have been quite advanced right after curing. On the other hand, there is also no indication that any degradation mechanisms influenced T_g in the applied number of thermal cycles. For these conclusions to have a higher statistical weight, more EOL samples should be tested.

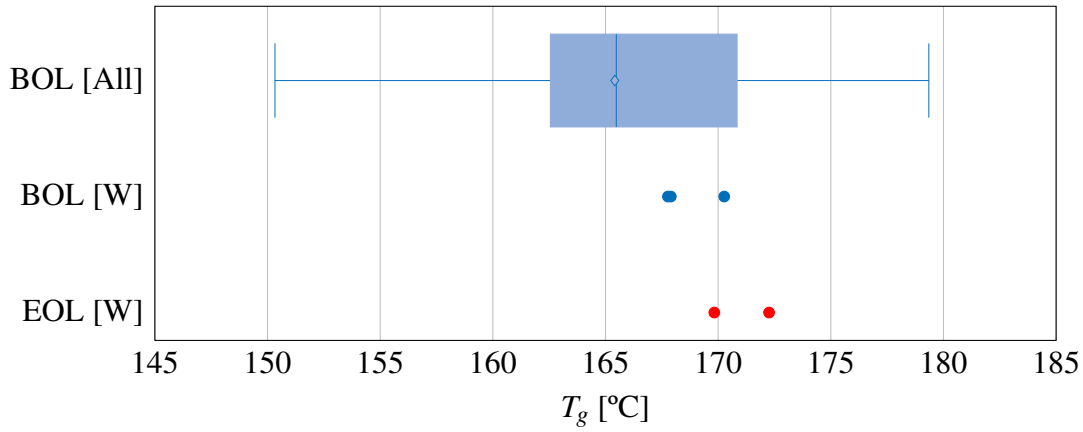


Figure 5.16: Values obtained for the glass transition temperature of every BOL sample (BOL [All]), BOL samples only from tube W (BOL [W]) and EOL samples also from tube W (EOL [W]).

Table 5.4: Summary of the glass transition temperature of BOL and EOL specimens.

Group	Tube (Samples)	$\overline{T_g} \pm s$
BOL	All (26)	165.41±7.64
	W (3)	168.65±1.41
EOL	W (2)	171.05±1.72

5.4 Discussion

The presence of defects resulting from the manufacturing process might be the most pressing concern raised by the microscopic observations, showing a high void content and detachment of innermost and outermost plies. The grinding process is a very likely cause for the damage of the outermost layers. In fact, this finishing process was supposed to only affect the sacrificial -85º layer, but it is removing axially oriented plies to comply with the required thickness. This is a consequence of the poor compaction of the wound layers, which do not present the expected thickness, obliging a more severe removal of material. It is plausible that the delamination of outermost layers is caused by the cutting and polishing

operations performed on the samples for microscopic observation, and further investigation on this matter is needed for a more incisive commentary. However, even through naked eye inspection it is possible to observe that the removal of the outermost material is quite uneven and random along the length of the tube in terms of how many layers it affects - which can be due to the natural ply waviness of filament wound components and inconstant width of the deposited tows. This uneven removal of $\pm 10^{o}$ plies exposes the interfaces between fibre tows, which has shown to be an ideal path for delamination in the presented micrographs. Even if the visible detachment of the outermost layers is due to the specimen preparation, it is not recommendable that the laminate is so exposed to this type of damage. Obtaining a layer thickness closer to what is predefined and reviewing the centerless grinding process is certainly advised. Contrary to the case presented up to this point, it is not likely that the removal of innermost plies in some regions is a result of specimen preparation. By visualising the interior of the CFRP tubes, severe scratches can be observed along its entire length. Although demolding is reported as being easily done by hand, without exerting any significant pressure, the shape and orientation of these defects strongly suggests that they originate from removing the tubes from the mandrel. The micrographs presented above showed how this detachment of portions of the innermost layer can lead to a 10% reduction in thickness, which is bound to affect the mechanical properties of the component. Again, this is a topic worthy of further study with a larger pool of specimens, and a review of the demolding step should be performed.

The significant presence of voids is another particularly worrying observation. The assessment of the void content through the appropriate methodologies is still under implementation and the results present a high dispersion, nonetheless, these studies point to void volume fractions commonly above 1%, with many evaluations close and even above 3%. The micrographs of previous production batches also showed many void riddled regions. This means that, even though only two samples were observed in this work, a high presence of voids is likely to be encountered in every produced tube, especially as they all stem from the same production parameters. The micrographs of BOL samples show that voids enable the propagation of intralaminar cracks at the end of the curing stage, which is not ideal. Additionally, when exposed to thermal fatigue or any other solicitation, the advancement of damage is still potentiated by the presence of voids due to stress concentration. This problem should be urgently tackled, as it weakens the composite component, impacting its mechanical properties and reducing its durability.

The problems encountered with the removal of outermost layers and excessive presence of voids can be mitigated by improving the compaction of the laminate during the winding process. Increasing fibre tension is known to aid laminate compaction, which could restrain the thickness of each layer, promote the expulsion of volatiles that generate voids, and

improve fibre alignment with reduced waviness. Altering the cross-sectional area of the fibre bands and the winding pattern can also lead to better results. Adopting wider and thinner bands combined with a less interwoven winding pattern can reduce the regions prone to capture volatiles, diminishing ply waviness. Shrink tapes are already applied, but their compression seems to be insufficient. On a complementary note, this measures could also improve the compression strength of the composite struts, which at this moment falls short of the project requirements - better fibre alignment is known to delay buckling mechanisms [95, 96].

One of the main goals of employing non-destructive inspection methodologies was reporting the progress of damage mechanisms due to thermal cycling. Microscopic observations and x-ray radiography were very successful in this regard, confirming that transverse matrix cracks are the first and most rapidly progressing damage mode to corrupt composite systems under fatigue environments. The amount of cracks encountered with both techniques is aligned with the findings summarised during the literature review, where 100 thermal cycles are often enough to reach a saturation phase of crack density that precedes the appearance of more severe damage mechanisms. As the EOL specimens were not examined before thermal cycling, it is not possible to distinguish cracks resulting from the curing stage from the ones provoked by thermal cycling. However, a large amount of specimens was visualised by x-ray radiography, showing an undeniably larger amount of cracks in EOL specimens than BOL samples. This perfectly constant trend should prove that thermal cycling caused the vast majority of cracks found in EOL specimens. There are no significant signs of delamination in the radiographs and the micrographs do not allow a clear distinction between preexisting voids at the ply interfaces and delamination phenomena - precisely because the EOL specimens were not observed before thermal fatigue.

Shifting the focus of this discussion to the effects of thermal cycling in the physical and mechanical properties of the composite struts, it is fascinating to observe that the large amount of intralaminar cracks degrading the EOL specimens did not significantly alter their characteristics. The flexural and compression response of composite systems is not as fibre-dominated as tensile characteristics, and there is an increased importance of the fibre-matrix adhesion and, at some point, the utter load-bearing capacity of the polymer matrix. The fact that compressive and flexural properties only dropped slightly - with the exception of the compression modulus - is indicative that no significant debonding phenomena occurred in the tubular specimens after the exposure to the defined thermal fatigue procedure. These results are quite coherent relatively to similar studies described during the literature review.

Thermal properties were not significantly affected either. The evaluation of the T_g

of EOL specimens was very reduced, but still indicated that no dramatic variation likely occurs as a result of the thermal fatigue environment conceived. This might be explained by an originally elevated degree of cross-linking, signalled by the DSC curves and the proximity of the glass transition temperature to the manufacturer prediction. It also appears that no severe chemical degradation mechanisms came into play, as the glass transition temperature did not become lower either. It is worth noting that the stable value of T_g is also aligned with the low alteration of the mechanical properties - during the literature review, it is found that increasing T_g often results in an improved mechanical response. The coefficient of thermal expansion did not show any relevant difference either. In fact, the small alteration encountered might be credited to the uncertainty of the test itself. Again, this is perfectly aligned with the information collected regarding the mechanical properties. If fibre-matrix debonding occurred at a large scale, a significantly weakened mechanical behaviour should be observed, and the average CTE should become less negative due to lack of constraint of the matrix - none of those cases are observed, which points to a residual prevalence of debonding phenomena.

It is not possible to state in which stage of damage progression the struts are encountered after the defined thermal cycling procedure, and only an extended study between a different number of cycles would allow a more detailed characterisation. Given the data collected and dissected along this work, it appears that no severe damage modes are affecting the laminate, as its properties are still close to intact. However, the high density of cracks visualised in the radiographs points to an advanced state of crack density, and if the tubes are not already at a stage of transverse damage saturation, they are likely to be quite close to reach it.

The influence of the design choices and manufacturing parameters on the thermal properties of the filament wound struts is not extensively examined by this experimental characterisation because the production batches considered for this study follow the same exact parameters. It is only by isolating and varying specific factors - such as the curing cycle, layup or winding machine configurations - that one can clearly identify its influence. Nonetheless, some general considerations can be made regarding that matter. Choosing the longest curing cycle recommended by the manufacturer appears to have resulted in a very high degree of cure, as was expected. Furthermore, it is undeniable that the coefficient of thermal expansion along fibre direction is a fibre-dominated property, as the values obtained fall between the indicated CTE for both fibres. Still under the scope of thermal response, it also became clear that the rivalling expansion and contraction of the different constituents during temperature changes originates stresses that lead to damage progression within the laminate.

Chapter 6

Conclusions and Future Work

Aerospace applications, due to their highly demanding requirements, push the development of composite materials to incredible heights, both literally and figuratively, accomplishing advancements that can then trickle down to more down-to-earth applications. The development of this work showcases the complex micromechanics and intricate phenomena that govern the behaviour of composite systems. These intrinsic connections between the various characteristics of a composite component are highlighted through the impact that every design decision has on its response, but it is precisely this complexity and broad possible outcome of physical and mechanical properties that propels composite systems to the forefront of many industries.

Section 6.1 attempts to summarise the behaviour encountered for the filament wound tubes studied throughout this work, touching on the role of the manufacturing process and the resistance to the harsh conditions that define the space environment. Finally, section 6.2 provides a critical assessment of how the characterisation of these composite components could be improved and what opportunities lay ahead in their development.

6.1 Conclusions

The studied filament wound struts are designed to withstand the harsh conditions of the space environment and meet the requirements for dimensional stability and mechanical response needed for its application in the frame of a deployable space antenna. One of the main obstacles for composite systems that orbit the Earth are the cyclic temperature changes that these materials become exposed to. This justifies the importance of studying the response of these tubes to temperature changes, and evaluating how thermal fatigue can reduce their durability.

Acquiring a deep understanding of how the manufacturing process and design choices affect the characteristics of the composite struts is a fundamental step in the prediction

of its response and in the critical evaluation of what alterations should be performed to tackle any problem encountered. As the tubes considered in this study were all produced under the same parameters, the conclusions drawn from the experimental studies on this matter are quite generic. They clearly confirm that the coefficient of thermal expansion along fibre direction is a fibre-dominated property. Additionally, the use of the longest recommendable curing cycle appeared to result in a high degree of cross-linking. Furthermore, the microscopic observations show the difficulties associated with filament winding, with compaction issues and high void content.

Another point of concern in subjecting CFRP laminates to severe temperature variations is the rivalling contraction and expansion of its constituents. This mismatch of the coefficient of thermal expansion between the fibres and matrix creates stresses that result in the progression of damage mechanisms within the composite part. This was successfully verified, as the microscopic observations and x-ray radiographs show a severe density of intralaminar cracks on specimens exposed to thermal cycling. The degradation of the laminates under these environments raises concerns regarding the maintenance of their properties. This study showed that even with a significant presence of transverse matrix cracks, the physical and mechanical properties of the composite parts may not be drastically altered. The compression and flexural properties, as well as T_g and CTE, suffered minimal fluctuations after exposure to thermal fatigue. Damage progression in composites tends to start with intralaminar cracks, and the prolonged exposure to fatigue environments can originate more severe damage mechanisms. It is plausible to assume that the mechanical properties of the laminate, as well as its CTE, were almost intact because debonding phenomena were still quite reduced. The value of T_g appears to also remain unchanged, which is coherent with the high degree of cure observed in BOL specimens, and may signal that no significant chemical degradation occurs under the adopted thermal fatigue procedure.

The work presented along this thesis certainly emphasises the complexity adjacent to composite systems, and more incisive conclusions could only be drawn with an extended experimental characterisation. Nonetheless, the experimental studies were already quite revealing, particularly regarding the intricate relation that exists between damage mechanisms and the properties of composite systems.

6.2 Future Work

The reflection on future works can begin by evaluating how the presented work could be improved regarding the achievement of more solid basis for the conclusions drawn and extending the detailed characterisation of the filament wound tubes.

Let us start with the influence of the production parameters and design choices on the thermal behaviour of the CFRP tubes. The production batches that this study considered for the experimental characterisation result from the same exact production choices, meaning that no variable was isolated and altered in order to study its influence. What this study performs in that topic is a generalised assessment of how the choices made presented expected consequences on the resulting composite parts. A more interesting evaluation would report on how the fluctuation of some parameters - for example, constituent selection, layup, winding tension, curing cycle - affects the response of the laminate. Moreover, this study identified a large presence of defects originated during the production stage, which are closely connected with a more severe nucleation of cracks. This is an additional cause of concern and motivation for changes in the adopted production parameters. With this in mind, it is advisable that a development phase is programmed to understand the plausible causes for these defects while searching for ways to adjust the thermal behaviour of the filament wound struts so that every requirement is met.

The study on the effect of thermal cycling stands on its own regardless of that matter, but its value is diminished by other factors. The most crucial improvement on the investigation of the consequences of thermal fatigue would be the assessment of the state of the material after various different numbers of thermal cycles. This is the most common methodology adopted in similar studies in the literature, and allows a deeper understanding of how the composite parts are reacting to that fatigue environment. It would then be possible to track the evolution of damage mechanisms, identifying the different stages of degradation, and those observations could be correlated with changes in the physical and mechanical properties noted at the same number of fatigue cycles. By only studying the characteristics of the material before and after a single set of cycles, the identification of any trends is tampered, as knowing only two states is hardly enough to establish meaningful predictions on the consequences of different levels of exposure to thermal cycling. Additionally, the various scheduling constraints encountered, which are always associated with projects of this nature, difficult a more advisable assessment of the effect of thermal fatigue on some points. First, the thermal cycling procedures should all be under vacuum, as that is a more correct approximation of the space environment. Also, as the manufacturing process is still allowing some significant dispersion on the properties of the final components, it would be best to test specimens that come from the same original tubes, as to eliminate the variance resulting from production - just like what was done regarding the CTE tests. Lastly, the non-destructive inspection should be performed on precisely the same specimens, before and after thermal fatigue, as to clearly determine the cause of each damage mode and report its progress.

The development of the composite tubes studied in this thesis is still at an intermediate

level. Many more investigations are to come, for example, regarding the effect of additional conditions encountered in the space environment on the degradation of the CFRP tubes. As this project is far from over, it is relevant to reflect on how to optimise it for the stages ahead. One of the main takeaways from this study is how damage progression is heavily related to alterations in the properties of composite materials under thermal fatigue.

The brief incursion on possible non-destructive inspection methods along this work showed their potential in the assessment of the state of the material. Adopting more complex non-destructive methodologies in a rigorous quality control stage, under a comprehensive development programme, could provide a detailed prediction of the physical and mechanical properties of the CFRP tubes at later phases - minimising the need for expensive and time consuming destructive tests. This area poses a great opportunity for the adoption of machine learning techniques that identify the encountered defects or damage and return an evaluation on the state of the material. Machine learning is a vast area, with a tremendous amount of solutions, but its problem-solving ability can be reduced to two main areas - classification and regression [97, 98]. Classification algorithms can be used to place any given data input in a predefined class. This could be extremely helpful to catalogue the CFRP tubes as fit for their application or defective, through an automatised evaluation of the information obtained through non-destructive inspection. Lets establish a practical example. The tubes arriving from the production stage tend to show signs of damage. Simple image-processing algorithms could quantify the amount of damage presented in a radiograph - or a similar technique - and the implementation of a machine learning classification algorithm could present a pass-fail evaluation of the tubes. Regression algorithms can be utilised in a more complex setting, as they return the value of a continuous variable based on the introduced data. With an extended characterisation of the filament wound tubes, a correlation could be established between the observed level of damage and the alteration of the physical and mechanical properties of the composite. The implementation of machine learning algorithms coupled with non-destructive testing could then lead to a faster and less costly assessment of the produced tubes, albeit under the assumption that a meaningful connection can be established between damage progression and weakened properties - which is entirely plausible.

The field of composite materials presents an exciting array of possibilities, and the many exciting challenges still to come in the development of these filament wound tubes is a perfect depiction of that. In hindsight, the work described along this thesis is filled with limitations and demands restrain in the conclusions drawn. Nonetheless, it was only by undertaking this study that what should be done ahead became clear. The natural path for new advancements in engineering resides precisely in critical thinking and defying the state of the art, so that new ideas become a reality.

References

[1] S.K. Mazumdar. *Composites Manufacturing: Materials, Product, and Process Engineering*. CRC Press, 2001. ISBN 9780429127427. doi: 10.1201/9781420041989.

[2] Tasdeeq Sofi, Stefan Neunkirchen, and Ralf Schledjewski. Path calculation, technology and opportunities in dry fiber winding: a review. *Advanced Manufacturing: Polymer & Composites Science*, 4(3):57–72, 2018. doi: 10.1080/20550340.2018.1500099.

[3] D.V. Rosato and C.S. Grove Jr. *Filament Winding: Its Development, Manufacture, Applications and Design*. Interscience Publishers, 1964. ISBN 0470733381.

[4] Sotiris Koussios. *Filament Winding: a Unified Approach*. Delft University Press, 2004. ISBN 90-407-2551-9.

[5] Rodrigo de Lacerda Aroso Furtado. Filament winding simulation. Master's thesis, Faculty of Engineering of University of Porto, Porto, March 2016.

[6] S. M. Sapuan. Chapter 3 - composite materials. In S.M. Sapuan, editor, *Composite Materials*, pages 57–93. Butterworth-Heinemann, Boston, 2017. ISBN 978-0-12-802507-9. doi: https://doi.org/10.1016/B978-0-12-802507-9.00003-9.

[7] S.T. Peters. *Composite Filament Winding*. ASM International, 2011. ISBN 978-1-61503-722-3.

[8] Bora Balya. Design and analysis of filament wound composite tubes. Master's thesis, Middle East Technical University, December 2004.

[9] Hugo Faria. *Analytical and Numerical Modelling of the Filament Winding Process*. PhD thesis, Faculty of Engineering of University of Porto, Porto, April 2013.

[10] Emrah Salim Erdiller. Experimental investigation for mechanical properties of filament wound composite tubes. Master's thesis, Middle East Technical University, July 2004.

[11] Pultrex. Fibre tension systems for filament winding equipment. https://pultrex.com/fibre-tension-systems-2/, 2018. Accessed on 09-03-2021.

[12] Nihat Akkus and Garip Genc. Influence of pretension on mechanical properties of carbon fiber in the filament winding process. *The International Journal of Advanced Manufacturing Technology*, 91(9-12):3583–3589, 2017. doi: 10.1007/s00170-017-0049-z.

[13] Pierre Mertiny and F. Ellyin. Influence of the filament winding tension on physical and mechanical properties of reinforced composites. *Composites Part A: Applied Science and Manufacturing*, 33:1615–1622, 12 2002. doi: 10.1016/S1359-835X(02)00209-9.

[14] Brian Ellul, Duncan Camilleri, Jana Grech, and Martin Muscat. Filament wound composite pressure vessels and pipes subject to an internal pressure - an experimental and material characterization study. *Journal of Pressure Vessel Technology*, 138: 060906–1,8, 01 2016. doi: 10.1115/1.4032506.

[15] S. Tompkins. Effects of thermal cycling on composite materials for space structures. 1989.

[16] Gerda Horneck. *Space Environment*, pages 2293–2299. Springer Berlin Heidelberg, Berlin, Heidelberg, 2015. ISBN 978-3-662-44185-5. doi: 10.1007/978-3-662-44185-5_1469.

[17] Miria M. Finckenor and Kim K. de Groh. *A Researcher's Guide to: Space Environmental Effects*. NASA ISS Program Science Office, 2020.

[18] Jerry Jon Sellers, William J. Astore, Robert B. Giffen, Wiley J Larson, Jerry Sellers, William Astore, Robert Giffen, and Wiley Larson. *Understanding Space: An Introduction to Astronautics*. McGraw-Hill Primis Custom Publishing, 2nd edition, 2003. ISBN 0072943645,9780072943641.

[19] Soheila Mahdavi. Thermal cycling of out-of-autoclave thermosetting composite materials. Master's thesis, Concordia University, Montreal, March 2017.

[20] John R. Wagner, Eldridge M. Mount, and Harold F. Giles. 19 - polymer structure. In John R. Wagner, Eldridge M. Mount, and Harold F. Giles, editors, *Extrusion (Second Edition)*, Plastics Design Library, pages 225–232. William Andrew Publishing, Oxford, second edition edition, 2014. ISBN 978-1-4377-3481-2. doi: https://doi.org/10.1016/B978-1-4377-3481-2.00019-3.

[21] Michel Biron. 2 - thermoplastic specific properties. In Michel Biron, editor, *Material Selection for Thermoplastic Parts*, pages 39–75. William Andrew Publishing, Oxford, 2016. ISBN 978-0-7020-6284-1. doi: https://doi.org/10.1016/B978-0-7020-6284-1.00002-7.

[22] Michel Biron. 8 - thermal properties. In Michel Biron, editor, *Material Selection for Thermoplastic Parts*, pages 339–375. William Andrew Publishing, Oxford, 2016. ISBN 978-0-7020-6284-1. doi: https://doi.org/10.1016/B978-0-7020-6284-1.00008-8.

[23] Frank H. Stillinger and Pablo G. Debenedetti. Glass transition thermodynamics and kinetics. *Annual Review of Condensed Matter Physics*, 4(1):263–285, 2013. doi: 10.1146/annurev-conmatphys-030212-184329.

[24] Giulio Biroli and Juan Garrahan. Perspective: The glass transition. *The Journal of chemical physics*, 138:12A301, 03 2013. doi: 10.1063/1.4795539.

[25] Koun Shirai. A thermodynamic description of the glass state and the glass transition. *Journal of Physics Communications*, 4(8):085015, 2020. doi: 10.1088/2399-6528/abae16.

[26] Ludovic Berthier and Giulio Biroli. Theoretical perspective on the glass transition and amorphous materials. *Reviews of Modern Physics*, 83(2):587–645, 2011. doi: 10.1103/revmodphys.83.587.

[27] Robert J Young and Peter A Lovell. *Introduction to Polymers: Third Edition*. CRC Press, United States, 3 edition, June 2011. ISBN 978-0-8493-3929-5.

[28] Ru-Min Wang, Shui-Rong Zheng, and Ya-Ping Zheng. *3 - Matrix materials*. Woodhead Publishing Series in Composites Science and Engineering. Woodhead Publishing, 2011. ISBN 978-0-85709-221-2. doi: https://doi.org/10.1533/9780857092229.1.101.

[29] John F Timmerman, Matthew S Tillman, Brian S Hayes, and James C Seferis. Matrix and fiber influences on the cryogenic microcracking of carbon fiber/epoxy composites. *Composites Part A: Applied Science and Manufacturing*, 33(3):323–329, 2002. ISSN 1359-835X. doi: https://doi.org/10.1016/S1359-835X(01)00126-9.

[30] Ricardo Carbas, E. Marques, L.F.M. Silva, and António Lopes. Effect of cure temperature on the glass transition temperature and mechanical properties of epoxy adhesives. *Journal of Adhesion*, 90, 01 2014. doi: 10.1080/00218464.2013.779559.

[31] Chengzhi Dong, Kai Li, Yuxi Jiang, Dwayne Arola, and Dongsheng Zhang. Evaluation of thermal expansion coefficient of carbon fiber reinforced composites using electronic speckle interferometry. *Opt. Express*, 26(1):531–543, Jan 2018. doi: 10.1364/OE.26.000531.

[32] Shubham Rupani, Rahul Dev, Shivang Jani, and G Acharya. Experimental evaluation of coefficient of thermal expansion of carbon fiber reinforced polymer tube. *International Journal of Advance Engineering and Research Development*, 4:428–433, 05 2017.

[33] Ru-Min Wang, Shui-Rong Zheng, and Ya-Ping Zheng. 11 - other properties of polymer composites. In Ru-Min Wang, Shui-Rong Zheng, and Ya-Ping Zheng, editors, *Polymer Matrix Composites and Technology*, Woodhead Publishing Series in Composites Science and Engineering, pages 513–548. Woodhead Publishing, 2011. ISBN 978-0-85709-221-2. doi: https://doi.org/10.1533/9780857092229.3.513.

[34] M.R. Vengatesan, A.M. Varghese, and V. Mittal. Chapter 3 - thermal properties of thermoset polymers. In Qipeng Guo, editor, *Thermosets (Second Edition)*, pages 69–114. Elsevier, second edition edition, 2018. ISBN 978-0-08-101021-1. doi: https://doi.org/10.1016/B978-0-08-101021-1.00003-4.

[35] Koshi Takenaka. Negative thermal expansion materials: technological key for control of thermal expansion. *Science and Technology of Advanced Materials*, 13(1):013001, 2012. doi: 10.1088/1468-6996/13/1/013001.

[36] Haleh Ardebili, Jiawei Zhang, and Michael G. Pecht. 6 - characterization of encapsulant properties. In Haleh Ardebili, Jiawei Zhang, and Michael G. Pecht, editors, *Encapsulation Technologies for Electronic Applications*, Materials and Processes for Electronic Applications, pages 221–258. William Andrew Publishing, second edition edition, 2019. ISBN 978-0-12-811978-5. doi: https://doi.org/10.1016/B978-0-12-811978-5.00006-7.

[37] Ray Walton Grenoble. *Mechanical Properties and Durability of a Composite Material at Cryogenic Temperatures*. PhD thesis, Old Dominion University, Virginia, May 2006.

[38] Dinabandhu Das, Tia Jacobs, and Len Barbour. Exceptionally large positive and negative anisotropic thermal expansion of an organic crystalline material. *Nature Materials*, 9:36–9, 11 2009. doi: 10.1038/nmat2583.

[39] Khushboo Yadava, Gianpiero Gallo, Sebastian Bette, Caroline Mulijanto, Durga Prasad Karothu, In-Hyeok Park, Raghavender Medishetty, Pance Naumov,

Robert Dinnebier, and Jagadese Vittal. Extraordinary anisotropic thermal expansion in photosalient crystals. *IUCrJ*, 7, 01 2020. doi: 10.1107/S2052252519014581.

[40] Robert R Johnson, M. Kural, and George B. Mackey. Thermal expansion properties of composite materials. 1981.

[41] N. Zobeiry and A. Poursartip. 3 - the origins of residual stress and its evaluation in composite materials. In P.W.R. Beaumont, C. Soutis, and A. Hodzic, editors, *Structural Integrity and Durability of Advanced Composites*, Woodhead Publishing Series in Composites Science and Engineering, pages 43–72. Woodhead Publishing, 2015. ISBN 978-0-08-100137-0. doi: https://doi.org/10.1016/B978-0-08-100137-0.00003-1.

[42] Kai Dong, Xiao Peng, Jiajin Zhang, Bohong Gu, and Baozhong Sun. Temperature-dependent thermal expansion behaviors of carbon fiber/epoxy plain woven composites: Experimental and numerical studies. *Composite Structures*, 176:329–341, 2017. ISSN 0263-8223. doi: https://doi.org/10.1016/j.compstruct.2017.05.036.

[43] Valery V. Vasiliev and Evgeny V. Morozov. Chapter 7 - environmental, special loading, and manufacturing effects. In Valery V. Vasiliev and Evgeny V. Morozov, editors, *Advanced Mechanics of Composite Materials (Second Edition)*, pages 359–435. Elsevier Science Ltd, Oxford, second edition edition, 2007. ISBN 978-0-08-045372-9. doi: https://doi.org/10.1016/B978-008045372-9/50007-5.

[44] Chao Kang, Yaoyao Shi, Bo Deng, Tao Yu, and Pengcheng Sun. Determination of residual stress and design of process parameters for composite cylinder in filament winding. *Advances in Materials Science and Engineering*, 2018:1–11, 03 2018. doi: 10.1155/2018/1821342.

[45] Malgorzata Chwal, Aleksander Muc, Adam Stawiarski, and Marek Barski. Residual stresses in multilayered composites - general overview. *Composites Theory and Practice*, 16:132–138, 10 2016.

[46] A S Kaddour, Salim Al-Hassani, and Mike Hinton. Residual stress assessment in thin angle ply tubes. *Applied Composite Materials*, 10:169–188, 05 2003. doi: 10.1023/A:1023990507666.

[47] Kenan Çınar, Umud Ozturk, Nuri Ersoy, and Michael Wisnom. Modelling manufacturing deformations in corner sections made of composite materials. *Journal of Composite Materials*, 48:799–813, 02 2014. doi: 10.1177/0021998313477896.

[48] H. Bakaiyan, H. Hosseini, and Ehsan Ameri. Analysis of multi-layered filament-wound composite pipes under combined internal pressure and thermomechanical loading with thermal variations. *Composite Structures*, 88:532–541, 05 2009. doi: 10.1016/j.compstruct.2008.05.017.

[49] Hongyan Zhang, P. M. Anderson, and Glenn S. Daehn. Analysis of thermally induced stress and strain in continuous fiber- reinforced composites. *Metallurgical and Materials Transactions A*, 25(2):415–425, 1994. doi: 10.1007/bf02647987.

[50] Valery V. Vasiliev and Evgeny V. Morozov. Chapter 3 - mechanics of a unidirectional ply. In Valery V. Vasiliev and Evgeny V. Morozov, editors, *Advanced Mechanics of Composite Materials (Second Edition)*, pages 57–132. Elsevier Science Ltd, Oxford, second edition edition, 2007. ISBN 978-0-08-045372-9. doi: https://doi.org/10.1016/B978-008045372-9/50003-8.

[51] Yasushi Miyano and Masayuki Nakada. *Durability of fiber-reinforced polymers*. Wiley-VCH Verlag., 2018. ISBN 978-3-527-34356-0.

[52] Kee Lee, Kyu Han Kim, S. Jeoung, S. Ju, JH Shim, Na-Hyung Kim, Seokjoon Lee, S. Lee, Jung-Kun Lee, and D. Paul. Thermal expansion behavior of composites based on axisymmetric ellipsoidal particles. *Polymer*, 48:4174–4183, 06 2007. doi: 10.1016/j.polymer.2007.05.036.

[53] S. Kobayashi, M. Tomite, M. Iwata, H.N. Tran, and K. Goto. Durability of carbon fiber reinforced composite laminates for large precise space structure under cyclic thermal loading. pages 7502–7509, 2013.

[54] Sang Yoon Park, Heung Soap Choi, Won Jong Choi, and Hyuk Kwon. Effect of vacuum thermal cyclic exposures on unidirectional carbon fiber/epoxy composites for low earth orbit space applications. *Composites Part B: Engineering*, 43(2):726–738, 2012. ISSN 1359-8368. doi: https://doi.org/10.1016/j.compositesb.2011.03.007.

[55] Yasir Nawab, Frédéric Jacquemin, Pascal Casari, Nicolas Boyard, Yann Borjon-Piron, and Vincent Sobotka. Study of variation of thermal expansion coefficients in carbon/epoxy laminated composite plates. *Composites Part B: Engineering*, 50:144–149, 2013. ISSN 1359-8368. doi: https://doi.org/10.1016/j.compositesb.2013.02.002.

[56] Timothy L. Brown. *The Effect of Long-Term Thermal Cycling on the Microcracking Behavior and Dimensional Stability of Composite Materials*. PhD thesis, Virginia Polytechnic Institute, Virginia, December 1997.

[57] John A. Nairn. 2.12 - matrix microcracking in composites. In Anthony Kelly and Carl Zweben, editors, *Comprehensive Composite Materials*, pages 403–432. Pergamon, Oxford, 2000. ISBN 978-0-08-042993-9. doi: https://doi.org/10.1016/B0-08-042993-9/00069-3.

[58] Stephen Tompkins, James Shen, and Andre Lavoie. Thermal cycling of thin and thick ply composites. *Engineering, Construction and Operations in Space IV*, 02 1994.

[59] Magdalena Urbaniak and K. Grudzinski. Time-temperature-transformation (ttt) cure diagram for epy® epoxy system. *Polimery*, 52:117–126, 02 2007. doi: 10.14314/polimery.2007.117.

[60] Joseph D. Menczel and Bruce Prime. *Thermal Analysis of Polymers, Fundamentals and Applications*. John Wiley & Sons, 2009. ISBN 978-0-471-76917-0.

[61] Ching-Shiun Wu. Influence of post-curing and temperature effects on bulk density, glass transition and stress-strain behaviour of imidazole-cured epoxy network. *Journal of Materials Science*, 27(11):2952–2959, 1992. doi: 10.1007/bf01154105.

[62] Pascal Hubert, Timotei Centea, Lessa Grunefelder, Steven Nutt, James Kratz, and Arthur Levy. 2.4 out-of-autoclave prepreg processing. In Peter W.R. Beaumont and Carl H. Zweben, editors, *Comprehensive Composite Materials II*, pages 63–94. Elsevier, Oxford, 2018. ISBN 978-0-08-100534-7. doi: https://doi.org/10.1016/B978-0-12-803581-8.09900-8.

[63] Jeffrey Gotro. Thermoset characterization part 9: Vitrification; putting it all together. `https://polymerinnovationblog.com/thermoset-characterization-part-9-vitrification-putting-together/`, May 2014. Accessed on 29-05-2021.

[64] Jeffrey Gotro. Practical tips for curing thermosets part two: Impact of cure temperature on the glass transition temperature. `https://polymerinnovationblog.com/practical-tips-curing-thermosets-part-two-impact-cure-temperature.-final-tg`, Sep 2016. Accessed on 29-05-2021.

[65] Magdalena Urbaniak. Glass transition temperature-cure temperature-transformation (tgtt) diagram for epy epoxy system. *Polimery*, 63:18–24, 01 2018. doi: 10.14314/polimery.2018.1.3.

[66] Oleksandr G. Kravchenko, Sergii G. Kravchenko, and R. Byron Pipes. Chemical and thermal shrinkage in thermosetting prepreg. *Composites Part A: Applied Science and*

Manufacturing, 80:72–81, 2016. ISSN 1359-835X. doi: https://doi.org/10.1016/j.compositesa.2015.10.001.

[67] Zhenyi Yuan, Yongjun Wang, Guigeng Yang, Aofei Tang, Zhenchao Yang, Shujuan Li, Yan Li, and Danlong Song. Evolution of curing residual stresses in composite using multi-scale method. *Composites Part B: Engineering*, 155:49–61, 2018. ISSN 1359-8368. doi: https://doi.org/10.1016/j.compositesb.2018.08.012.

[68] L.G. Zhao, N.A. Warrior, and A.C. Long. A micromechanical study of residual stress and its effect on transverse failure in polymer–matrix composites. *International Journal of Solids and Structures*, 43(18):5449–5467, 2006. ISSN 0020-7683. doi: https://doi.org/10.1016/j.ijsolstr.2005.08.012.

[69] H. Zrida, P. Fernberg, Z. Ayadi, and J. Varna. Microcracking in thermally cycled and aged carbon fibre/polyimide laminates. *International Journal of Fatigue*, 94:121–130, 2017. ISSN 0142-1123. doi: https://doi.org/10.1016/j.ijfatigue.2016.09.017.

[70] Satoshi Kobayashi, Tomoaki Shimpo, and Ken Goto. Microscopic damage behavior in carbon fiber reinforced plastic laminates for a high accuracy antenna in a satellite under cyclic thermal loading. *Advanced Composite Materials*, 28:1–11, 11 2018. doi: 10.1080/09243046.2018.1551745.

[71] Firas Awaja, Shengnan Zhang, Manoj Tripathi, Anton Nikiforov, and Nicola Pugno. Cracks, microcracks and fracture in polymer structures: Formation, detection, autonomic repair. *Progress in Materials Science*, 83:536–573, 2016. ISSN 0079-6425. doi: https://doi.org/10.1016/j.pmatsci.2016.07.007.

[72] M. Kaminski, F. Laurin, J. Maire, C. Rakotoarisoa, and E. Hémon. Fatigue damage modeling of composite structures: the onera viewpoint. *AerospaceLab*, (9):1–12, 2015. doi: 10.12762/2015.AL09-06.

[73] Alberto D'Amore and Luigi Grassia. Phenomenological approach to the study of hierarchical damage mechanisms in composite materials subjected to fatigue loadings. *Composite Structures*, 175:1–6, 2017. ISSN 0263-8223. doi: https://doi.org/10.1016/j.compstruct.2017.04.071.

[74] Thomas Jollivet, Catherine Peyrac, and Fabien Lefebvre. Damage of composite materials. *Procedia Engineering*, 66:746–758, 2013. ISSN 1877-7058. doi: https://doi.org/10.1016/j.proeng.2013.12.128. Fatigue Design 2013, International Conference Proceedings.

[75] M.C. Lafarie-Frenot. Damage mechanisms induced by cyclic ply-stresses in carbon–epoxy laminates: Environmental effects. *International Journal of Fatigue*, 28 (10):1202–1216, 2006. ISSN 0142-1123. doi: doi.org/10.1016/j.ijfatigue.2006.02.014. The Third International Conference on Fatigue of Composites.

[76] L. Maragoni, P.A. Carraro, M. Peron, and M. Quaresimin. Fatigue behaviour of glass/epoxy laminates in the presence of voids. *International Journal of Fatigue*, 95: 18–28, 2017. ISSN 0142-1123. doi: https://doi.org/10.1016/j.ijfatigue.2016.10.004.

[77] M.M. Shokrieh and F. Taheri-Behrooz. Progressive fatigue damage modeling of cross-ply laminates, i: Modeling strategy. *Journal of Composite Materials*, 44(10): 1217–1231, 2010. doi: 10.1177/0021998309351604.

[78] Kenneth L. Reifsnider. Chapter 2 - damage and damage mechanics. In K.L. Reifsnider, editor, *Fatigue of Composite Materials*, volume 4 of *Composite Materials Series*, pages 11–77. Elsevier, 1991. doi: https://doi.org/10.1016/B978-0-444-70507-5.50006-8.

[79] Javier Cabrera Barbero. *Thermal-Fatigue and Thermo-Mechanical Equivalence for Transverse Cracking Evolution in Laminated Composites*. PhD thesis, West Virginia University, Morgantown, December 2018.

[80] Xi Li, Julian Kupski, Sofia Teixeira De Freitas, Rinze Benedictus, and Dimitrios Zarouchas. Unfolding the early fatigue damage process for cfrp cross-ply laminates. *International Journal of Fatigue*, 140:105820, 2020. ISSN 0142-1123. doi: https://doi.org/10.1016/j.ijfatigue.2020.105820.

[81] C. Henaff-Gardin and M.C. Lafarie-Frenot. Specificity of matrix cracking development in cfrp laminates under mechanical or thermal loadings. *International Journal of Fatigue*, 24(2):171–177, 2002. ISSN 0142-1123. doi: https://doi.org/10.1016/S0142-1123(01)00070-6.

[82] J.-M. Berthelot, A.El Mahi, and J.-F. Le Corre. Development of transverse cracking in cross-ply laminates during fatigue tests. *Composites Science and Technology*, 61(12): 1711–1721, 2001. ISSN 0266-3538. doi: https://doi.org/10.1016/S0266-3538(01)00068-9.

[83] J. Tong, F.J. Guild, S.L. Ogin, and P.A. Smith. On matrix crack growth in quasi-isotropic laminates—i. experimental investigation. *Composites Science and Technology*, 57(11):1527–1535, 1997. ISSN 0266-3538. doi: https://doi.org/10.1016/S0266-3538(97)00080-8.

[84] Keiichiro Tohgo, Shuji Nakagawa, and Hiroyasu Araki. Damage behavior and life prediction in cfrp cross-ply laminates under fatigue loading. *Journal of Solid Mechanics and Materials Engineering*, 2(3):342–353, 2008. doi: 10.1299/jmmp.2.342.

[85] Jinxin Meng, Yong Wang, Haiyang Yang, Panding Wang, Qin Lei, Hanqiao Shi, Hongshuai Lei, and Daining Fang. Mechanical properties and internal microdefects evolution of carbon fiber reinforced polymer composites: Cryogenic temperature and thermocycling effects. *Composites Science and Technology*, 191:108083, 2020. ISSN 0266-3538. doi: https://doi.org/10.1016/j.compscitech.2020.108083.

[86] Qi Yu, Ping Chen, Yu Gao, Jujie Mu, Yongwu Chen, Chun Lu, and Dong Liu. Effects of vacuum thermal cycling on mechanical and physical properties of high performance carbon/bismaleimide composite. *Materials Chemistry and Physics*, 130 (3):1046–1053, 2011. ISSN 0254-0584. doi: https://doi.org/10.1016/j.matchemphys.2011.08.033. URL `https://www.sciencedirect.com/science/article/pii/S0254058411007115`.

[87] W.A. Imbriale, Steven Gao, and Luigi Boccia. *Space Antenna Handbook*. 05 2012. ISBN 9781119993193. doi: 10.1002/9781119945147.

[88] Satomi Asai, Ken Goto, Satoru Yoneyama, Shuichi Arikawa, and Satoshi Kobayashi. Effect of space environment on thermal and mechanical properties of cfrp. 2015.

[89] Shinji Ogihara, Akira Kobayashi, Takamoto Ishiguro, and Nobuo Otani. Experimental characterization of matrix cracking behavior in thermally cycled cfrp laminates. *International Journal of Damage Mechanics*, 11(3):287–305, 2002. doi: 10.1106/105678902026414.

[90] Byung-Hahn Yeh and Yong-Gu Won. Cryogenic and elevated temperature cycling of carbon polymer composites for reusable launch vehicle cryogenic tanks. pages 38–42, 2002.

[91] Sergio González, Gianluca Laera, Sotiris Koussios, Jaime Domínguez, and Fernando A Lasagni. Simulation of thermal cycle aging process on fiber-reinforced polymers by extended finite element method. *Journal of Composite Materials*, 52 (14):1947–1958, 2018. doi: 10.1177/0021998317734625.

[92] Le Cuong, Nguyen Quang, Tran Cuong, Dao Khanh, and Nguyen Khanh. Experimental investigation and modeling of the thermal cycling effect on the mechanical properties of cfrp. pages 41–45, 07 2016. doi: 10.1109/ICMAE.2016.7549505.

[93] Yu Gao, Song He, Dezhuang Yang, Yong Liu, and Zhijun Li. Effect of vacuum thermocycling on physical properties of unidirectional m40j/ag-80 composites. *Composites Part B: Engineering*, 36(4):351–358, 2005. ISSN 1359-8368. doi: https://doi.org/10.1016/j.compositesb.2004.10.002.

[94] Kwang-Bok Shin, Chun-Gon Kim, Chang-Sun Hong, and Ho-Hyung Lee. Prediction of failure thermal cycles in graphite/epoxy composite materials under simulated low earth orbit environments. *Composites Part B: Engineering*, 31(3):223–235, 2000. ISSN 1359-8368. doi: https://doi.org/10.1016/S1359-8368(99)00073-6.

[95] Ole Thomsen and K.K. Kratmann. Experimental characterisation of parameters controlling the compressive failure of pultruded unidirectional carbon fibre composites. *Applied Mechanics and Materials*, 24-25:15–22, 06 2010. doi: 10.4028/www.scientific.net/AMM.24-25.15.

[96] J. Lee and C. Soutis. A study on the compressive strength of thick carbon fibre–epoxy laminates. *Composites Science and Technology*, 67(10):2015–2026, 2007. ISSN 0266-3538. doi: https://doi.org/10.1016/j.compscitech.2006.12.001.

[97] Catarina Silva and Bernardete Ribeiro. *Aprendizagem Computacional em Engenharia*. Imprensa da Universidade de Coimbra, Coimbra, 2018 2018. ISBN 978-989-26-1507-3. doi: https://doi.org/10.14195/978-989-26-1508-0.

[98] Jay H. Lee, Joohyun Shin, and Matthew J. Realff. Machine learning: Overview of the recent progresses and implications for the process systems engineering field. *Computers and Chemical Engineering*, 114:111–121, 2018. ISSN 0098-1354. doi: https://doi.org/10.1016/j.compchemeng.2017.10.008.